DYNAMIQUE DES SYSTÈMES DÉSORDONNES:UNE ÉTUDE PAR DIFFUSION DE NEUTRONS

Elisa Fabiani

THÈSE

présentée pour obtenir le grade de

DOCTEUR DE L'UNIVERSITE JOSEPH FOURIER

spécialité

Physique des Matériaux

par

Elisa FABIANI

DYNAMICS IN STRONG GLASSES:

AN INELASTIC NEUTRON SCATTERING ANALYSIS

DYNAMIQUE DES SYSTEMES DESORDONNES:

UNE ETUDE PAR DIFFUSION DE NEUTRONS

Directeur de thèse	Prof. Marc Bée
Rapporteurs:	Prof. Ulrich Buchenau
	Dr. Christiane Alba-Simionesco
Examinateurs:	Prof. Aldo Fontana
	Dr. Helmut Schober
	Dr Pierre Bastie

Contents

Preface

The main task of this thesis is to perform a systematic investigation of the dynamics of glassy materials at temperatures T much smaller than T_g, the glass transition temperature.

Both theoretical and experimental studies (Elliot 1990; Fontana and Viliani 2002; Fontana and Viliani 2003), performed over the last two decades on different aspects of the glassy state, have established a number of peculiar properties that concern low energy dynamics and manifest themselves in low temperature specific heat, thermal conductivity, and inelastic scattering experiments (Sette et al. 1998; Pilla et al. 2000). Some of the fundamental questions in this field have found a satisfactory and widely accepted answer. Despite of these efforts, some questions about the microscopic nature of the dynamics and the origin of the "universal" features concerning the density of vibrational states in glasses, have not found at present a

Préface

Le but principal de cette thèse est d'effectuer une recherche systématique sur la dynamique des matériaux vitreux à des températures T beaucoup plus petites que la température de transition vitreuse T_g.

Des études théoriques et expérimentales (Elliot 1990; Fontana et Viliani 2002; Fontana et Viliani 2003), exécutées pendant les deux dernières décennies sur différents aspects de l'état vitreux, ont établi un certain nombre de propriétés particulières qui concernent la dynamique à basse énergie et qui se manifestent dans la chaleur spécifique à basse température, dans la conductivité thermique, et dans la diffusion inélastique expérimentale (Sette et al. 1998; Pilla et al. 2000). Certaines questions fondamentales dans ce domaine ont trouvé une réponse satisfaisante et largement admise. Cependant, en dépit de tous ces efforts, quelques questions relatives à la nature microscopique de la dynamique et à l'origine des caractéristiques "universelles" de la densité des états

generally accepted answer (Fontana and Viliani 2002; Fontana and Viliani 2003). Among them some effects which are observed both in inelastic neutron scattering (Buchenau et al. 1986; Buchenau et al. 1988; Fontana et al. 1990; Cicognani et al. 1999; Fontana et al. 1999) and first order Raman scattering (Brodin et al. 1994; Carini et al. 1995) at low frequency are of interest for the present work:

(i) the existence of a broad structure-less band in the 20-100 cm^{-1} range, the so-called Boson Peak (BP), whose origin is not still well understood (Buchenau et al. 1986; Buchenau et al. 1988; Fontana et al. 1990; Rat et al. 1999; Foret et al. 2002)

(ii) the conceptual understanding of the sound attenuation mechanisms in vitreous systems (Ruocco et al. 2000, Benassi et al. 1996)

(iii) the observation of a quasi-elastic Raman scattering, at frequencies lower then 20 cm^{-1}, usually referred to as extra-scattering, which shows a peculiar temperature dependence (Benassi 1996) and which is attributed to relaxation mechanisms (Phillips 1981; Carini 1995)

(iv) the study of the Raman Coupling

vibrationnels dans les verres, n'ont pas trouvé actuellement une réponse généralement admise (Fontana et Viliani 2002; Fontana et Viliani 2003). Parmi eux certains effets qui sont observés dans les données inélastiques de diffusion de neutron (Buchenau et al. 1986; Buchenau et al. 1988; Fontana et al. 1990; Cicognani et al. 1999; Fontana et al. 1999) et de diffusion de Raman (Brodin et al. 1994; Carini et al. 1995) à basse fréquence sont examinés dans ce travail:

(i) l'existence d'une large bande sans structure dans la gamme de 20-100 cm^{-1}, le pic de Bose (BP), dont l'origine n'est pas encore bien comprise (Buchenau et al. 1986; Buchenau et al. 1988; Fontana et al. 1990; Rat et al. 1999; Foret et al. 2002);

(ii) la compréhension conceptuelle des mécanismes d'atténuation dans les systèmes vitreux (Ruocco et al. 2000, Benassi et al. 1996)

(iii) l'observation d'une diffusion quasi-élastique dans les données Raman, à des fréquences plus basses que 20 cm^{-1}, habituellement désignée sous le nom de diffusion supplémentaire, qui montre une dépendance particulière avec la température (Benassi et al. 1996) et qui est attribuée aux mécanismes de relaxation (Phillips 1981; Carini et al. 1995)

Function C(ω), which can give useful information about the microscopic characteristics of vibration modes.

In order to understand if these effects are general features of strong glasses, different systems have been investigated.

Here we present new results on two strong glasses, vitreous silica (v-SiO_2) and vitreous germania (v-GeO_2), which are very similar on the structural characteristics.

The technique employed was Inelastic Neutron Scattering (INS); in particular Time-Of-Flight (TOF) and Three-Axis Spectrometers (TAS) were used in order to investigate the dynamics in a wide range of energies and wave-vectors exchanged. In particular the study of v-GeO_2 has been undertaken because of its lower sound velocity, which allows the direct observation by INS of the dispersion relation over the (Q,ω)-region intermediate between hydrodynamic and single particle dynamics.

The studies of these samples have been done in order to develop the following objectives:

- the development of a new procedure to extract the density of states from coherent systems extending the usual incoherent approximation;

(iv) l'étude de la fonction de couplage Raman C(ω), qui donne des informations utiles sur les caractéristiques microscopiques des modes de vibration.

Afin de comprendre si ces effets sont généraux des verres forts, nous avons étudié différents systèmes. Ici nous présentons de nouveaux résultats sur deux verres forts, le quartz fondu (v-SiO_2) et l'oxyde de germanium vitreux (v-GeO_2), qui sont très proches du point de vue des caractéristiques structurales.

La technique utilisée est la dispersion inélastique des neutrons (INS); en particulier nous avons utilisé les spectromètres à Temps-De-Vol (TOF) et les spectromètres Trois-Axes (TAS) afin d'étudier la dynamique dans une grande gamme d'échange d'énergie et de vecteur d'onde. L'étude de v-GeO_2 a été effectuée en raison de sa faible vitesse du son, qui permet l'observation directe par INS des relations de dispersion dans la région (Q, ω) intermédiaire entre l'hydro- dynamique et la dynamique de la particule simple. Les études de ces échantillons avaient pour objectifs:

- *le développement d'une nouvelle procédure pour extraire la densité des états à partir des systèmes cohérents en étendant l'approximation incohérente habituelle;*
- *l'étude de la diffusion quasiélastique de nos échantillons dans la région de très de basse fréquence en utilisant des spectromètres Raman et TOF, afin de comparer aux*

- the study of the QES of our samples at very low frequency range by using Raman and TOF spectrometers, in order to compare with Brillouin data and to asses a correlation with the mechanism causing the sound attenuation;
- the comparison of the previous scattering data above-mentioned, in order to calculate the Raman coupling function C(ω) and its low frequency limit.
- the investigation of v-GeO_2 to asses that both longitudinal and transverse acoustic branches are still somewhat defined also in glassy system (Bove et al. 2004). Indeed, even though a satisfactory understanding of the high frequency longitudinal and transverse dynamics has been achieved in vitreous silica, it is not evident to what extent it could be generalized to describe other glassy systems (Ruocco et al. 2000; Ruzicka et al. 2004; Angell 1998);

The results obtained in this work can explain some aspects, which are still unresolved in the field of vitreous systems.

The thesis is structured as following:

- the most important physical properties

données de diffusion Brillouin pour trouver une corrélation entre cette diffusion et le mécanisme responsable de l'atténuation acoustique;

- *la comparaison des données de dispersion précédemment mentionnées, afin de calculer la fonction de couplage Raman C(ω) et sa limite à basse fréquence ;*
- *l'étude du v-GeO_2 afin de prouver que les branches acoustiques longitudinales et transversales sont aussi définies dans le système vitreux (Bove et al. 2004) comme dans les cristaux. En fait, même si une compréhension satisfaisante de la dynamique longitudinale et transversale à haute fréquence a été réalisée dans le quartz fondu, il n'est pas évident dans que ce resultat puisse être généralisé pour décrire d'autres systèmes vitreux (Ruocco et al. 2000; Ruzicka et al. 2004; Angell 1998).*

Les résultats obtenus dans ce travail peuvent expliquer des aspects, qui ne sont pas encore bien définis dans le domaine des systèmes vitreux.

La thèse est structurée de la manière suivante:

- *les propriétés physiques et les plus importantes anomalies des matériaux vitreux par rapport au cristal*

and anomalies of glassy materials with respect to the corresponding crystal are reminded in the first Chapter;

- the general properties of oxide glass formers (structure, specific heat, thermal conductivity) are treated in Chapter 2 in order to focalise the important characteristics of the systems studied;
- the main experimental techniques used, are presented in the third chapter: a detailed explanation of neutron scattering experiments and of light scattering technique is given;
- the description of the treatment of data and in particular the new method for the data analysis involving the extension of the incoherent approximation are the subject of Chapter 4;
- the aim of the Chapters 5 is to present new inelastic neutron scattering data for the network glass formers v-SiO_2 and v-GeO_2 and to compare them with those measured by Raman, specific heat (Sokolov 1993) and molecular dynamics simulations in order to:
  1. study the crossover from quasielastic to vibrational scattering at low frequency in both Raman and neutron spectra;
  2. explore the Brillouin scattering

correspondant sont rappelées dans le premier chapitre;

- *les propriétés générales des verres d'oxyde (structure, chaleur spécifique, conductivité thermique) sont traitées dans le chapitre 2 ansi que les caractéristiques importantes des systèmes que nous avons étudiés;*
- *les techniques expérimentales principalement utilisées sont présentées dans le troisième chapitre dans lequel nous donnons également une explication détaillée des expériences de diffusion de neutron et de la technique de dispersion de la lumière;*
- *la description du traitement des données et en particulier la nouvelle méthode pour l'analyse de données qui est basée sur l'extension de l'approximation incohérente, est le sujet du chapitre 4;*
- *le but du chapitre 5 est de présenter les nouvelle données de dispersion inélastique de neutron pour les verres de v-SiO_2 et de v-GeO_2 et de les comparer à celles mesurées par la spectroscopie Raman, la chaleur spécifique (Sokolov 1993) et les simulations moléculaires de dynamique pour:*
  1. *étudier le crossover entre la diffusion quasiélastique et le spectre vibrationnel de basse fréquence dans des spectres Raman et de neutrons;*
  2. *explorer le pic de diffusion Brillouin*

with increasing momentum on vitreous germania, to see how far the conventional dispersion approach holds;

3. find an appropriate description of the coherent vibrational scattering, comparing the conventional dispersion approach to a new extension of the incoherent approximation;
4. determine the spectral shape of the coupling function C(ω) and its low frequency limit.

- The evaluation of the neutron time-of-flight spectra in terms of the extension of the incoherent approximation (extended approximation) described in chapter 4 is presented in Chapter 6.
- The last results obtained about the determination of the spectral shape of the coupling function C(ω) and its low frequency limit (comparing inelastic scattering data collected by Raman and neutron experiments) are shown in Chapter 7
- the conclusions of this thesis work are resumed in Chapter 8
- finally, the paper related are listed in Chapter 9.

en fonction du vecteur d'onde sur l'oxyde de germanium vitreux, pour voir jusqu'où la dispersion conventionnelle reste valide ;

3. *trouver une description appropriée de la dispersion vibratoire cohérente, en comparant l'approche conventionnelle de la dispersion de neutron à une nouvelle extension de l'approximation incohérente;*
4. *déterminer la forme spectrale de la fonction de couplage C(ω) et sa limite de basse fréquence.*

- *L'analyse des spectres de temps-de-vol de neutrons par la méthode de l'extension de l'approximation incohérente (approximation prolongée) décrite en chapitre 4 est présentée dans le chapitre 6.*
- *Les derniers résultats obtenus au sujet de la détermination de la forme spectrale de la fonction de couplage C(ω) et de sa limite à basse fréquence (en comparant les données inélastiques de dispersion obtenues par des expériences de Raman et de neutron) sont exposés dans le chapitre 7.*
- *Les conclusions de ce travail de thèse sont reprises dans le chapitre 8.*
- *Enfin, les publications relatives à ce travail sont énumérées dans le chapitre 9.*

REFERENCES

ANGELL A., *Nature* **393**, 521 (1998).

BENASSI P., KRISCH M., MASCIOVECCHIO C., MAZZACURATI V., MONACO G., RUOCCO G., SETTE F., and VERBENI R., *Phys. Rev. Lett.* 77, 3835 (1996).

BOVE L.E., FABIANI E., FONTANA A., PALETTI F., PETRILLO C., PILLA O. and VIEIRO-BENTO I.C., submitted to *Phys. Rev. Lett.* (2004).

BRODIN A., FONTANA A., BORJESSON L., CARINI G. and TORELL L.M., *Phys. Rev. Lett.* **73**, 2067 (1994).

BUCHENAU U., PRAGER M., NUKER N., DIANOUX A.J., AHMAD N. and PHILLIPS W.A., *Phys. Rev.***B 34**, 5665 (1986).

BUCHENAU U., ZHOU H.M., NUKER N., GILROY K.S. and PHILLIPS W.A., *Phys. Rev. Lett.* **60**, 1318 (1988).

CARINI G., D'ANGELO G., TRIPODO G., FONTANA A., LEONARDI A., SAUNDERS G.A. and BRODIN A., *Phys. Rev.* **B 52**, 9342 (1995-I).

CICOGNANI G., DIANOUX A.J., FONTANA A., ROSSI F., MONTAGNA M., SCOPINO T., PELOUS J., TERKI F., PILLEZ J. N. and WOIGNIER T., *Philos. Mag.* **B. 79**, 2091 (1999).

ELLIOT S.R. , *Physics of amorphous materials* (Longman Scientific & Technical) (1990).

FORET M., VACHER R., COURTENS E. and MONACO G., *Phys. Rev.* **B 66,** 024204 (2002).

FONTANA A., ROCCA F., FONTANA M.P., ROSI B. and DIANOUX A.J., *Phys. Rev.* **B 41**,3778 (1990).

FONTANA A., DELL'ANNA R., MONTAGNA M., ROSSI F., VILIANI G., RUOCCO G., SAMPOLI M., BUCHENAU U. and WISCHNEWSKI A., *Europhysics Letters* **47**, 56 (1999).

FONTANA A. AND VILIANI G. *Philos. Mag.* **B**, Volume 82, Number 2/6, Special issue: 8th International Workshop on Disordered Systems, Andalo 2001 and references therein (2002).

FONTANA A. AND VILIANI G., *Philos. Mag.* **B**, Special issue: 9th International Workshop on Disordered Systems, Molveno-Andalo 2003 (in press).

PHILLIPS W. A., *"Amorphous Solids: Low-Temperature properties"* (Springer, Berlin, 1981).

PILLA O., CUNSOLO A., FONTANA A., MASCIOVECCHIO C., MONACO G., MONTAGNA M., RUOCCO G., SCOPIGNO T. and SETTE F., *Phys. Rev.Lett.* **85**, 2136 (2000).

RAT E., FORET M., COURTENS E., VACHER R., and ARAI M., *Phys. Rev. Lett.* **83**, 1355 (1999).

RUOCCO G., SETTE F., DI LEONARDO R., MONACO G., SCAMPOLI M., SCOPINO T., and VILLANI G., *Phys. Rev. Lett.* **84**, 5788 (2000).

RUZICKA B., SCOPIGNO T., CAPONI S., FONTANA A., PILLA O., GIURA P., MONACO G., PONTECORVO E., RUOCCO G., and SETTE F., *Phys. Rev.* **B 69**, 100201(R) (2004).

SETTE F., KRISCH M., MASCIOVECCHIO C., RUOCCO G. and MONACO G., *Science* **280**, 1550 (1998).

SOKOLOV A. P., KISLIUK A., QUITMANN D., and DUVAL E., *Phys. Rev.* **B 48**, 7692 (1993).

1. The Physics of Disordered Materials

This introductory chapter presents the most important dynamical and structural characteristics of glassy materials and the evidence of the anomalies that they manifest with respect to the corresponding crystal state. The general features of glasses presented in this part are experimental results obtained in the last twenty years by using of different techniques as inelastic neutron scattering, inelastic Raman scattering, specific heat and thermal conductivity.

Cette introduction présente les propriétés dynamiques et structurales les plus importantes des matériaux vitreux et met en évidence les anomalies qu'ils manifestent par rapport à l'état cristallin correspondant. Les caractéristiques générales des verres présentées dans cette partie sont des résultats expérimentaux obtenus dans les dernières vingt années en employant différentes techniques comme la diffusion inélastique des neutrons et la diffusion Raman, la mesure de la chaleur spécifique et de la conductivité thermique.

1.1 Introduction: Amorphous materials

An amorphous material can be defined as a solid, which does not possess the characteristic periodicity of a crystal (Elliot 1990, Zachariasen 1932). That means that some kinds of disorder, which can occur in several forms, are present.

The different types of disorder, which can be spin, substitutional, vibrational and topological disorder, are schematically illustrated in Figure 1.1.

With the *substitutional disorder* (Figure 1.1a) the underlying perfect crystal is preserved but one type of atom is randomly substituted for another in the lattice. The next category of randomness considered is the *vibrational disorder* of a crystalline lattice (Figure1b). Whit *spin disorder* (Figure 1c), the underlying perfect crystal is still preserved but each atomic site bears a oriented randomly spin or magnetic moment.

The last form of randomness is the *topological disorder* (Figure 1d) in which there is no translational periodicity; in fact the system is characterised by a short range order but the atoms are linked at random to each other.

In this context, a *glass* can be defined as an amorphous solid completely lacking of long range order and characterized by a typical temperature parameter called *glass transition temperature* T_g, as explained in the following section.

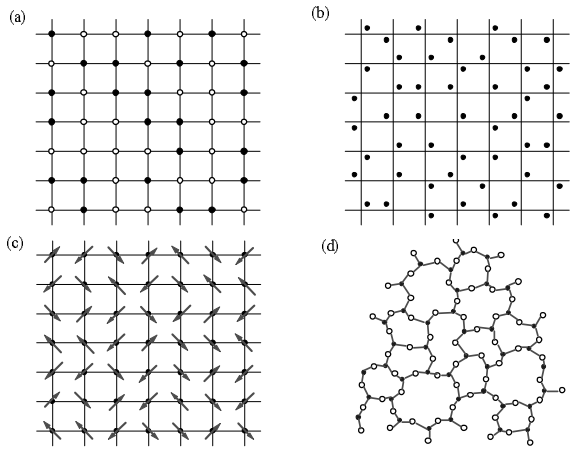

Figure 1.1: Different forms of disorder: substitutional (a), vibrational (b), spin (c) and topological (d)

1.2 The Glass Transition Temperature T_g

Any material, inorganic, organic, or metallic, formed by any technique, which exhibits glass transformation behavior, is a glass.

The glass has the mechanical properties of a solid and lacks the long-range order as in a liquid. At short distance, the order is well defined and corresponds to structural units of the lattice, like tetrahedra SiO_4 or GeO_4 in the examples of v-SiO_2 and v-GeO_2, respectively (Figure 1.1d).

By definition a material is a glass if its viscosity is greater than about 10^{13} kg/ms.

Viscosity is related to the stress relaxation time, which is of the order of several minutes, so that the criterion specifies when the material will behave as a rigid solid for experiments carried out on a macroscopic time scale. However by waiting long enough it is possible to observe relaxation to a new configuration of Equilibrium State. Since the viscosity is strongly temperature dependent, the above criterion also defines a *temperature at which the relaxation times are of the order of minutes*: this is the glass transition temperature T_g.

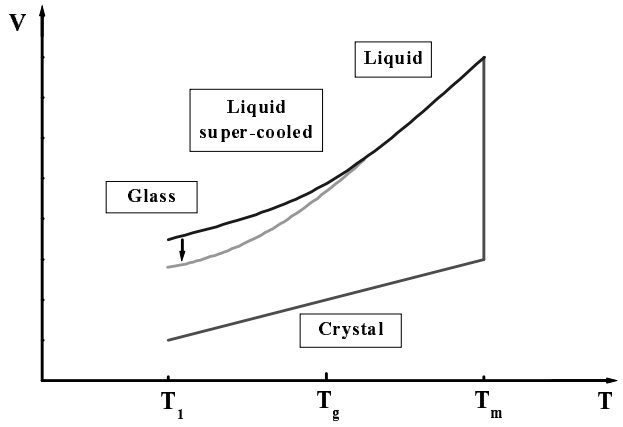

Figure 1.2: Thermodynamic behaviour of the glass transition

Glass transformation behavior can be discussed on the basis of either enthalpy or volume *versus* temperature diagrams[1], such as that shown in Figure 1.2. In either case, we can monitor the change with temperature of the volume, V, or enthalpy, H, above the melting temperature of the substance.

When cooling the liquid, the atomic structure of the melt will gradually change down to the melting temperature (T_m). Cooling again to any temperature below, the liquid will normally crystallize, with the formation of a long range, periodic atomic arrangement. If this occurs, the enthalpy will decrease abruptly to corresponding crystal value.

If the liquid is cooled below the melting temperature of the crystal without crystallization, it will become a super-cooled liquid. The structure of the liquid continues to rearrange as the temperature decreases and its viscosity increases, but the enthalpy does not decrease abruptly if the cooling is fast enough. The enthalpy begins to deviate from the equilibrium line, following a curve of gradually decreasing slope, until the viscosity becomes so great that the liquid structure is arrested and there is no longer temperature dependence. The temperature region lying between the limits where the enthalpy is that of the equilibrium liquid and that of the frozen solid is known as the glass transformation region. The frozen liquid is now a glass. In the plot of the volume as a function of temperature the crystallization is characterised by a strong break in the slope at T_m, while the glass forming is characterized by a gradual changing of the gradient as a function of temperature.

Although the glass transformation actually occurs over a temperature range, it is convenient to define a term, which allows us to express the difference in thermal history between the glass and the super-cooled liquid. If we extrapolate the glass and supercooled liquid lines, they intersect at a temperature defined as the fictive temperature. This temperature is termed *glass transition temperature* (T_g) (Shelby 1997).

[1] Since enthalpy and volume behave in a similar way, the choice of the ordinate is somewhat arbitrary.

This definition of glass includes a wide variety of materials, the most common of which are the inorganic glasses formed by super-cooling the melt.
In this category are the network structures, single constituent materials, plus a wide range of more complex compositions. Selenium is the only element, which forms a stable glass from the melt. Many inorganic compositions, which cannot be super-cooled to give vitreous materials, may be prepared as glasses by other techniques.

1.3 The relaxation process in glassy materials

As we have just said, the glass can be obtained by the super-cooling of a liquid. The super-cooling *freezes* the system in a disordered liquid configuration, which does not correspond to the absolute minimum of the free energy F, but only to a local minimum. Even if the system is not in an equilibrium state, its energy is not enough to jump the gap to another energy configuration. This means that the system is in a *metastable* state.

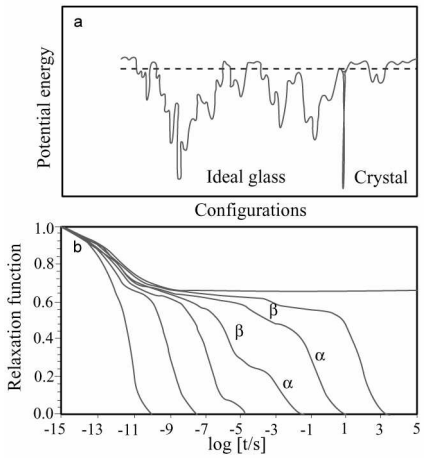

Figure 1.3: a) Energy-landscape representation for a glass: the internal energy of a system depends on the configuration of all its particles. b) The relaxation function shows the approach to equilibrium over time. (Angell 1998)

It is possible to have many configurations with similar free energy but different structure: the system can easily jump from one to another when the gap is small. These structural changes are called *relaxation process*. They are always present in glassy materials and the relaxation time is of the order of seconds if $T \sim T_g$, and of the order of years if $T \leq T_g$ (Angell 1998).

In vitreous materials it is possible to distinguish two main relaxation processes (Figure 1.3b):

- a slow α-dynamics below the GHz regime
- a fast β-dynamics in the GHz regime and below, but faster than the α-dynamics

The α process is a cooperative effect and has a strong temperature dependence especially near the glass transition (T_g) while the β processes is observed at temperatures below T_g (Goldstein 1969). In general the presence of an active relaxation process influences the width of the Brillouin peak (Ruocco *et al.* 2000) as well as the shape of the susceptibility function. The susceptibility at high frequencies can be obtained by the low frequency Raman scattering, called Quasi-Elastic Scattering (QES), which is present also in the inelastic neutron scattering measurements. The correlation between the relaxation process and the QES was studied in the present work and will be presented in Chapter 5.

1.4 Characteristics of glasses at low temperature

Extensive research performed over the last two decades on different aspects of the glassy state has established some physical properties that are strikingly different from those of the respective crystalline solids and there are commonly referred as universal for disordered systems. Performing inelastic scattering experiments as well as specific heat and thermal conductivity measurements anomalous properties can be observed at low frequency in the first case and at low temperature in the second one.

An important conceptual result of the low energy behaviour is that disordered systems support, in addition to Debye-like phonons, some other excess modes. In the following the main thermal anomalies of glasses are reported.

1.4.1 The Specific Heat

The lowest-energy excitations corresponding to $T < 1$ K can be successfully described in terms of Two-Level Systems (TLS) or more generally Tunnelling Systems coexisting and interacting with phonons. A nearly constant density of states of TLS provides a linear excess contribution to the specific heat at low temperature (Figure 1.4a). However at higher temperature effects are observed which cannot be accounted for this TLS model (Figure 1.4b).

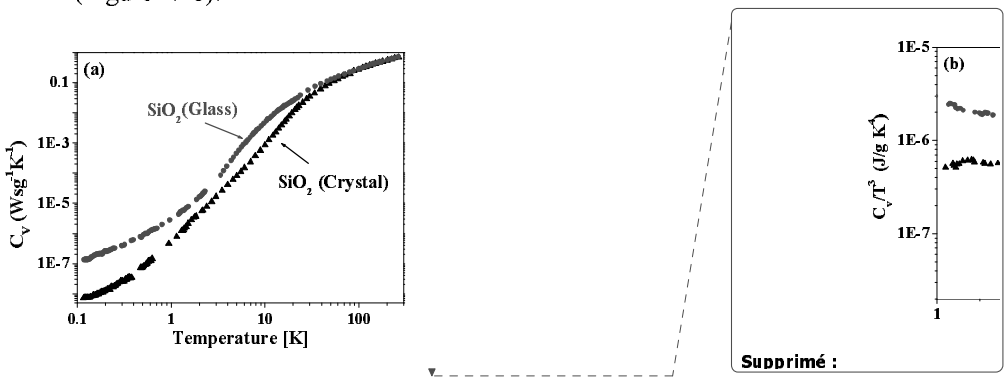

Figure 1.4: Specific heat C_V (a) and reduced specific heat C_V/T_3 (b) for vitreous silica and the corresponding crystal (Zeller and Pohl 1971)

Above 1 K the specific heat for vitreous silica and the corresponding crystal, exhibits further excess over that predicted by the Debye model and manifests itself in a broad peak in *reduced specific heat*[2] C_V/T^3 plot in the temperature range between 10 K

[2] We divide the specific heat for T^3 to emphasise the differences respect with to the crystalline systems that have a Debye behaviour ($C_V \propto T^3$)

and 40 K (Figure 1.4b). This peak indicates the presence of an excess of states in the low energy range with respect to the Debye model, which is explained, in the crystal, by the presence of more states in the lowest transverse branch, close to the first Brillouin zone. For the glass, the origin of the modes responsible for this excess is still under study.

The anomaly in the specific heat gives evidence for a departure from the Debye behaviour found at low temperatures in crystals. The excess in the specific heat reflects, for disordered systems, an excess in the vibrational density of states, $g(\omega)$. In fact C_V can be written in terms of $g(\omega)$ as:

$$C_P \approx C_V = 3Nk_B \int_0^{\omega_0} g(\omega) \left(\frac{\hbar\omega}{k_B T} \right)^2 \times \frac{e^{\left(\hbar\omega/k_B T\right)}}{\left[e^{\left(\hbar\omega/k_B T\right)} - 1 \right]^2} d\omega \qquad (1.1)$$

where N is the number density, ω_0 the highest vibrational frequency.

1.4.2 The Thermal Conductivity

The temperature dependence of the thermal conductivity of glassy materials is quite different from that of crystalline materials. The main difference between the glass and corresponding crystal is that the thermal conductivity of glasses is considerably lower than that of the crystal. Moreover, the spread of values of the conductivity from one glass to another, at a given temperature, is usually smaller than the spread in the case of crystalline materials. This subject has been of considerable interest for many years but while the mechanism of thermal conductivity in crystals is well understood, a completely satisfactory explanation of the corresponding processes in the glasses has not been found yet.

In the region below 1 K, complementary acoustic measurements have demonstrated that heat is carried by Debye phonons (sound waves) which are scattered by two-level systems (tunneling states) (Phillips 1981).

The least understood region is that between about 1 and 10 K, where the thermal conductivity varies only slightly with temperature, before increasing again above 10 K (Jones 1983) (Figure 1.5). In this region, the thermal conductivity shows a *plateau* for the glass and a maximum for the crystal.

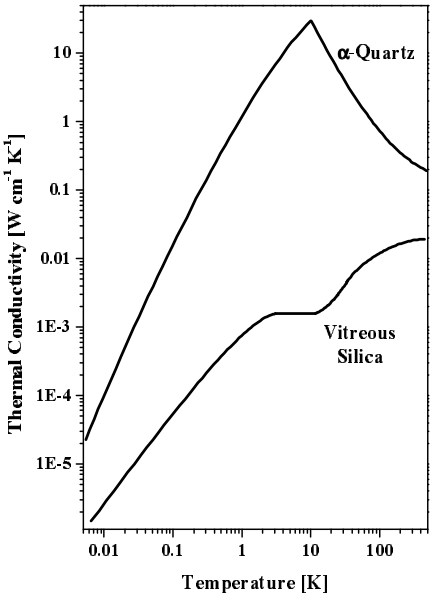

Figure 1.5: Thermal conductivity of vitreous silica in comparison with that of the corresponding crystal (Zeller and Pohl 1971)

1.4.3 Inelastic Scattering Experiments

At frequency below 10 meV, where the Debye's theory for crystals predicts a constant, a broad band is present in the plot $g(\omega)/\omega^2$ *versus* ω, in inelastic neutron and Raman scattering spectra, that seems to be an universal feature of disordered materials. The intensity of this maximum follows the Bose-Einstein law:

$$I \propto \frac{1}{e^{(\hbar\omega/k_B T)} - 1} \tag{1.2}$$

and for this reason it is called Boson Peak.

The Boson Peak can be related to an excess of the vibrational density of states (VDOS) (Fontana and Viliani 2002, 2003). A first hypothesis is that the excess of states is due to the localization of vibrations induced by the static disorder in the glass (Foret *et al.* 1996). A second hypothesis is that this excess is due to collective propagating modes (Ruocco *et al.* 2000).

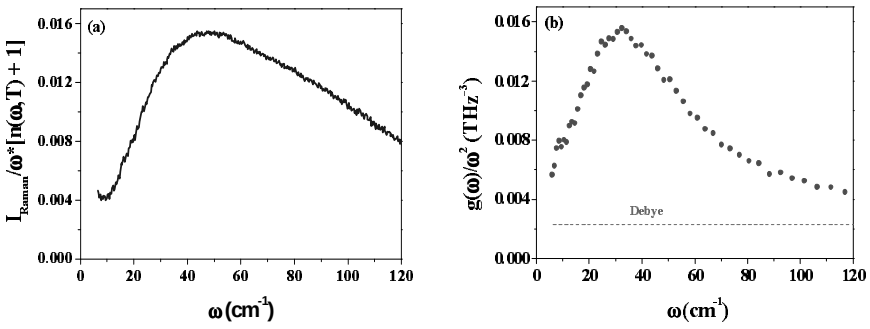

Figure 1.6: Inelastic Raman (a) and Neutron (b) scattering spectra for vitreous silica. The dashed line in the (b) is the Debye prediction

The excitations responsible of the Boson Peak will be shown in following Chapters, where the experiments performed and the results obtained are presented.

1.5 How can we study low energy behaviour in glasses?

The low energy vibrations responsible of the Boson Peak can be studied using three main scattering techniques: x-ray, neutron and light scattering. Each of these is characterised by a different energy and momentum transfer range:

- light scattering is a high-resolution probe (δE=24μeV-240 μeV) but is characterized by a small momentum transfer;

- inelastic x-ray scattering can probe a wide momentum (10^{-2} Å^{-1}-10^{2} Å^{-1}) and energy transfer range (10^{-3} meV-10^{3} meV) but with a worse resolution as compared to that of the light (δE = 2meV);
- inelastic neutron scattering is a good compromise between the two techniques because allows to investigate wide energy and momentum transfer ranges, with a resolution similar to that of the light scattering (δE = 15 μeV – 170 μeV).

In addition to their good resolution and wide momentum and energy transfer range, neutrons are useful in the condensed matter study because:

- their wavelengths are of the same order of interatomic distances in solids and liquids,
- their energy is of the same order as many excitations in condensed matter,
- they have no charge, thus, they can penetrate deeply into the target.

A more detailed explanation of these techniques will be given in Chapter 3.

REFERENCES

ANGELL A., *Nature* **393**, 521 (1998).

ELLIOT S.R., *Physics of amorphous materials*, Longman Scientific & Technical (1990).

FONTANA A. and VILIANI G., *Philos. Mag.* **B**, Volume 82, Number 2/6, Special issue: *8th International Workshop on Disordered Systems*, Andalo 2001 and references therein (2002).

FONTANA A. and VILIANI G., *Philos. Mag.* **B**, Special issue: *9th International Workshop on Disordered Systems*, Molveno-Andalo 2003 (in press).

FORET M., COURTENS E., VACHER R. and SUCK J.-B., *Phys. Rev. Lett.* **77**, 3831 (1996).

GOLDSTEIN M.J., *J. Chem. Phys.* **51,** 3728 (1969).

JONES D.P. and PHILLIPS W.A., *Phys. Rev.* **B 27**, 3891 (1983).

PHILLIPS W. A., *"Amorphous Solids: Low-Temperature properties"*, (Springer, Berlin, 1981).

RUOCCO G., SETTE F., DI LEONARDO R., MONACO G., SCAMPOLI M., SCOPINO T., and VILLANI G., *Phys. Rev. Lett.* **84**, 5788 (2000).

SHELBY J.E. *"Introduction to Glass Science and Technology"* (The Royal Society of Chemistry, Cambridge, England) (1997).

ZACHARIASEN W.H., *J. Am. Chem. Soc.* **54**, 3841 (1932).

ZELLER R.C. and POHL R.O. *Phys. Rev.* **B 4**, 2029 (1971).

2. General Structural Properties of Oxide Glassy Materials

The goal of the present chapter is to summarise the knowledge concerning the common characteristics between vitreous silica and vitreous germania.

L'objectif de ce chapitre est de résumer les connaissances qui concernent les caractéristiques communes entre les verres de SiO_2 et GeO_2.

2.1 The structure

Vitreous silica and vitreous germania are very similar strong glasses. Both exhibit a *Continuous Random Network* (CRN) structure based on covalent bonding. The idea was put forward in1932 by Zachariasen (Zachariasen 1932).

In Zachariasen's random network theory the nature of the bonding between the atoms in glass is the same as that in the corresponding crystal. In the case of vitreous silica and vitreous germania, the structural unit is a tetrahedron of four oxygen atoms bonded to a four-valent silicon (Si) or germanium (Ge) atom at the centre. Each oxygen atom is the common vertex of two such tetrahedra and therefore it is bonded to two Si or Ge atoms (see Figure 2.2). The principal difference between the crystal and the glass is that, in the latter, the structural units are connected together "randomly" to give a structure which lacks periodicity, extended symmetry and long-

range order, as illustrated schematically in two dimensions in Figure 2.1 and in three dimensions in Figure 2.2 (Wright 1994).

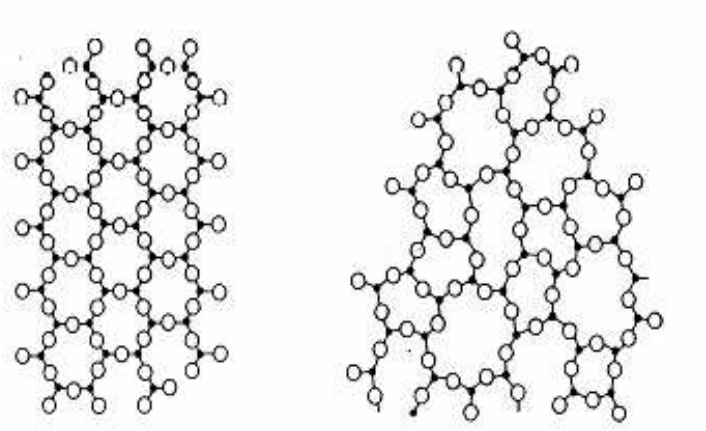

(a) (b)

Figure 2.1: Zachariasen's original random network diagram: SiO_4 tetrahedra are joined at common oxygen atoms, for a crystal (a) and for the disordered system (b).

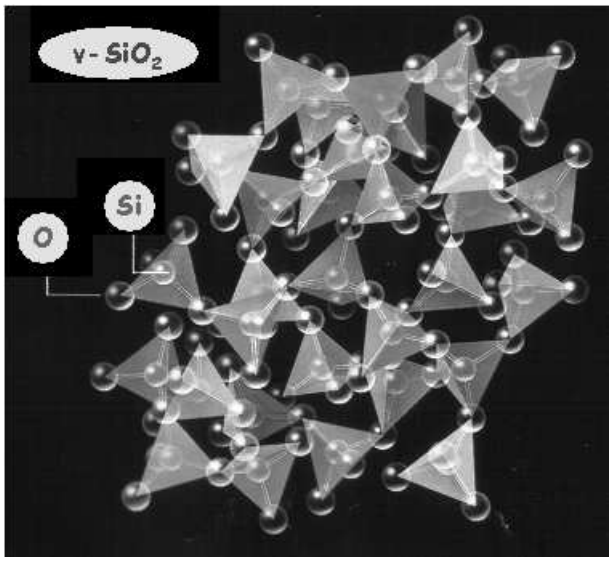

Figure 2.2: Three-dimensional structure for vitreous silica. The silicon atom is in the middle of the SiO_4 tetrahedron.

2.2 Static and Dynamic Structure Factor

When performing inelastic neutron scattering experiments, the Static Structure Factor for vitreous silica and vitreous germania can be determined and the same information can be obtained as from diffraction experiments. The procedure is explained later in more detail in Chapters 4 and 6.

Figure 2.3 reports the neutron static structure factors $S(\boldsymbol{Q})$ for vitreous silica (a) and vitreous germania (b) obtained from INS data taken at the IN4 spectrometer, using a incident wavelength of 1.53 Å which corresponds to an incident energy of about 35 meV. The dynamic range, which can be explored by using this set-up, is between 1 and 6.5 $Å^{-1}$.

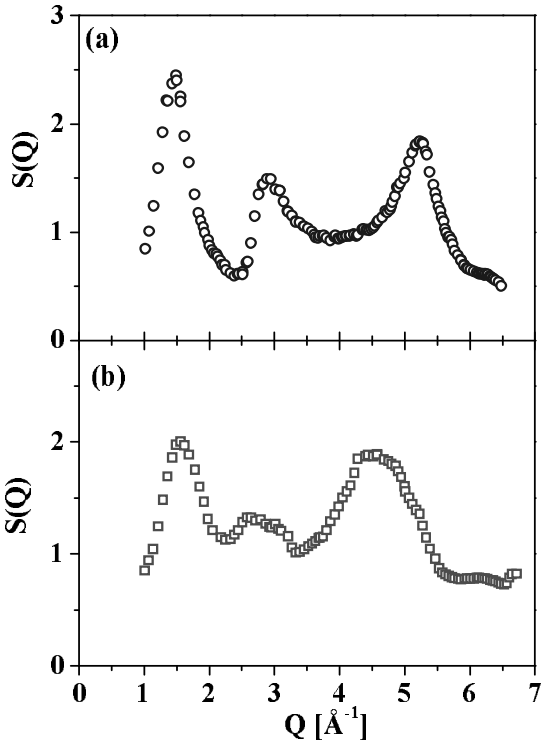

Figure 2.3: Static structure factors $S(\boldsymbol{Q})$ for vitreous silica (a) and vitreous germania (b), determined from neutron scattering data collected on IN4.

The structures observed in $S(\boldsymbol{Q})$ are due to the structural short range ordering of the glasses.

The origin of the main elastic feature, centred at about 1.5 $Å^{-1}$, has been assigned to the spatial correlations induced by the presence in the network of ring like structures (Elliott 1991), and is usually referred to as First Sharp Diffraction Peak (FSDP).

The *dynamic structure factor* $S(\boldsymbol{Q}, \omega=\omega_{BP})$ is represented in Figure 2.4. The frequency ω_{BP} is the Boson Peak energy maximum at about 4 meV for vitreous silica and 3.5 meV for vitreous germania.

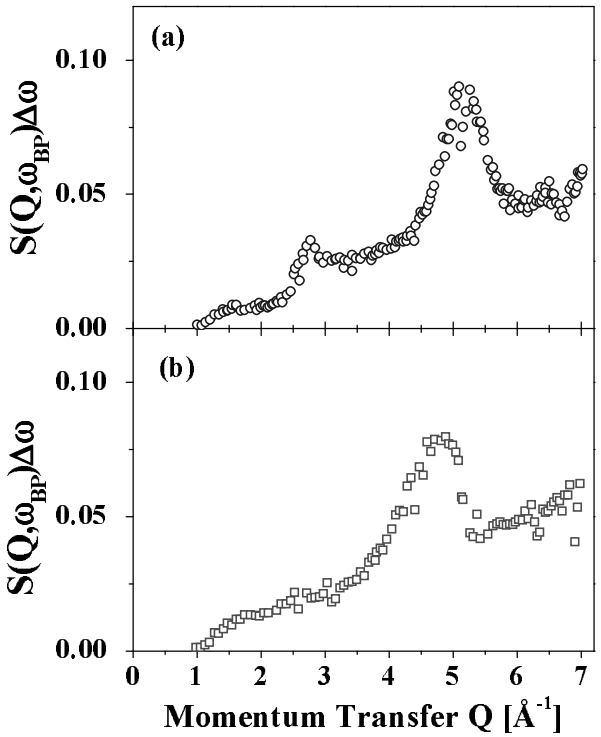

Figure 2.4: Dynamic structure factors $S(\boldsymbol{Q}, \omega=\omega_{BP})$ for vitreous silica (a) and vitreous germania (b), determined from inelastic neutron scattering data collected on IN4, following the procedure described in Chapters 4 and 6.

In $S(\boldsymbol{Q}, \omega=\omega_{BP})$ the inelastic contributions observed coincide approximately with the position of the peaks present in the static structure factors shown in Figure 2.3.

2.3 The vitreous silica structure

Among disordered systems, vitreous silica is a typical strong glass former and it has widely been studied both experimentally (by diffraction and inelastic scattering techniques) and numerically because it exhibits all the typical features of disordered materials.

The distance Si–O, O–O and Si–Si and the coordination number have been obtained by x-ray diffraction studies (Wright 1994) and they are shown in Table 2.1.

	Si-O	O-O	Si-Si
Maximum position	1.62±0.02 Å	2.6±0.03 Å	3.08±0.02 Å
Peak Width	0.07±0.03 Å	0.10±0.04 Å	0.10±0.04 Å
Coordination Number	4.1±0.4 Å	5.8±0.8 Å	3.4±0.4 Å

Table 2.1

It is possible to divide the vitreous SiO_2 structure in two "regions": the first one is defined by the distance between an atom of silicon and the four atoms of oxygen around it, characterising the tetrahedra which build the structure of the system. The bond angle α, O-Si-O, is 109.7°, a larger value in comparison with the standard tetrahedral angle (109.47°).

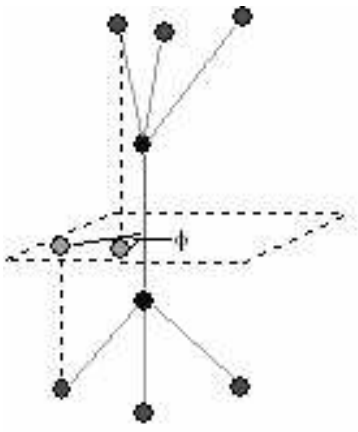

Figure 2.5: Definition of the angle ϕ in the three-dimensional network

The distance between the atoms of Silicon and between the structural units, characterise the second region. The bond angle β, Si-O-Si, is smaller than 180°, because the distance between the closer couple of Si atoms is smaller than twice the distance between the Si and the next-neighbouring oxygen atom.

We need to define a third angle, the torsion angle ϕ, which characterises the orientation between the SiO_4 tetrahedra connected in the network (Figure 2.5).

The most important characteristics of vitreous silica and vitreous germania are listed in Table 2.2.

	Glass Transition Temperature Tg [K]	**Melting Temperature T_m [K]**	**Refraction index n**	**Density ρ [g/cm^3]**	**Longitudinal Velocity v_L [m/s]**	**Transversal Velocity v_T [m/s]**
v-SiO_2	1473	2003	1.461	2.2	5970	3800
v-GeO_2	853	1378	1.663	3.65	3637	2233

Table 2.2

Vitreous silica and vitreous germania are very similar to each other, but the latter is characterised by a lower sound velocity than the first one. The lower sound velocity makes possible the direct observation by Inelastic Neutron Scattering experiments of the dispersion relation over the (Q, ω)-region intermediate between hydrodynamic and single particle dynamics.

REFERENCES

ELLIOTT S.R., *Phys.Rev.Lett.* **67,** 711 (1991).

WRIGHT A.C., *Journal of Non-Cryst. Solids* **179**, 84 (1994)

ZACHARIASEN W. H. *J. Am. Chem. Soc.* **54**, 3841 (1932).

3. Experimental procedures

The properties of condensed matter can be investigated using several techniques. Usually, the application of different techniques on the same sample is useful to obtain complementary information in order to have a complete picture of the problem under study.
In this section, Neutron Spectroscopy is presented and some information about Raman Spectroscopy are given. In the present work, both techniques have been combined to investigate the dynamics of vitreous silica and vitreous germania.

Les propriétés de la matière condensée peuvent être étudiées en utilisant plusieurs techniques. Habituellement, l'application de différentes techniques sur le même échantillon est utile pour obtenir des informations complémentaires afin d'avoir une image complète du problème étudié.
Dans cette section, la spectroscopie neutronique est présentée et quelques informations sur la spectroscopie Raman sont fournies. Dans ce travail de thèse, les deux techniques ont été combinées pour étudier la dynamique de l'oxyde de silice et de l'oxyde de germanium vitreux.

3.1 Neutron Spectroscopy

3.1.1 Introduction

The neutron is a particularly good probe for studying both the structure and the dynamics of condensed matter. To examine the structure of matter, a scattering process in which the radiation has a wavelength comparable in magnitude with the spacing between atoms is needed. A neutron with a mass m and a velocity v has an associated De Broglie wavelength λ and a wave-vector k such as:

$$m\mathrm{v} = \hbar k = \frac{h}{\lambda} \tag{3.1}$$

For thermal neutron the wavelength is of the order of Å, and is comparable to atomic distances. Additionally, thermal neutrons have kinetic energies E (~25 meV) comparable to typical excitations (fluctuations in time) in condensed matter:

$$E = k_B T = \frac{m\mathrm{v}^2}{2} = \frac{\hbar^2 |\boldsymbol{k}|^2}{2m} \tag{3.2}$$

where k_B and $\hbar$ are the Boltzman and the Plank constants, respectively, $\boldsymbol{k}$ is the wave vector, m the mass and v the velocity. Thermal neutrons correspond to a temperature of 300 K, an energy of 25 meV and a wavelength of 1.8 Å (v = 2200 m/s). In an inelastic scattering process, one can readily observe that the neutrons loose or gain energy in the same order as their kinetic energy. This means that using inelastic neutron scattering, we can obtain complete information on the vibrations of atoms or molecules, diffusion, re-orientations and relaxation processes.

Besides the possibility of inelastic scattering, neutrons have other advantages:

- Neutrons interact with the atomic nucleus. The amplitude of the neutron wave scattered by an individual nucleus depends on the nature of the nucleus and so varies between different isotopes of the nucleus and between the two spin states of the

neutron-nucleus system. Therefore neutrons can easily distinguish atoms which are comparable in atomic number. The variation of the scattering amplitude from isotopes of the same atomic species gives rise to a process know as incoherent scattering, which is characterised by the absence of interference between the waves scattered by different atoms. The cross-section consists, therefore, of a coherent part, with interference occurring between the scattered waves, and an incoherent part. Their magnitude can be altered by changing the isotopic composition of the sample: each part provides different information and, using polarisation analysis, can be measured separately.

- Neutrons, as neutral particles, interact rather weakly with matter, so they can penetrate deeply into the sample, so that generally bulk properties can be studied.
- Finally, neutrons carry a magnetic moment and can be polarised, so they are particularly suited to investigate magnetic structures and magnetic excitations.

In Table 3.1 the fundamental properties of the neutron are reported.

Mass	m_n = 1.008664924 u = $1.675 \cdot 10^{-27}$ kg
Spin	s = ½
magnetic moment	μ_n =1.91304275(45) μ_N
	(μ_N=$5.051 \cdot 10^{-27}$ J T^{-1})
electric charge:mean square radius	r_n =0.11±0.02 fm
electric dipole moment	d_n =(-0.7±0.4) $\cdot 10^{-21}$ e cm
Polarizability	α =(1.2±1.0) $\cdot 10^{-3}$ fm^3
β decay of a free neutron	$n \rightarrow p^+ + e^- + \nu$
life time	τ = 888 ± 3 s
half life	$T_{1/2} = \tau \ln 2$ = 615 ± 3 s
Charge	0

Table 3.1: Properties of the neutron (Hercules book 1993)

Beside, in Table 3.2, we report some important and useful relations between the wavelength, the energy, the velocity, the wave vector and the temperature of neutron.

$$\lambda = 6.283\frac{1}{k} = 3.956\frac{1}{\mathrm{v}} = 9.045\frac{1}{\sqrt{E}} = 30.81\frac{1}{\sqrt{T}}$$

$$E = 0.0861T = 5.227\mathrm{v}^2 = \frac{81.81}{\lambda^2} = 2.072k^2$$

Table 3.2: Relations between the wavelength λ in Å, wave vector k in $Å^{-1}$, velocity v in km/s, energy E in meV and temperature T in K for the neutron

For the production of neutron large-scale facilities are required as reactors or spallation sources. All experiments explained in the following chapters have been carried out at the Institut Laue-Langevin (ILL) in Grenoble.

ILL use the fission process where a neutron hit a Uranium 235 atom, which is divided in two light nuclei and two or more neutrons are created. It is a High Flux Reactor used for research. It is a continuous source having a compact core to produce the highest possible flux (of about 56 MW).

3.1.2 Theoretical aspects

The microscopic dynamics is described in terms of two-particle space- and time-dependent correlation functions. Spectroscopic investigations probe the atomic motions in the space of the Fourier-conjugated variables $\boldsymbol{Q}$ and ω. The Fourier components are plane-wave-like excitations with wave vector $\boldsymbol{Q}$ and frequency ω.

In an idealised neutron scattering experiment a neutron beam with flux Φ, wave vector $\boldsymbol{k}$ and energy E (defined by the formula 3.2) impinges on the target.

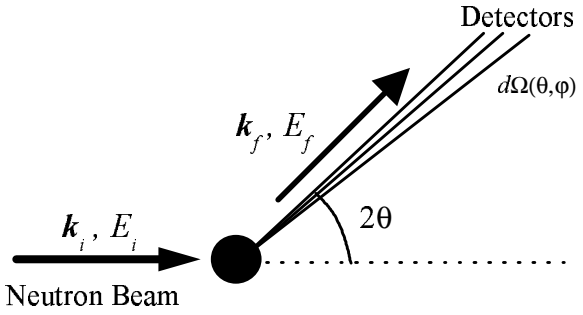

Figure 3.1: The *ideal* scattering experiment

The physics to be observed is described by the momentum $\hbar\boldsymbol{Q}$ and the energy $\hbar\omega$ transfer from the probe to the sample, defined by the conservation law as:

$$\hbar\boldsymbol{Q} = \hbar\boldsymbol{k}_i - \hbar\boldsymbol{k}_f \tag{3.3}$$

$$\hbar\omega = E_i - E_f = \frac{\hbar^2 k_i^2}{2m} - \frac{\hbar^2 k_f^2}{2m} \tag{3.4}$$

where $\boldsymbol{k}_i$ and $\boldsymbol{k}_f$ are the incident and scattered wave vector, respectively (see Figure 3.1). The relevant quantities are, therefore, the measured scattering intensity, the scattering cross-section and the dynamical and static structure function.

3.1.3 The double differential cross section

The number of scattered neutrons is measured by the double differential cross section, which can be written as:

$$\frac{\partial^2\sigma}{\partial\Omega\partial\omega} = N\frac{k_f}{k_i}\left\langle\overline{b^2}\right\rangle S(\boldsymbol{Q},\omega) \tag{3.5}$$

where N is the total number of particles in the target, $\left\langle \overline{b^2} \right\rangle = \frac{1}{N}\sum_{i=1}^{N} \overline{b_i^2}$ and $\overline{b_i}$ is the neutron scattering length of atom i ($\overline{b_i} = \overline{b_i}^*$). The so defined scattering function $S(\boldsymbol{Q},\omega)$ takes the name of *dynamical structure factor* and can be written in the form:

$$S(\boldsymbol{Q},\omega) = \frac{1}{2\pi\hbar N\left\langle \overline{b^2} \right\rangle}\int_{-\infty}^{+\infty} \mathrm{d}t\, \mathrm{e}^{-i\omega t} \sum_{i=1}^{N}\sum_{j=1}^{N} \overline{b_i b_j} \left\langle \mathrm{e}^{-i\boldsymbol{Q}\cdot\boldsymbol{R}_i(0)}\, \mathrm{e}^{i\boldsymbol{Q}\cdot\boldsymbol{R}_j(t)} \right\rangle \tag{3.6}$$

where $\boldsymbol{R}_i(t)$ is the position of the atom i in space and time t.

For a defined element, the average $\overline{b_i}$ of the scattering length b_i over all isotopes and spin is called *coherent scattering length* while the mean-square deviation of the scattering lengths from their average values is known as the *incoherent scattering length*.

$$\begin{aligned} b_i^{coh} &= \overline{b_i} \\ b_i^{inc} &= \sqrt{\overline{b_i^2} - \overline{b_i}^2} \end{aligned} \tag{3.7}$$

which are related to the coherent and incoherent cross section by the formula:

$$\begin{aligned} \sigma_{\mathrm{coh}} &= 4\pi\left(\overline{b_i}\right)^2 \\ \sigma_{\mathrm{inc}} &= 4\pi\left[\overline{b_i^2} - \overline{b_i}^2\right] \end{aligned} \tag{3.8}$$

The scattering function $S(\boldsymbol{Q},\omega)$ contains all information about the structure and the dynamics of the material. It can be divided into two contributions:

- the incoherent scattering $S_{inc}(\boldsymbol{Q}, \omega)$, which yields information on the self-correlation function, i.e. the probability to find a particle at r at time t, if the same particle was at $r = 0$ at time $t = 0$
- the coherent scattering $S_{coh}(\boldsymbol{Q}, \omega)$, which contains information about the correlations in time and space between different atoms. It is given by Fourier-transform of the sum of the self and the pair correlation function. The pair

correlation function gives the probability to find a particle at r at t, if another particle has been at $r = 0$ at $t = 0$.

The self correlation term, $i = j$, is as well included in the coherent scattering.

To see how $S(\boldsymbol{Q},\omega)$ is related to the dynamics properties of our sample we can perform the time and space Fourier transform of $S(\boldsymbol{Q}, \omega)$ to define the real space van Hove correlation function:

$$G(\boldsymbol{R}, t) = \frac{1}{2\pi^3} \int_{-\infty}^{+\infty} e^{-i(\boldsymbol{Q}\cdot\boldsymbol{R}-\omega t)} S(\boldsymbol{Q}, \omega) d\boldsymbol{Q} d\omega \tag{3.9}$$

Evaluating the integral the physical meaning of $G(\boldsymbol{R},t)$ is clearer:

$$G(\boldsymbol{R}, t) = \frac{1}{N} \left\langle \int d\boldsymbol{R}' \rho(\boldsymbol{R}', 0) \rho(\boldsymbol{R}' + \boldsymbol{R}), t \right\rangle \tag{3.10}$$

where $\rho(\boldsymbol{R}', t)$ is the microscopic particle density operator.

The van Hove correlation function describes the correlation between the particle density at any place $\boldsymbol{R}'$ at any time t=0, and the particle density at $\boldsymbol{R}'+\boldsymbol{R}$ at some time t.

An important limiting case is $G(\boldsymbol{R}, t=0)$, which represent a static picture, i.e. a snapshot of the structure. This is obtained by integrating $S(\boldsymbol{Q},\omega)$ over all frequencies:

$$G(\boldsymbol{R},0) \leftrightarrow \int S(\boldsymbol{Q},\omega) d\omega = S(\boldsymbol{Q}) \tag{3.11}$$

to obtain the *static structure factor*, $S(\boldsymbol{Q})$, which will be discussed further in the next section.

3.1.4 Coherent and incoherent scattering

The scattering function $S(\mathbf{Q}, \omega)$ can also be expressed in terms of the time-Fourier transform $F(\boldsymbol{Q}, t)$:

$$S(\boldsymbol{Q},\omega)=\frac{1}{2\pi}\int_{-\infty}^{+\infty}\mathrm{d}t\,\mathrm{e}^{-i\omega t}\,F(\boldsymbol{Q},t) \tag{3.12}$$

where $F(\boldsymbol{Q}, t)$ is *intermediate scattering function*:

$$\mathrm{F}(\boldsymbol{Q},t)=\frac{1}{\mathrm{N}}\sum_{\mathrm{i,j=0}}^{\mathrm{N}}\left\langle e^{-i\boldsymbol{Q}\cdot\boldsymbol{R}_i(0)}\,e^{i\boldsymbol{Q}\cdot\boldsymbol{R}_j(t)}\right\rangle \tag{3.13}$$

The incoherent and coherent scattering laws can be written as:

$$\begin{aligned}S_{inc}(\boldsymbol{Q},\omega)&=\frac{1}{2\pi}\int_{-\infty}^{\infty}F_{inc}(\boldsymbol{Q},t)\,\mathrm{e}^{-i\omega t}\,\mathrm{d}t=\int_{-\infty}^{+\infty}\mathrm{e}^{-i\omega t}\sum_{i=1}^{N}\left\langle \mathrm{e}^{-i\boldsymbol{Q}\cdot\boldsymbol{R}_i(0)}\,\mathrm{e}^{i\boldsymbol{Q}\cdot\boldsymbol{R}_i(t)}\right\rangle \mathrm{d}t\\ S_{coh}(\boldsymbol{Q},\omega)&=\frac{1}{2\pi}\int_{-\infty}^{\infty}F_{coh}(\boldsymbol{Q},t)\,\mathrm{e}^{-i\omega t}\,\mathrm{d}t=\int_{-\infty}^{+\infty}\mathrm{e}^{-i\omega t}\sum_{\mathrm{i,j=1}}^{\mathrm{N}}\left\langle \mathrm{e}^{-i\boldsymbol{Q}\cdot\boldsymbol{R}_i(0)}\,\mathrm{e}^{i\boldsymbol{Q}\cdot\boldsymbol{R}_j(t)}\right\rangle \mathrm{d}t\end{aligned} \tag{3.14}$$

The difference between coherent and incoherent scattering represents a particular feature of neutron scattering.

In coherent scattering the scattered amplitudes are summed up and then squared while in incoherent scattering the intensities (amplitudes squared) from individual particles are summed up. Therefore coherent scattering contains interference between different particles, as just said in the previous section. This interference is absent in incoherent scattering. But interference may occur if one incoherent scattering particle is distributed over several positions with a certain probability.

Taking the intermediate scattering function at $t = 0$, one obtains the integral $S(\boldsymbol{Q})$ of $S(\boldsymbol{Q},\omega)$ over all frequencies:

$$S(\boldsymbol{Q})=\int_{-\infty}^{+\infty}\mathrm{d}\omega\,S(\boldsymbol{Q},\omega)\approx\frac{1}{N}\sum_{\mathrm{i,j=1}}^{\mathrm{N}}\left\langle \mathrm{e}^{-i\boldsymbol{Q}\cdot\boldsymbol{R}_i}\mathrm{e}^{i\boldsymbol{Q}\cdot\boldsymbol{R}_j}\right\rangle \tag{3.15}$$

In this way, one takes the correlations between different atoms at the same time. To see the fundamental important of this result, one can consider the consequences for the

coherent and incoherent scattering. For the coherent case, one has a snapshot of the instantaneous spatial atomic correlation, averaged over long times, so one gets information about the structure by measuring the integral over all possible energy transfer. If one has only coherent scattering, $S(\boldsymbol{Q})$ shows long-range density and concentration fluctuations at small momentum transfer $\boldsymbol{Q}$. At higher $\boldsymbol{Q}$, there is often a first diffraction peak, followed by oscillations around 1 which die out at high $\boldsymbol{Q}$. For the incoherent case, the correlation between different atoms is not visible, so $S(\boldsymbol{Q}) = 1$.

Now we denote by $R_{j\boldsymbol{Q}}(t)$ the component of the atomic position vector parallel to the momentum vector $\boldsymbol{Q}$. If $R_{j\boldsymbol{Q}}(t)$- $R_{j\boldsymbol{Q}}(0)$ has a gaussian distribution for different choices of the zero point in time, one can make use of the Bloch identity:

$$\left\langle e^{-i\boldsymbol{Q}\cdot\boldsymbol{R}_j(0)} e^{i\boldsymbol{Q}\cdot\boldsymbol{R}_j(t)} \right\rangle = e^{-\left\langle Q^2 \left\langle \left(R_{j\boldsymbol{Q}}(t)-R_{j\boldsymbol{Q}}(0)\right)^2 \right\rangle \right\rangle / 2} \tag{3.16}$$

One can use the Bloch identity to formulate an approximation to the incoherent scattering law, the Gaussian approximation for the intermediate incoherent scattering function:

$$F(\boldsymbol{Q},t) = e^{-Q^2\gamma(t)} \tag{3.17}$$

where $\gamma(t)$ is an average time-dependent mean square displacement for all atoms in the sample[1]. If there are only vibrations and in the framework of the *one-phonon approximation*, $\gamma(t)$ is related to the vibrational density of states $g(\omega)$:

$$\gamma(t) = \frac{k_B T}{M} \int_0^{\omega_{max}} d\omega \frac{g(\omega)}{\omega^2} (1 - \cos\omega t) \tag{3.18}$$

[1] This approximation is often a useful simplification even if several reason exist for its failure. One is the deviation of the distribution of the time-dependent atomic displacement from a gaussian. For example an atom jumping between two potential minima: the displacement distribution function has two maxima, obviously different from a gaussian. Moreover, even if all atoms have a gaussian distribution of their displacements, the gaussian approximation requires the same width of the distribution for each atom in each direction.

The intermediate scattering function can be expressed in terms of $G(\boldsymbol{R},t)$ as following:

$$F(\boldsymbol{Q},t)=\int d\boldsymbol{R}\, e^{i\boldsymbol{Q}\cdot\boldsymbol{R}}[G(\boldsymbol{R},t)-\rho] \tag{3.19}$$

3.1.5 The dynamic range Q-ω

In an experiment one observes very generally a signal as a function of $\boldsymbol{Q}$ and ω. This could be a peak in measured intensity *versus* energy transfer $\hbar\omega$. Such signals contain physical information from the sample blurred by the limited resolution of the instrument. The particular type of experiment will dictate the portions of ($\boldsymbol{Q}$, ω) space which are probed.

The dynamic range available can be calculated by using the formula (3.3) as:

$$Q^2 = k_i^2 + k_f^2 - 2k_i k_f \cos 2\theta \tag{3.20}$$

where 2θ is the angle between the wave vectors $\boldsymbol{k}_i$ and $\boldsymbol{k}_f$ and can be represented in the Figure 3.2. In the picture, each red line corresponds to a different angle.

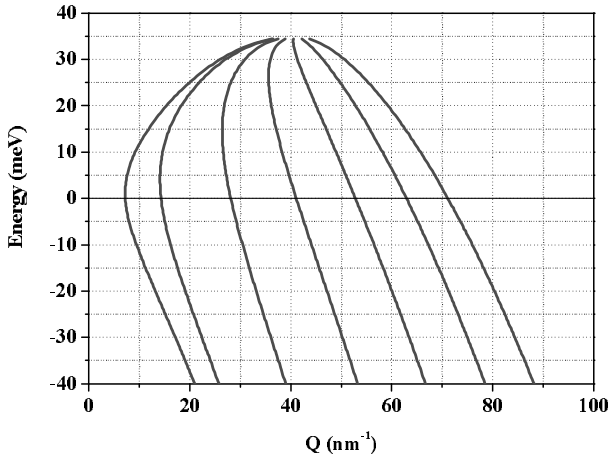

Figure 3.2: Dynamic range for a time-of-flight instrument, using a incident wavevector k_i of 41 nm^{-1}

3.1.6 The neutron Time-Of-Flight technique

Time-Of-Flight (TOF) is a general method for finding the energy of a neutron by measuring the time that it takes to fly between two points. High-energy neutrons fly fast whilst low-energy or "cold" neutrons are much slower.

In the primary part of the spectrometer, i.e. before the sample, we wish to select a pulse of neutrons with a fixed speed from a continuous beam of neutrons with mixed speeds.

At the sample some neutrons gain or loose energy and are scattered with new velocities in many directions. We know the time at which the neutrons hit the sample and we wish to know the time of their arrival at the detectors. Counting the number of neutrons arriving within different time periods, we obtain a histogram of the number of neutrons arriving at the detectors within a given period at different times: the time-of-flight spectrum. Time focussing forces all neutrons that have transferred the same amount of energy to the sample to arrive at the detectors together, regardless of their incident and final energies. Knowing that all neutrons hit the sample with equal velocity at the same time, we can calculate how the energy was absorbed or released by various atomic motions in the sample.

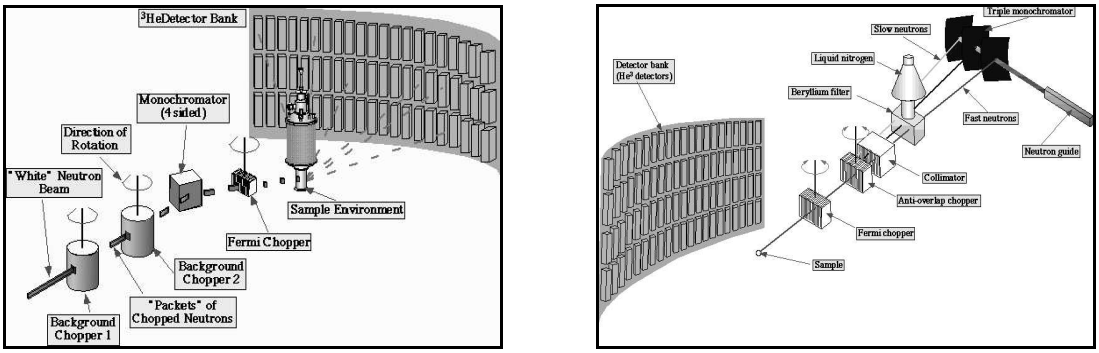

Figure 3.3: Experimental set-up of TOF spectrometers IN4 and IN6 at ILL

Two schematically examples of TOF spectrometer present at ILL are represented in Figure 3.3.

The time-of-flight spectra measured at various angles are further treated in order to obtain the scattering function $S(\boldsymbol{Q},\omega)$. For a detailed description of TOF technique see Bacon's book (Bacon 1975).

Time-of-flight spectrometers may be divided into two classes (Figure 3.4):

Direct geometry spectrometers in which the incident energy, E_i, is defined by a device such as a crystal or a chopper and the final energy E_f, is determined by time of flight.

Indirect geometry spectrometers in which the sample is illuminated by a white beam and E_f is defined by a crystal or a filter and E_i is determined by time of flight.

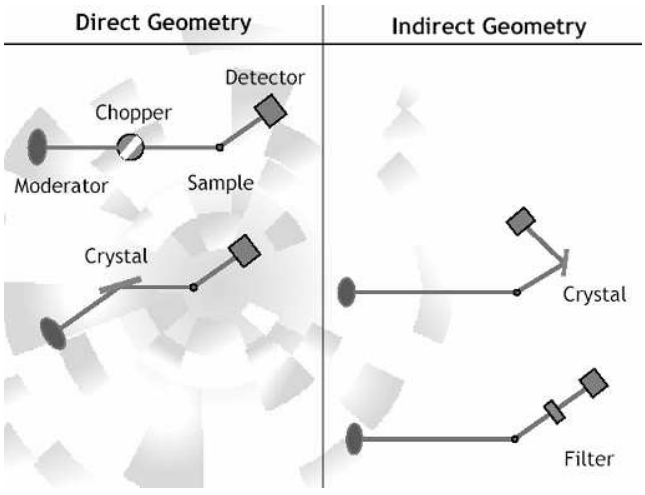

Figure 3.4: Schematic drawing of direct and indirect geometry

3.1.7 The neutron Three-Axis technique

The three-axis spectrometer (TAS) was invented by Brockhouse in 1962. This type of instrument is common in reactor centre and is one of the most important instruments for

the measurement of neutron scattering from single crystals. It is designed to study the collective motion of the atoms in the sample (phonons) and their magnetic excitations (magnons). Its name refers to the three axes of the monochromator, sample and analyzer crystal, the orientation of which can be varied independently. It gives us information about the excitation spectrum at a given point $\boldsymbol{Q}$ in reciprocal space. At each point of the scan the triangle ($\boldsymbol{k}_i$, $\boldsymbol{k}_f$, $\boldsymbol{Q}$) is modified so that $\boldsymbol{k}_i$ and $\boldsymbol{k}_f$ will close at the same momentum transfer **Q**, but the length of one of the wave vectors is varied to provide for the required energy transfer.

It's clear that in addition to the $\boldsymbol{k}_i$ and $\boldsymbol{k}_f$ modification, also all the angles of the scattering triangle will change.

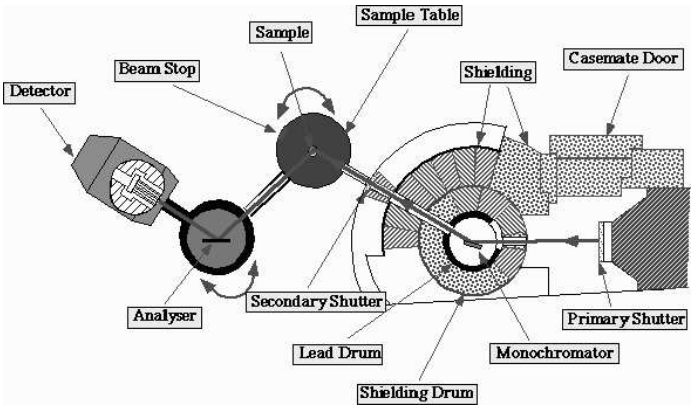

Figure3.5: Schematic overview of TAS spectrometer IN1 at ILL

This measuring technique allows the determination of the energy transfer between the neutrons and the sample, as a function of the scattering angle, which itself is related to the momentum transfer by the formula (3.10). The neutron scattering from single crystals is limited by selection rules, which connect the scattering in a particular direction (momentum transfer $\boldsymbol{Q}$), to a certain change in energy ω. The measured intensity as a function of $\boldsymbol{Q}$ and ω is mainly determined by two factors: the resolution of the instrument, and the dynamic scattering function $S(\boldsymbol{Q}, \omega)$. Harmonic excitations such

as phonons give a sharply peaked scattering function, and $S(\boldsymbol{Q}, \omega)$ describes the phonon or magnon dispersion curve. More complex scattering functions are associated with the anharmonic phenomena, which manifest themselves, for example, near phase transformations. In parallel with the experiment, $S(\boldsymbol{Q}, \omega)$ can be calculated theoretically, normally as an ω-spectrum for a constant value of $\boldsymbol{Q}$. Therefore, the ability to perform constant $\boldsymbol{Q}$ scans is one of the outstanding advantages of a three-axis spectrometer. But generally any scan in $\boldsymbol{Q}$-ω space can be performed.
ILL supports several Three-Axis instruments (IN1, IN3, IN8, IN20, IN14, IN12). In this work, the results obtained by measurement performed on IN1, IN8 and IN3 will be shown in the Chapter 5.

3.1.8 The TOF and TAS choice

TOF is more efficient whenever one needs to explore large sections of $(\boldsymbol{Q}, \omega)$ space, e.g. when:

- one does not know where the interesting physics lies
- one knows that the interesting physics is diffuse.

TAS is more efficient whenever:

- one knows what one wants to measure and where to find it
- one knows that it is well localised in $(\boldsymbol{Q}, \omega)$ space

In the Chapter 5 we will show that carrying out experiments using both TOF and TAS spectrometers, a wide range $(\boldsymbol{Q}, \omega)$ can be explored because these instruments operated over complementary kinematics ranges with different energy resolutions.

3.2 Raman Spectroscopy

In inelastic light scattering, photons couple to excitations in matter (phonon, electronic excitations or magnetic excitations) and scatter inelastically.

The part of the inelastic spectrum associated with scattering from optical phonons, molecular modes and magnetic and electronic interactions, is traditionally called Raman scattering.

The typical frequency of the excitations studied is of the order on 0.1-100 THz, i.e. 1-3500 cm^{-1}. Inelastic scattering arising from the interaction with acoustic phonons is called Brillouin light scattering, BLS, and the frequency is of the order of the 10 GHz.

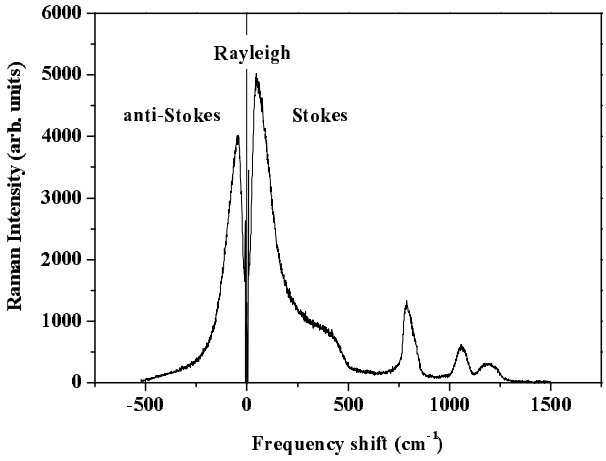

Figure 3.6: Experimental light scattering spectrum for vitreous silica

The inelastic light can create as well as annihilate excitations, hence two inelastic branches are observed: Stokes and anti-Stokes. Elastically scattered light is commonly called Rayleigh scattering. A experimental light scattering spectrum for Stokes, anti-Stokes and Rayleigh corresponding process is represented in Figure 3.6.

3.2.1 General Raman Theory

Raman scattering can be described through the interaction of the incident radiation with an initial energy state of the system, E_i causing a transition to a final state E_f. The scattering is dependent on the geometry of the excitation through the normal co-ordinate derivative of the polarisability tensor. If there is no change in the polarisability through a vibrational motion, that particular mode will not be Raman active. Thus the polarisation of the incident and scattered light will provide selection rules for Raman scattering. Moreover, the temperature dependence of the Raman scattering is introduced through the Bose-Einstein factor. Taking the ratio of the Stokes to the anti-Stokes scattering intensities, the temperature of the sample can be determined in the actual experimental situation. The temperature dependence of Raman scattering for glassy systems has been mentioned in Chapter 1 when the anomalous features of the BP and the QES are treated. Both effects are strictly connected to the overall, vibrational and relaxational, density of states. It is then clear that a crucial information for understand completely their nature is the knowledge of the "true" density of states of the material.

In general one can experimentally deduce the density of states, $g(\omega)$, from Raman, neutron and specific heat measurements (Sokolov *et al.* 1993) , but all these techniques have nevertheless some drawbacks. In the case of Raman scattering, the direct evaluation of the vibrational density of states from experimental spectra is not straightforward because of the presence of a coupling spectral function, i.e. the *Raman coupling function* $C(\omega)$, which measures the efficiency of the coupling between the incident photon to the vibrations of the system.

The first order Raman scattering intensity (Stokes) I_R for harmonic excitations at a given temperature T, is connected to the vibrational density of states (Galenneer and Sen 1978, Price and Carpenter) by:

$$I_R(\Omega_0+\omega)=\frac{(\Omega_0+\omega)^4}{2\pi c^3}\hbar V E_0^2\,\frac{n(\omega,T)+1}{\omega}\sum_{p,b}C_b^p(\Omega_0,\omega)g_b(\omega) \tag{3.21}$$

where Ω_0 is the frequency of the incident light, ω is the Raman shift, E_0 is the incident field amplitude, V is the scattering volume, $n(\omega,T)$ is the Bose-Einstein population factor, b indicates the vibrational bands, p the polarization of light, $g_b(\omega)$ is the corresponding density of states and

$$C_b^p(\Omega_0,\omega)=\left|\sum_l P_l^p u_l^b(\omega)\right|^2 \tag{3.22}$$

$P_l^p u_l^b(\omega)$ is the first order term of the expansion of the electronic polarizability tensor as a function of the displacement eigenvectors $u_l^b(\omega)$. In the low frequency acoustic region we assume $C_b^p(\Omega_0,\omega)\equiv C_{ac}^p(\Omega_0,\omega)\equiv C(\omega)$, the *probe-excitation coupling function*, and $g_b(\omega)\equiv g(\omega)$, the *density of states*.

When one assumes the disordered solid to be constitutively isotropic, the polarizability tensor is found to contain only two independent quantities: P_{VV} and P_{HV}. It is these two quantities which are probed in the usual 90° scattering configuration. The polarization of the experiment p is VV when the incident and the scattered electric fields E are parallel, and is HV when they are perpendicular. When not indicated we report to comparing Raman and neutron scattering measurements the quantity P_{HV}.

The first order Raman scattering intensity I_R of the formula (3.21) can be simplified as:

$$I_R(\omega,T)\propto\frac{n(\omega,T)+1}{\omega}g(\omega)C(\omega) \tag{3.23}$$

Different theoretical models have been so far proposed for the frequency dependence of $C(\omega)$ under different approximations (Nemanich and Solin 1977, Winterling 1975, Martin and Galeener 1981, Alexander and Orbach 1982, Duval *et al.* 1987, Fontana *et al.* 1997, Dell'Anna *et al.* 1998). The direct comparison between Raman scattering and

inelastic neutron scattering measurements is the most faithful procedure to evaluate $C(\omega)$ to assess the validity of the proposed models and it will be the topics of Chapter 7.

REFERENCES

ALEXANDER S. and ORBACH R., *J. Phys. (Paris) Lett.* **43**, L625 (1982).

BEE M., "*Quasielastic Neutron Scattering*" (Adam Hilger, Bristol and Philadelphia) (1988).

BACON G. E., "*Neutron Diffraction*" (Oxford Univ. Press, London) (1975).

BUCHENAU U. Lecture Notes: "*Neutron and X-ray scattering from glasses*".

DELL'ANNA R., RUOCCO G., SAMPOLI M. and G. VILIANI, *Phys. Rev. Lett.* **80**, 1236 (1998).

DORNER B., Lecture Notes for the Introductory Course 30-31 August 1999, in connection with ECNS'99, 1-4 September 1999.

DUVAL E., MARIOTTO G., MONTAGNA M., PILLA O., VILIANI G. and BARLAND M., *Europhys. Lett.* **3**, 333 (1987).

FONTANA A., ROSSI F., CARINI G., D'ANGELO G., TRIPODO G. and BARTOLOTTA A., *Phys. Rev. Lett.* **78**, 1078 (1997).

GALENNEER F.L. and SEN P.L., *Phys. Rev.* **B 17**, 1928 (1978).

HERCULES BOOK: BARUCHEL J., HODEAU J.L., LEHMANN M.S., REGNARD J.R. and SCHLENKER C., "*Neutron and Synchrotron Radiation for Condensed Matter*", Vol. **1** (EDP SCIENCES-SPRINGER-VERLAG) (1993).

MARTIN R.M. and GALEENER F.L., *Phys. Rev.* **B 23**, 3071 (1981).

MATIC A. "*Glassy Materials: Fundamental aspects and ionic conduction*" PhD Thesis, Göteborg University, Sweden (1999).

NEMANICH R.J. and SOLIN S.A., *Solid State Commun.* **23**, 417 (1977).

PRICE D.L. and CARPENTER J.M., *J. Non-Cryst. Solids*, **92**,153 (1987).

SCHOBER H. Lecture Notes: "*Neutron spectroscopy: an ideal tool for the material scientist*".

SOKOLOV A. P., KISLINK, A., QUITMANN, D. and DUVAL E., *Phys. Rev.* **B**, **48**, 7692 (1993).

WILLIS B.T.M "*Chemical Applications of thermal neutron scattering*", (Oxford University Press-1973)

WINTERLING G., *Phys. Rev.* **B 12**, 2432 (1975).

4. Neutron and Raman Data Analysis

A new data treatment for Inelastic Neutron Scattering data is shown in this chapter. The most important steps of the neutron analysis to obtain the vibrational density of states and the dynamical structure factor are explained for the cases of vitreous silica and vitreous germania. For the Raman analysis the presence of an underlying weak background of luminescence is taken into account to obtain the exact determination of its spectral shape and temperature dependence.

Dans ce chapitre nous décrivons une nouvelle analyse pour les données inélastiques de neutrons. Nous expliquons les étapes les plus importantes de l'analyse de ces données pour obtenir la densité des états de vibration et le facteur dynamique de structure pour les cas des oxydes de silice et de germanium vitreux. Dans l'analyse Raman la présence d'un faible fond de luminescence est prise en considération afin d'obtenir la détermination exacte de sa forme spectrale et de sa dépendance de la température.

4.1 Neutron data analysis

4.1.1 Fundamentals

When performing inelastic neutron scattering experiment on a TOF spectrometer, the physical quantity which is measured the number of neutrons, Δn, detected within

each time channel of width Δt, by a detector covering a solid angle $\Delta\Omega$, during a period T with a sample illuminated by an incident beam of Φ_0 incident neutrons per second (with energy E_0).

Δn can be expressed as:

$$\Delta n = \Phi_0 T \Delta\Omega \cdot eff(E) \cdot SAF(E) \left(\frac{\partial^2 \sigma}{\partial\Omega \partial\omega} \right) \Delta t \tag{4.1}$$

where $\frac{\partial^2 \sigma}{\partial\Omega \partial\omega}$ is the double differential cross section (equation 3.5, Chapter 3), $eff(E)$ is the detector efficiency and $SAF(E)$ is the Self-Attenuation Factor, due to absorption and scattering losses because of the sample geometry.

The neutron counts per unit energy are obtained from the neutron counts per time channel using:

$$\frac{\partial n}{\partial E} = \frac{\partial n}{\partial t} \times \frac{\partial t}{\partial E} \tag{4.3}$$

where

$$E = \frac{1}{2} m \frac{l^2}{t^2} \rightarrow \frac{\partial t}{\partial E} = \frac{t}{2E} \tag{4.4}$$

The velocity of thermal neutrons is of the order of km s^{-1}; consequently their energy can be determined by measuring their time-of-flight over the distance of a few metres. Measuring the time of arrival of the neutron at to detector, and knowing the flight path, we can calculate its velocity and hence its wavelength. The incident energy and the energy transfer are determined for each detector by knowing the TOF.

4.1.2 Data treatment of Time of Flight Data

The first correction to apply to experimental TOF data is to remove the background. The result obtained is normalised to a vanadium spectrum to correct for the different detector efficiencies.

Finally corrections for the absorption and scattering losses from the sample and the container have to be made. This last step depends on the geometry used[1].

A typical time of flight spectrum of v-SiO_2 taken at room temperature, after the subtraction of empty cell contribution is shown in Figure 4.1.

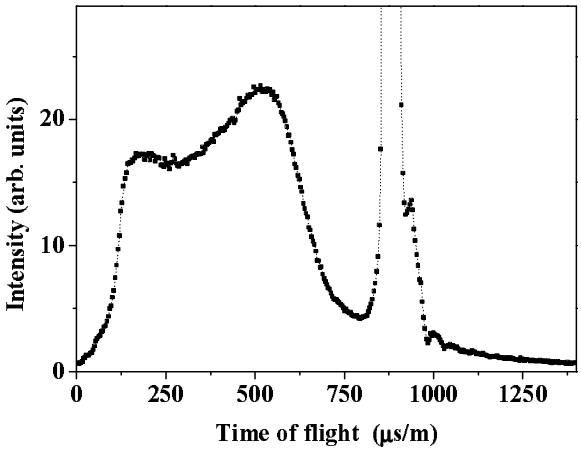

Figure 4.1: Time-of flight spectrum of vitreous silica sample, taken at 300 K on the TOF spectrometer IN4

The sharp peak around 800 μs/m corresponds to the neutrons which have been scattered from the sample without exchange of energy. When no movements of the atomic equilibrium positions are present, the width of this peak is the experimental resolution.

The decrease in elastic scattering with increasing Q is described by the Debye-Waller factor. It is approximately proportional to the temperature T (Marshall and Lovesey 1971):

[1] This part of treatment of data has been made used INX program. More detailed information about the methods used in the program, the approximations that have been made, the actual calculations performed etc. will be found in the web site: http://www.ill.fr.

$$W(Q) = \frac{\hbar^2 Q^2}{2M} \frac{3k_B T}{(k_B \theta_D)^2} \tag{4.5}$$

where M is the atomic mass, k_B is the Boltzmann constant and θ_D is the Debye-temperature.

Formula 4.5 yields numerically:

$$e^{-W(Q)} = e^{-\alpha Q^2} \tag{4.6}$$

where $\alpha = \frac{0.0067\,T}{300}$ for v-SiO_2.

On the left part of the elastic peak, one can remark the increasing of intensity due to the fast neutrons. This part of the spectrum corresponds to the inelastic scattering and the exchanged energy corresponds to the intermolecular vibrations or phonons.

The right part of the spectrum corresponds to the slow neutrons which suffered a loss of energy due to the sample.

Actually the strong asymmetry between left and right parts of the spectrum is somewhat artificial and originates from the recording of the data with a constant time interval.

When the TOF spectra are converted into energy spectra, the asymmetry of the inelastic parts in the spectrum is strongly reduced. One has to refer to the vibrational density of states to obtain information about the movements of the atoms.

4.1.3 Definition of the classical scattering law $S(Q,\omega)$

Mise en forme : Puces et numéros

After the standard time-of-flight to energy conversion, the output file obtained is the experimental scattering function $S_{exp}(\boldsymbol{Q}, \omega)$. The following derivation is formulated in terms of the classical scattering law $S(\boldsymbol{Q},\omega)$, where the frequency ω is related to the energy transfer E of the scattering process by:

$$E = \hbar\omega \tag{4.7}$$

and $\boldsymbol{Q}$ is the momentum transfer. This classical law $S(\boldsymbol{Q}, \omega)$ can be calculated from the measurement of the double differential cross section

$$S(\boldsymbol{Q},\omega)=\frac{k_B T}{\hbar\omega}\left(e^{\hbar\omega/k_B T}-1\right)\frac{k_i}{k_f}\frac{4\pi}{N\bar{\sigma}}\frac{\partial^2\sigma}{\partial\omega\partial\Omega} \qquad (4.8)$$

taking ω to be positive in energy gain of the scattered neutron (ILL convention).

Here T is the temperature, k_i and k_f are the wave vectors values of incoming and scattered waves, respectively, N is the number of atoms in the beam, $\bar{\sigma}$ is the average scattering cross section of the atoms and Ω is the solid angle. The definition requires a completely isotropic glass and it is valid for glasses with more than one kind of atoms, as it is usually the case. Formula 4.8 does not make distinction between coherent and incoherent scattering.

4.1.4 The inelastic scattering: the incoherent approximation

Mise en forme : Puces et numéros

A useful quantity that can be derived from the scattering law $S(\boldsymbol{Q},\omega)$ is the *vibrational density of states* (VDOS). This quantity can be obtained by using different procedures, which invoke several approximations especially when coherent scattering dominates in the system under study (as with silicon, germanium and oxygen atoms).

One of the most important approximations applied to extract the VDOS from TOF data is the so-called "*incoherent approximation*" which is invoked especially when dealing with a purely coherent sample.

The incoherent approximation assumes that the scattering equation 4.8 can be described in terms of a single average atom, which scatters only incoherently. The time-dependent displacement of this average atom from its equilibrium position is assumed to have a gaussian distribution (as explained in Chapter 3). From the Bloch identity (Marshall and Lovesey 1971), the intermediate scattering function can be written as

$$F(\boldsymbol{Q},t) = \mathrm{e}^{-Q^2\gamma(t)} \tag{4.9}$$

where $\gamma(t)$ is the time-dependent mean square displacement of the average atom (equation 3.18). Within the frame of the *one-phonon approximation*, the inelastic scattering from our classical isotropic incoherent scatterer (Marshall and Lovesey 1971) can be so written as:

$$S(\boldsymbol{Q},\omega) = Q^2 \mathrm{e}^{-2W} \frac{k_B T}{2\overline{M}} \frac{g(\omega)}{\omega^2} \tag{4.10}$$

where e^{-2W} is the Debye-Waller factor defined by formula (4.5), $\overline{M}$ is the average atomic mass, and $g(\omega)$ the required VDOS.

However, to compare the experimental results with the dynamical models, it is very important to make an accurate determination of the *multi-phonon neutron scattering contributions* (MPNS) to the experimental spectra. These contributions are significant for measurements carried out at high temperature and large neutron momentum transfer $\boldsymbol{Q}$. Therefore, development of techniques for MPNS calculations is essential to understand the dynamics of the given system. An elegant way to correct for the influence of multi-phonon scattering is to express $S(\boldsymbol{Q},\omega)$ as:

$$S(\mathbf{Q},\omega) = \frac{1}{\pi}\int_0^\infty \mathrm{e}^{-\gamma(t)Q^2} \cos\omega t \, \mathrm{d}t \tag{4.11}$$

Mise en forme : Puces et numéros

4.1.5 Density of states in the incoherent approximation and multi-phonon contribution

The vibrational density of states can be correctly calculated within the incoherent approximation if one takes into account the different scattering amplitudes depending on the individual atomic components. Moreover one can not neglect that different energy excitation probes (i.e. neutron wavelength), and consequently different exchanged $\boldsymbol{Q}$ explored, give different spectral shapes in the low frequency region.

Finally the use of a specific model is essential in order to deduce the density of states from an uncomplete basis in the wave-vector space spanned in the experiments.
On these bases, using equation (4.8) the neutron differential scattering cross section can be written as:

$$\frac{\partial^2\sigma}{\partial\omega\partial\Omega} = \frac{k_i}{k_f} b^2 e^{-\hbar\omega/k_B T} S(\boldsymbol{Q},\omega) \tag{4.12}$$

In the formula, b is the scattering length and $S(\boldsymbol{Q},\omega)$ is directly related to the $g(\omega)$ by (4.10).

Using the reduced variables $\alpha = \frac{\hbar^2 Q^2}{2Mk_B T}$ and $\beta = \frac{\hbar\omega}{k_B T}$ (with M the reduced atomic mass) the scattering law may be written as:

$$\tilde{S}(\alpha,\beta) = e^{-Q^2\langle u^2\rangle} g(\omega) \frac{\alpha}{2\beta sinh\frac{\beta}{2}} \tag{4.13}$$

where $\tilde{S}(\alpha,\beta)$ is the symmetrised form of $S(\boldsymbol{Q},\omega)$.

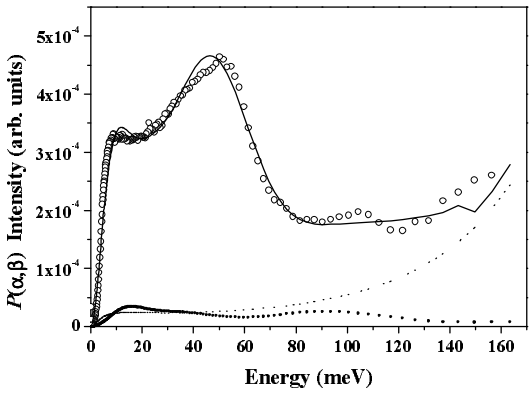

Figure 4.2: $P(\alpha, \beta)$ calculated from vitreous silica data, taken at 300 K on the TOF spectrometer IN4

The *Generalised Distribution* $P(\alpha,\beta)$ can be calculated from the (4.13) as:

$$P(\alpha,\beta) = 2\beta sinh\left(\frac{\beta}{2}\right)\frac{\tilde{S}(\alpha,\beta)}{\alpha} \sim g(\omega)e^{-Q^2\langle u^2\rangle} \qquad (4.14)$$

Actually, this function contains in addition to the density of states contributions from multi-phonon scattering as well as a smooth background.

The density of states $g(\omega)$ can be obtained by using an iterative procedure (Dianoux *et al.*). A first estimation of $g(\omega)$ is calculated by using a defined number of vibrational modes, each characterized by 5 parameters, i.e. the mass, the frequency, the intensity, the cutoff frequency, and the shape of the peak in the spectrum. Then, both the Debye-Waller factor and the multi-phonon contribution are estimated and used to evaluate a model $P(\alpha,\beta)$ which is compared with the experimental one. The initial parameters are then varied until a satisfactory agreement is achieved (see Figure 4.2).

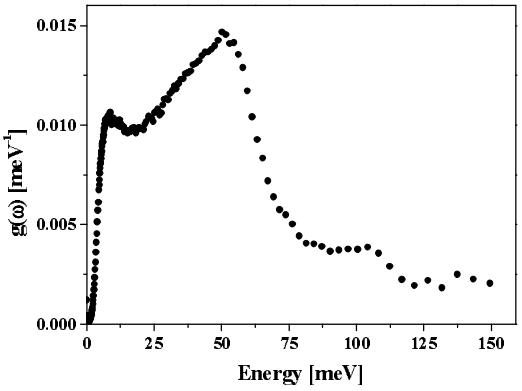

Figure 4.3: Vibrational density of states of v-SiO_2 at room temperature

At this point the procedure is inverted and $g(\omega)$ is obtained after subtraction of the evaluated multi-phonon contribution from the experimental data. In Figure 4.3 the final evaluated $g(\omega)$ is shown. In our case, this fitting procedure has been done at all

the measured temperatures even if at 50 K the multi-phonon correction does not affect the data significantly.

In the case of a glass consisting of two or more elements, this density is named the *generalized vibrational density of states*, to emphasize that it is not the true density of states, but its reflection in the scattering, weighted by the respective cross sections and masses of the different atoms of the sample.

The incoherent approximation works astonishingly well for the two coherently scattering glasses silica and germania. But it does not provide any information on the vibrational eigenvectors. To do that an *extension* of the incoherent approximation is needed. Such extension will be introduced in one of the following sections.

4.1.6 Where can we trust the incoherent approximation?

Mise en forme : Puces et numéros

The validity of the incoherent approximation is based on the assumption that the spectral distribution averaged over the momentum transfer $\boldsymbol{Q}$ has a coherent cross section, which approximates the incoherent cross section.

At large energy transfers this should be the case, since the related momentum transfers are also large. In that case the combination of powder averaging and detector (or $\boldsymbol{Q}$-) averaging guarantees the validity of the approximation. Conversely, for low energy transfers the $\boldsymbol{Q}$-volume to average is quite sensitive to the incident neutron energy E_0 and to the angular range of the detector. The ratio between the averaging $\boldsymbol{Q}$-volume of the Brillouin zone of the sample determines the applicability of the incoherent approximation (Requardt *et al.* 1997).

4.1.7 Determination of the VDOS by using the specific heat

Mise en forme : Puces et numéros

Looking at other techniques, the low temperature specific heat is in principle determined only by the true $g(\omega)$, which contains in addition to the vibrations all the

extra degrees of freedom due to the presence of relaxations and/or two-level systems (Phillips 1981). This technique is also very sensitive to the exact nature of the sample (chemical composition, impurity content) (Phillips 1981), but does not give a direct estimate of the $g(\omega)$, being an integral quantity and loosing in principle any spectral information. Specific heat gives nevertheless very precious hints to solve the cited problems in the analysis of inelastic scattering data (Sokolov *et al.* 1993), even if the inversion of the integral function that must be done to deduce the density of states is not a computationally stable problem. Recently a contribution to solve the question has been suggested, by using the Tikonhov regulation method (Sokolov *et al.* 1993). The inversion problem has been solved to find a reliable vibrational density of states. Indeed the results strongly depends both on the signal to noise ratio at low temperatures and on an independent estimate of the spectral shape of the two level systems (TLS) distribution (Sokolov *et al.* 1993).

It is clear from what we so far exposed that taken separately the specific heat, the Raman spectroscopy and the inelastic neutron scattering to deduce a density of states one can not obtain reliable and complete information so that for the deduction of the $g(\omega)$ the convergent use of all those techniques is needed.

As a by-product of this simultaneous analysis one could also experimentally determine the Raman coupling function $C(\omega)$ which is of a great importance when one is interested in the knowledge of the nature of the vibrational modes (Chapter 7).

4.1.8 Extension of the incoherent approximation

Mise en forme: Puces et numéros

In the case of INS a new procedure has been developed to calculate the vibrational density of states (Fabiani *et al.* to be submitted).

Taking into account that the VDOS is a function of the frequency, an extension of the incoherent approximation has been done in the frequency domain. The vibrational eigenvectors change with changing frequency, so each frequency window

has its own coherent dynamic structure factor. The interference between different scattering atoms does not change the overall scattering intensity, but leads to oscillations in the momentum transfer dependence. To take this into account, we define the quantity $S_\omega(\boldsymbol{Q})$ which is *dynamical structure factor*. Like $S(\boldsymbol{Q})$, this function equals 1 in the incoherent case (Chapter 3). Its coherent part shows long-range density and concentration fluctuations at small scattering angles, again like $S(\boldsymbol{Q})$, but now divided into elastic and inelastic parts. In a glass, the elastic part show the frozen density and concentration fluctuations, the inelastic part the Brillouin scattering. At large momentum transfer, the interference effects lead to oscillations around the 1 of the incoherent part. These oscillations will be close to those of $S(\boldsymbol{Q})$ at the elastic line, but may show a different interference pattern in the inelastic, depending on the vibrational modes at the given frequency. With the help of this function, the incoherent approximation expressed by the equation (4.11) transforms into the *extended approximation*:

$$S(\boldsymbol{Q},\omega) = S_{dyn}(\boldsymbol{Q},\omega)\frac{1}{\pi}\int_0^\infty \mathrm{e}^{-\gamma(t)Q^2}\cos\omega t\,\mathrm{d}t \qquad (4.15)$$

The approximation allows to fit not only a density of states, but a frequency-dependent dynamic structure factor as well. For coherent scatterers, the introduction of $S_\omega(\boldsymbol{Q})$ provides not only an enormous reduction of the deviation between theory and experiment, but opens up the possibility to analyze the vibrational eigenvectors (Buchenau *et al.* 1986, Wischnewsky *et al.* 1998). If this analysis is successful, one can proceed to calculate the *true* vibrational density of states, because then one knows the weight of a given mode in the scattering. In the following Chapters we applied this new method to silica and germania measurements.

4.2 Raman analysis

The exact determination of the spectral shape and temperature dependence of Raman spectra, is a crucial point in the data treatment for a quantitative determination of the coupling function $C(\omega)$ at low frequency (<20cm^{-1}) and low temperature (<70K) (Chapter 7). Even if the highest vibrational frequencies of glass under investigation are well below 1500 cm^{-1} we extended the scans on a much wider range due to the presence of an underlying background of luminescence.

As previously cited, Raman spectra contain two main contributions in addition to the one phonon scattering: the Quasi-Elastic Scattering (QES) and luminescence background. Both induce a great uncertainty in the determination of the density of states from the experimental data, and it is necessary to minimise their influence. As explained in Chapter 5, the QES intensity, located in the $\omega <$ 20 cm^{-1} region is strongly dependent on temperature. In order to reduce as much as possible its contribution to the scattering, the Raman measurements were done at low temperatures.

On the other hand the intensity of the luminescence relative to that of the Raman signal increases with decreasing temperature. The origin of the luminescence background can be due to several concurring effects but it is generally accepted that it originates mainly from the presence in the sample of impurities, holes, and surface defects. When the exciting laser light hits the sample near its surface the intensity of the luminescence increases enormously while the Raman intensity remains unchanged. It is useful to collect two sets of measurements in the bulk (near and far from the surface and) extending up the spectra to very high frequencies where the luminescence falls to zero. The comparison of these spectra directly allows a precise estimate of the luminescence contribution.

In Figure 4.4a the Raman contribution is represented by the sharp lines below 1500 cm^{-1}, while the luminescence background extends well above 3500 cm^{-1}. The spectral shape of the luminescence background was deduced as follows.

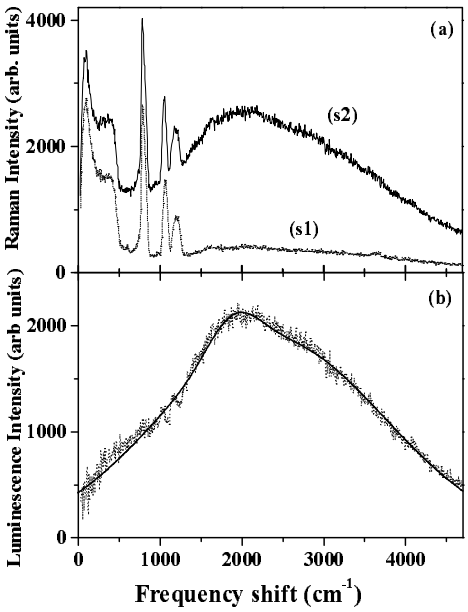

Figure 4.4: (a) Raman spectra of vitreous silica obtained in the bulk (*s*1) and near the surface (*s*2). (b) Luminescence contribution in comparison with its best fit obtained by means of a suitable polynomial function

The spectrum obtained in the bulk (*s*1) multiplied by a factor was subtracted from the one taken near the surface (*s*2), in order to cancel the Raman peaks, whose intensity, as said, is independent on the beam position inside the sample. The obtained luminescence contribution is shown in Figure 4.4b together with its best fit obtained by means of a suitable polynomial function. This procedure was repeated for each temperature. The Raman spectra taken in the bulk were then corrected for the luminescence by subtracting the polynomial curve, obviously rescaled to the intensity of the background effectively measured in the 1500-3000 cm^{-1} range (Figure 4.4a).

In figure 4.5 the ratio between the Raman intensity and the luminescence background contribution taken at 10 cm^{-1} (open dots) and 15 cm^{-1} (open triangles) is shown as a function of temperature.

These ratios can be used as an upper limit to estimate the error in the determination of $C(\omega)$ from Raman data, since at 10 cm^{-1} the Raman intensity reaches the minimum measured value.

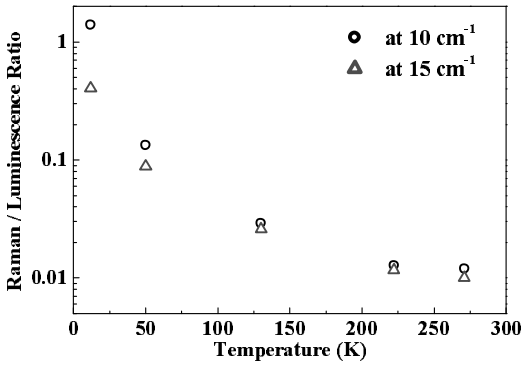

Figure 4.5: Ratio between the Raman intensity and the luminescence background contribution taken at 10 cm^{-1} (open dots) and 15 cm^{-1} (open triangles) as a function of temperature.

REFERENCES

BUCHENAU U., PRAGER M., NUKER N., DIANOUX A.J., AHMAD N. and PHILLIPS W.A., *Phys. Rev.* **B 34**, 5665 (1986).

DIANOUX A.J, CURRAT R. and ROLS S., Private Communication.

FABIANI E., FONTANA A. and U. BUCHENAU to be submitted

MARSHALL W. and LOVESEY S.W., *Theory of Thermal Neutron Scattering*, Oxford, Claredon Press (1971)

PHILLIPS W.A., *Low temperature properties*, Springer Berlin (1981)

REQUARDT H., CURRAT R., MONCEAU P., LORENZO J. E., DIANOUX A. J., LASJAUNIAS J.C. and MARCUS J., *J. Phys.: Condens. Matter* **9** 8639 (1997)

SOKOLOV A. P., KISLIUK, A., QUITMANN, D. and DUVAL, E., *Phys. Rev.* **B**, **48** , 7692 (1993) .

WISCHNEWSKI A., BUCHENAU U., DIANOUX A.J., KAMITAKAHARA W. A. and ZARESTKY J. L., *Phys. Rev.* **B**, **57**, 2663 (1998)

5. Neutron and Raman experiments

New inelastic Raman and neutron scattering experiments for the network glass formers SiO_2 and GeO_2 were performed at temperatures from 10 to 300 K.

The measurements were motivated by the following objectives:

1. *to study the crossover from quasielastic to vibrational scattering at low frequency in both Raman and neutron spectra;*
2. *to study the Brillouin scattering with increasing momentum on vitreous germania, to see how far the conventional dispersion approach holds;*
3. *to find an appropriate description of the coherent vibrational scattering, comparing the conventional dispersion approach to a new extension of the*

De nouvelles expériences de diffusion inélastique de Raman et de neutron portant sur les verres de SiO_2 et GeO_2 ont été exécutées pour des températures allant de 10K jusqu'à 300 K.

Ces mesures ont été motivées par les objectifs suivants:

1. *étudier le 'recouvrement' entre les régimes quasi élastique et vibrationnel à basse fréquence dans les spectres Raman et neutron;*
2. *étudier la diffusion Brillouin en fonction du transfert de moment Q dans le verre de germanium, pour estimer la limite de validité de l'approche conventionnelle de dispersion;*
3. *trouver une description appropriée de la diffusion cohérente, en comparant l'approche conventionnelle de diffusion à une nouvelle procédure*

incoherent approximation;

4. *to determine the spectral shape of the coupling function C(ω), comparing inelastic scattering data obtained by Raman and neutron experiments, and in particular, its low frequency limit.*

basée sur la prolongation de l'approximation incohérente;

4. *déterminer la forme spectrale du coefficient de couplage C(ω), en comparant les données inélastiques de dispersion obtenues par des expériences de spectroscopie Raman et de neutrons, et en particulier, sa limite à basse fréquence.*

5.1 Samples

It is well known that different samples of SiO_2 can be obtained, depending on thermal history and OH-content. They are commercially available with a large number of names containing a different number of OH^- bonds such as spectrosil, puropsil, heralux etc. The content of OH^- bonds goes from 2-3 ppm (for the puropsil) up to 1200 ppm (for the spectrosil-B).

Nevertheless it has been demonstrated (Ahmad 1993) by Raman and specific heat measurements that the low-frequency dynamics is not modified by different content of OH^- bonds.

The sample of v-SiO_2 used for our experiments was a commercial grade spectrosil sample, purchased from SILO. It had a disk shape with a diameter of about 50 mm and a thickness of 4.8 mm.

In the case of v-GeO_2, appropriate amounts for the neutron scattering experiments of reagent-grade GeO_2 powder (Aldrich 99.99+%) were melted in platinum crucibles for about 1h at *ca.* 1600°C. The homogeneous and bubble-free melt was subsequently quenched in water and glassy samples of irregular shape were removed from the bottom of the crucible. This preparation technique results in completely transparent glasses.

5.2 Raman experiments

Raman scattering experiments were done using a standard experimental set-up Jobin Yvon U1000 in a wide frequency range (from 3 to 3000 cm^{-1}). We are mainly interested in the frequency range below 100 cm^{-1}, but we extended the scans to a much wider range, because of the presence of an underlying weak background of luminescence, as explained in a previous chapter.

At very low frequency (< $3cm^{-1}$) the double monochromator Sopra was used, setting the slits to 100μm to obtain $0.1cm^{-1}$ resolution. The Raman spectra were taken in polarised (VV) and depolarised (HV) geometries.

5.3 Neutron experiments

The inelastic neutron scattering data were obtained using five different spectrometers at the Institut Laue Langevin (ILL) in Grenoble (France), in order to cover the whole range of interest in the Q-ω plane. The low Q-high ω region has been investigated using the three axis spectrometers (TAS) IN1, and IN8; the low Q-low ω region was explored by the TAS IN3, while for the high Q region, two time of flight spectrometers (TOF) were employed: the cold-neutron time-of-flight IN6 with incoming neutrons of 4.1 Å wavelength and the thermal time-of-flight IN4 with 1.53 Å and 2.2 Å wavelength.

The TAS measurements were only done for the vitreous germania sample, because the high sound velocity of silica does not allow neutron Brillouin experiments. On the other hand, no IN6 measurement was performed for germania. Most experiments were done at room temperature, but the time-of-flight measurements were in some cases extended to lower temperatures.

In order to gain access to the small Q region with an energy transfer high enough to probe an extended dynamical range, the IN1 and IN8 spectrometer configuration was

optimised to operate at low scattering angles (down to 1°) with sufficiently high incoming intensity and high energy resolution. The analyser energy was set at a fixed final wavevector of 7.3 $Å^{-1}$ (IN1) and 4.8 $Å^{-1}$(IN8), determining an elastic resolution function having a Gaussian shape with a FWHM of 2.5 meV and 4.1 meV respectively. The scattered intensity from the sample was measured at six different exchanged wave-vectors $\boldsymbol{Q}$, namely, 0.3, 0.5, 0.7 and 1.2 $Å^{-1}$ on IN1 and 0.65 and 0.8 $Å^{-1}$ on IN8.

For the low-ω low-$\boldsymbol{Q}$ range probed on IN3, high-resolution spectrometer configuration was accomplished by means of the tight 15', 40', 40', and 40' Soller collimations from the reactor to the detector, with the analyser set to select a fixed final wave vector $\boldsymbol{k}$ = 2.66 $Å^{-1}$. This configuration allowed investigating the energy range between –10 and 8 meV with a Gaussian elastic resolution having a FWHM of 0.8 meV. The intensity scattered from the sample was measured at four wave-vector transfers $\boldsymbol{Q}$, namely, 0.75, 1, 1.5 and 2 $Å^{-1}$.

Because of the non-negligible small angle background, deriving both from the cell walls and from the sample environment, careful measurements of the background contribution were carried out by collecting the intensity scattered from the empty cell, at the same wave vectors as the sample, and from a full absorber, a 1-mm-thick Cd slab inside the cell.

After normalization of the measured data to the monitor, the background intensity was subtracted and multiple scattering contribution was also accounted for.

High $\boldsymbol{Q}$ neutron spectra were obtained on the thermal TOF spectrometer IN4, using a fixed incoming neutron wavelength of 1.53 Å, allowing to an accessible exchanged-wave vector, $\boldsymbol{Q}$, range between 1.5 and 7 $Å^{-1}$ with an energy resolution of 1.3 meV FWHM. After the standard time of flight to energy conversion, the raw data were corrected by using the procedure explained in Chapter 4. The constant-$\boldsymbol{Q}$ cuts of the dynamic structure factor $S(\boldsymbol{Q},\omega)$ were then obtained by interpolation, binning the scattering data every 0.5 $Å^{-1}$.

5.4 Study of Raman and Neutron data as a function of temperature: the origin of the Quasi-Elastic Scattering at low frequency

Performing the neutron measurement for different temperature values in v-SiO_2 and v-GeO_2, we can compare the results with the measurements of Raman scattering from the same samples in the temperature range 12 K to 1200 K for silica and 13 K to 300 K for germania. The result shows the presence at low frequency of an extra-scattering close to the elastic line, which does not follow the temperature-dependence expected for harmonic vibrations: the Quasi-Elastic Scattering (QES)[1].
In this section, we have concentrated our study on v-SiO_2. Comparing these studies to the acoustic attenuation measured at 30 GHz by Brillouin light scattering (Vacher and Pelous 1976), we found a close parallel between the QES and the acoustic attenuation in the temperature range between 10 and 800 K.

5.4.1 The experimental results obtained from Raman and neutron scattering

In Figure 5.1 the HV Raman spectra divided by the Bose-Einstein population factor at some significant temperatures are represented for the samples studied. The spectra were normalised at high frequency as shown in the inset of the same picture. Here we discuss only the low frequency region because the general features at higher frequencies are already discussed in the literature (Flubacher *et al.* 1959, Hass 1970). In the spectra of vitreous silica the boson peak is clearly present for $\omega < 100$ cm^{-1}. For $\omega < 50$ cm^{-1} the scattered intensity decreases with decreasing ω. The very low

[1] QES is not necessarily a broadening or spreading of the elastic line. It can also be a quasielastic line sitting under a perfectly unbroadened elastic line. In fact, this is the usual case in a glass, where the atoms only jump back and forth, maintaining well-defined equilibrium positions in a structure which lives forever (at least on the time scale accessible to neutrons)

frequency data, as displayed in Figure 5.1, indicate a minimum of the scattered intensity around 10 cm^{-1} and an increase for $\omega < 10cm^{-1}$. At 12 K, no such increase of the intensity has been detected. The sharp increase below 4 cm^{-1} stems from elastic scattering contribution due to the finite resolution of the spectrometer (~1.8 cm^{-1}). The strong QES contribution appears in the spectra already at low temperature and increases almost linearly in T (Figure 5.1a). At high temperature the QES tends to saturate. This tendency is even clearer in Figure 5.1b, where we report the high temperature spectra.

Moreover, we note at high temperatures a shift of the maximum of the Boson peak to higher frequency.

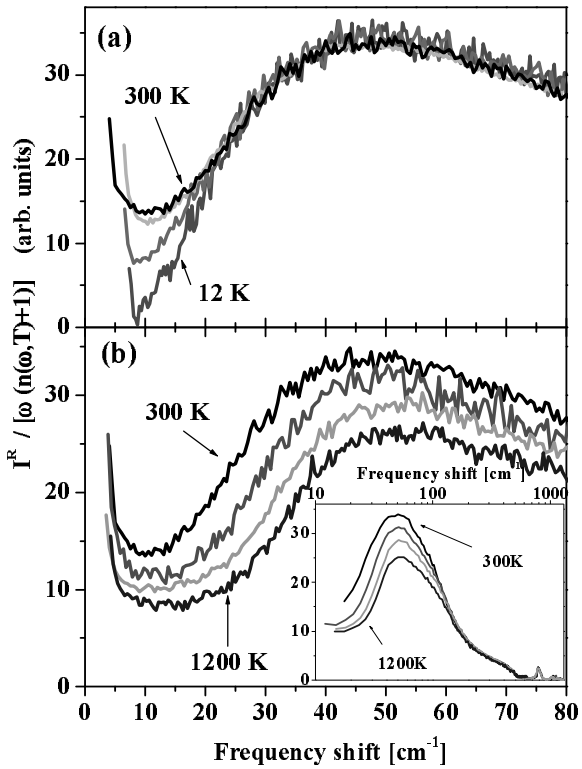

Figure 5.1: Raman scattering spectra of vitreous silica between 12K and 1200K (T =12K, 50K, 133K, 300K (1a) and T=300K, 620K, 995K, 1200K (1b)). The spectra were normalised at high frequency as shown in the inset of the figure, where we report the high temperature spectra in logarithmic scale.

A finite scattering intensity for $\omega \rightarrow 0$ requires a careful investigation of the instrumental profile. This has been done by monitoring the scattering intensity as a function of resolution, changing the widths of the spectrometer slits.

A true increase towards $\omega \rightarrow 0$ was found in all types of v-SiO_2 and independent from the OH^- concentration (Figure 5.2), confirming the results previously mentioned, obtained by Ahmad (Ahmad 1993). Hence, the QES existing in v-SiO_2 has an intrinsic nature, which does not depend on the OH^- content.

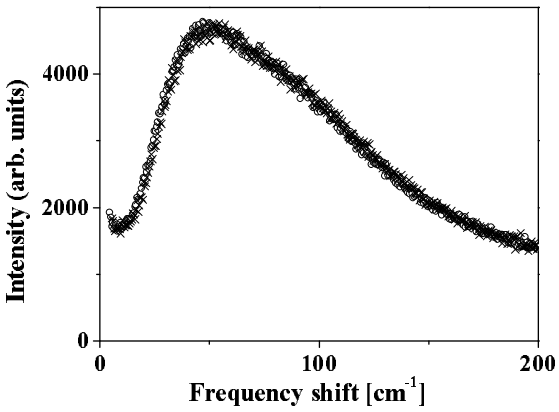

Figure 5.2: Raman scattering spectra of different vitreous silica containing a different number of OH^- bonds

The neutron spectra depicted in Figure 5.3 show a similar spectral shape and temperature behaviour of Raman spectra in Figure 5.1. The inset of Figure 5.3 shows the significant increase of the QES with temperature between 35 and 300 K.

Note that v-SiO_2 shows two different temperature changes in Figure 5.3. The first is the onset of the quasielastic scattering between 35 and 300 K shown in Figure 5.3a, a feature observed in many glasses. The second is an upward shift of the boson peak between 300 and 1100 K, shown in Figure 5.1 b, which is a feature unique to silica.

The differences between the neutron and Raman spectra above 30 cm^{-1} can be described in terms of the Raman coupling function (Fontana *et al.* 1999) which will be discussed in the next chapter.

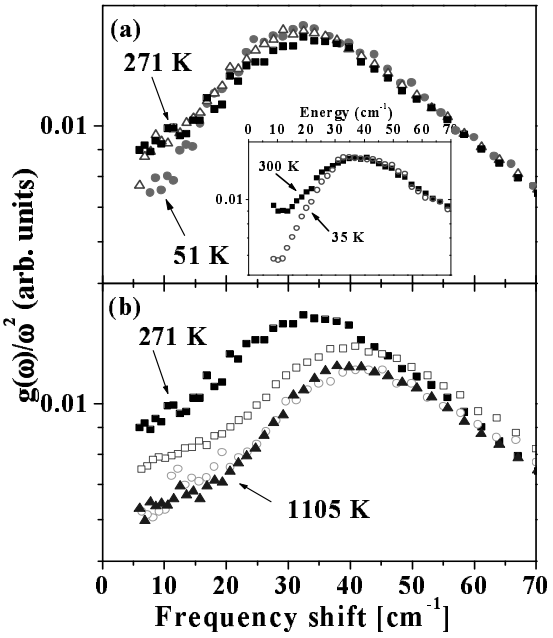

Figure 5.3: Neutron scattering spectra of vitreous silica between 35K and 1104K. *T* =51K, 155K, 271K (1a); T=271K, 693K, 893K, 1104K (1b). Inset: Low frequency spectra at 35K and 300K.

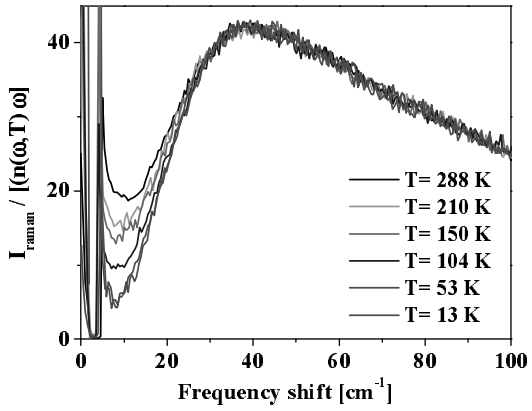

Figure 5.4: Raman scattering spectra of vitreous germania between 13K and 300K. The spectra were normalised at high frequency.

For vitreous germania the presence of the QES is evident at temperatures up to 300 K, as well as in vitreous silica, as is reported in Figure 5.4. In this case, the

comparison to neutron data is missing, because no cold neutron data were taken. The thermal time-of-flight data on the IN4 do not allow to see such a clear quasielastic signal, because the resolution is limited.

The intensity of the QES at low frequency in neutron data collected on silica is more difficult to evaluate as it can be noticed in the Figure 5.3. In fact, the Raman technique is better suited to observe the quasielastic scattering.

The QES intensity was assessed in Raman as well as in neutron measurements to estimate the intensity at 10 cm^{-1} (~1.2 meV) in a window of 5 cm^{-1} as a function of the temperature and the results for vitreous silica are reported in Figure 5.5 as squares and crosses respectively. Both results have a similar spectral shape and temperature behaviour.

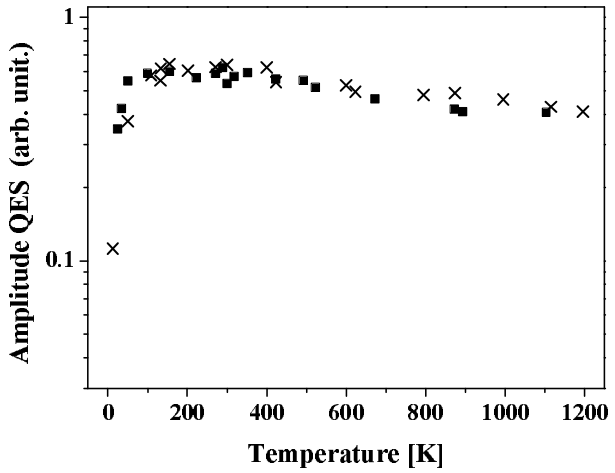

Figure 5.5: Results of the QES amplitude measured at 10 cm^{-1}, by Raman (crosses) and neutron scattering (full squares).

5.4.2 The origin of the Quasi-Elastic Scattering in vitreous silica

Even if the nature of the microscopic origin of the QES is not well understood, it is now clear that different effects can contribute to its amplitude. The thermal history of the used sample (Caponi *et al.* 2003 and references therein), the high mobility in

superionic glasses (Benassi *et al.* 1991), the presence of hydrogen bonds (chemical water) in the sample matrix as well as free water (physical water) in porous system (Terki *et al.* 1999) could influence the QES. Besides in the paper of Carini *et al.* (1995), the authors explain the QES in terms of relaxation process.

But how can we relate the relaxation mechanism to the origin of the extra-scattering in glasses?

As explained in Chapter 1 the relaxation processes can be divided in two classes: the α-processes, which represents the slow dynamics below the GHz regime and the β-processes, which follow an Arrhenius behaviour. The fast dynamics in the GHz regime is supposed to belong to this second class, with a low Arrhenius barrier of only a few times $k_B T$.

When a relaxation process is present it can cause a spreading of the width of the Brillouin peak, changing the shape of the susceptibility, which gives the evaluation of the QES intensity in Raman and Neutron scattering data.

The width of the Brillouin peak is related to the acoustical attenuation (Jäckle 1981, Ruocco *et al.* 1999) by the formula

$$\alpha = \frac{2\pi\Gamma}{h\nu} \tag{5.1}$$

Here α is the extinction coefficient of the Brillouin wave energy, Γ is the full width at half maximum of the Brillouin line and ν is the sound velocity. It is plausible to assume that the Brillouin damping is proportional to the number of relaxations, which have a relaxation time of the order of the inverse Brillouin frequency. Similarly, one guesses that the quasielastic scattering from the atomic mean square displacements of these relaxations will be proportional to their number. Taking into account this relation between the relaxation mechanism and the QES scattering, the comparison between Raman, Neutron and Brillouin scattering data makes sense.

Figure 5.6 represents the above-mentioned comparison between the data collected and the acoustic attenuation data from literature (Vacher *et al.* 1997), applying appropriate calibration factors. As evident from the figure, the agreement between

the temperature dependence of the QES intensity and the width of the Brillouin line between 10 K to 800 K is excellent, indicating a common origin of the two phenomena.

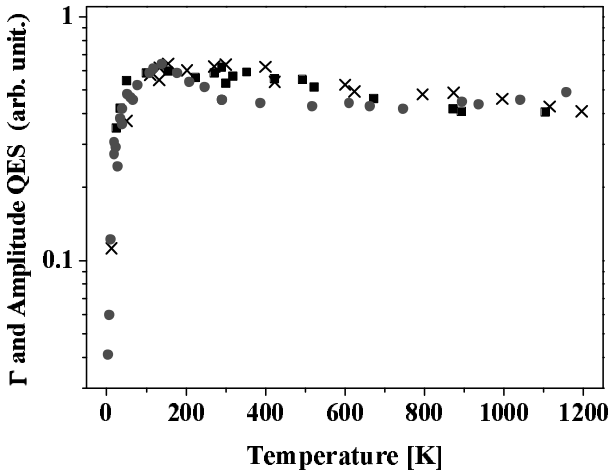

Figure 5.6: Comparison between the Raman data (crosses), neutron data (squares) and acoustic attenuation

At temperatures higher than 800K the parallel ends and the sound attenuation increases more strongly than the QES. In fact, while the QES tends to decrease, the sound attenuation tends to increase. This difference could be due to the shift of the maximum of the BP at high temperatures mentioned above.

5.4.3 Interpretation of experimental results

As already suggested in the literature (Winterling 1975), this excess of scattering intensity is neither due to second order processes nor to the high frequency tails of the Brillouin lines, but to the scattering from structural defects or damped sound waves which are characteristic of the glassy state. In fact, two level states can couple to light scattering directly, as was originally proposed by Jäckle (Jäckle 1981, Hunklinger and Arnold 1976). However, a more probable mechanism would involve

a coupling of the light to the phonons, which in turn couple to relaxational jumps; this indication can be deduced from the fact that the depolarisation ratio is the same for QES and the boson peak. The microscopic origin of QES should then be the same than the one of the acoustic attenuation peak, which is at about 150K when measured at 30 GHz.

The interpretation of the experimental data can be given on the basis on the double well potential characterising the structural defects present in glasses (Winterling 1975, Anderson and Bömmel 1955). When an atom or groups of atoms undergo a transition between two energy minima, the polarizability tensor changes its spatial orientation. Anderson and Bömmel (Anderson and Bömmel 1955) have suggested that the structural defects involve the motion of oxygen atoms, a conclusion corroborated for the BP by a recent Hyperraman experiment (Hehlen *et al.* 2000). Hence, it is reasonable that the polarizability of the oxygen is anisotropic taking into account that the polarizability depends on the spatial disordered location of the defects.

The picture we are thinking about here is similar to the situation found in liquids. If the polarizability of a molecule is isotropic, then the light scattering is polarised and we have a Brillouin doublet and a central line, if the polarizability is anisotropic, there is in the Raman spectrum an additional depolarised contribution named reorientational scattering (Rayleigh wing). It corresponds to the incoherent neutron scattering, which also permits the study of the motion of individual atoms.

Hence the excess of scattering can be interpreted as due to structural relaxing defects (β- processes) which causes the acoustic attenuation measured by the HWHM of the Brillouin line-shape.

In any case, the quasielastic scattering is limited to frequencies below 15 cm^{-1} (energy transfers below 2 meV). Above that frequency, one sees essentially harmonic vibrations. But again, the question what these vibrations are, is by no means settled. We will turn to this question in the rest of this chapter, as well as in the next chapter.

5.5 Study of vitreous germania in THz region: the dispersion of longitudinal and transverse modes in strong glasses

5.5.1 Introduction

As we have just discussed in previous chapters, vitreous silica is the most important glass-forming material. Vitreous germania (v-GeO_2) is a chemical and structural analogue of silica glass. Inelastic neutron scattering experiments performed on this sample are able to provide fundamental information on the origin of the general features of these glasses at low frequency. In the next paragraph, data collected on vitreous germania are reported.

In particular we want to focus the attention on new results, obtained by a combination of different inelastic neutron spectrometers. The aim of this study was to cover a wide energy transfer range at low frequency, to assess whether the dispersion branches are still present in vitreous germania, as claimed for vitreous silica (Ruzicka *et al.* 2004).

5.5.2 The investigation of the low-Q region by TAS spectrometers

The INS data collected on IN1 and IN8 are reported, for four selected Q-values, in Figure 5.7. Well-defined Brillouin peaks, fairly resolved from the elastic tail also at the minimum Q value, are identified on the data, independently of any model or data treatment. With increasing Q, the peak position shifts towards higher energies with a high propagating velocity (~23 meV Å, 3497 m/s, close to the measured acoustic

longitudinal sound velocity of 3600 m/s), revealing the propagating nature of this excitation.

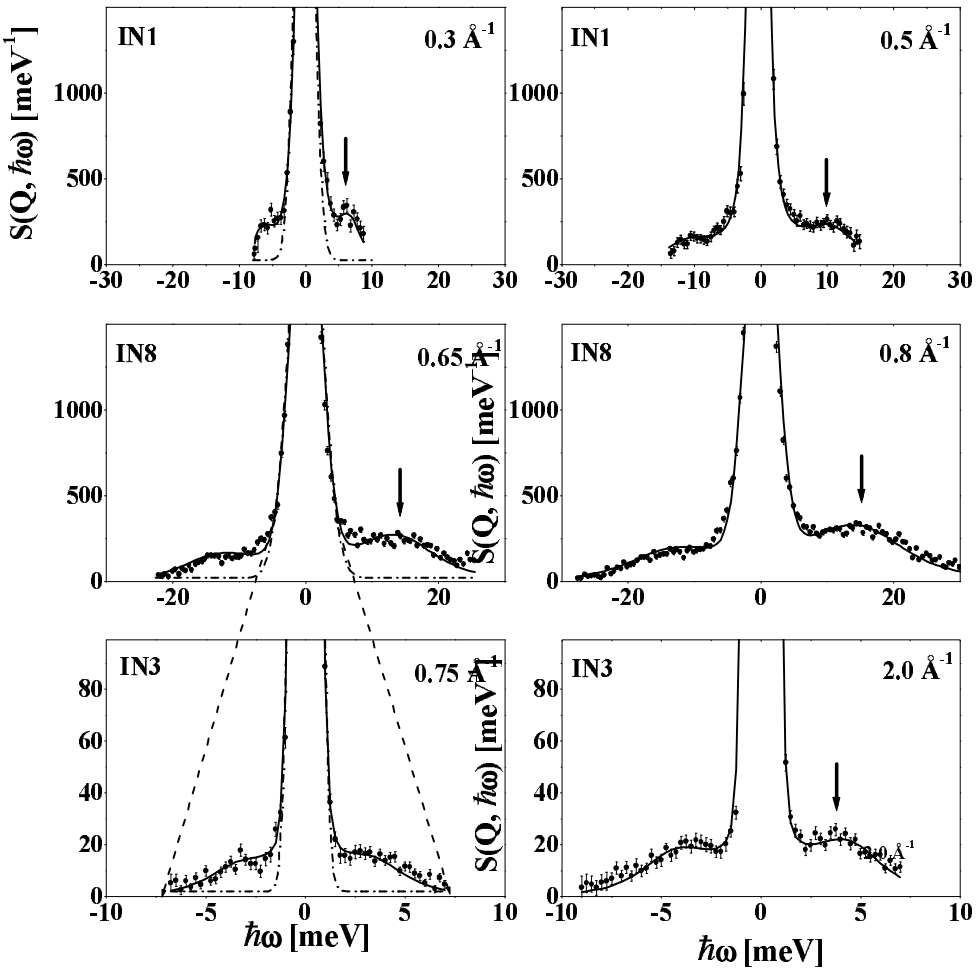

Figure 5.7: INS spectra of v-GeO_2 at 300K, collected on 3 different three-axis spectrometers, as a function of Q. IN1 and IN8 spectra show a well defined high frequency-peak dispersing with a velocity of 23 meV Å. IN3 spectra present a low-frequency inelastic feature, well resolved from the elastic line, and slightly dispersing. Dashed lines represent the measured spectrometer resolutions.

At low Q, aside the Brillouin peaks associated with the longitudinal sound mode, theoretical and numerical studies also find a second dispersing excitation in the dynamical response function (masked here by the resolution) suggesting the

existence of a transverse-like dynamics propagating in disordered systems (Horbach *et al.* 2001, Taraskin and Elliott 1997).

In spite of several numerical results (Pilla *et al.* 2000), there is little experimental evidence on the crossover from Brillouin to high-momentum transfer scattering. Accurate information can be gained on the existence and on the propagating or localised nature of the predicted low frequency excitation at low $\boldsymbol{Q}$-values, by the IN3-TAS spectra, also presented in Figure 5.7. Beside an intense central line, the spectra show a slightly $\boldsymbol{Q}$ dependent well-resolved inelastic signal. The high resolution employed enabled the determination of its position, which shifts from 4.6 to 5.3 meV in the range from 0.75 to 2 Å^{-1}, while its intensity grows as Q^2.

The dispersing longitudinal mode was fitted in terms of a damped harmonic oscillator

$$S(Q,\omega) = \frac{1}{\pi}\frac{k_B T}{\bar{M}}\frac{\Gamma Q^2}{(\omega^2 - c^2Q^2)^2 + \omega^2\Gamma^2} \qquad (5.2)$$

where Γ is the damping of the phonon and c is the longitudinal sound velocity. As pointed out above, c turned out to be close to the sound velocity measured in ultrasonic and light scattering Brillouin experiments.

The fit results for Γ are shown in Figure 5.8 in a double-logarithmic plot versus the momentum transfer $\boldsymbol{Q}$. Also included are data from a recent simulation of vitreous germania (Pilla *et al.* 2004) and from Brillouin light scattering experiments at 20 and 300 K.

Note that the two light scattering Brillouin values are markedly different, as pointed out in the previous section. The 20 K value lies close to the extrapolation of the neutron Brillouin data with a Q^2 law. The existence of a Q^2 law agrees with earlier findings in vitreous silica (Benassi *et al.* 1996), which are, however, debated controversially (Rat *et al.* 1999).

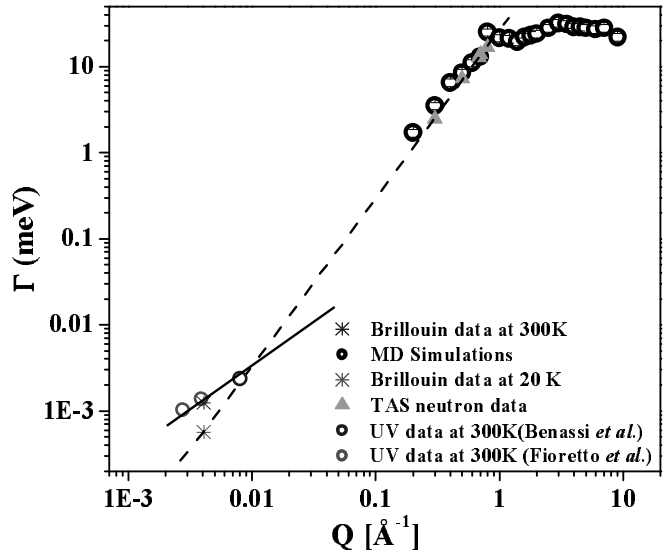

Figure 5.8: Brillouin damping in vitreous germania from experiment and simulation. The crosses represent the Brillouin data at room and low temperature of Hunklinger and Arnold (1976). The green triangles are the TAS neutron data collected at ILL. The dashed line is a fit in terms of proportionality to Q^2 while the continuous line in terms of proportionality to Q. Finally, the open dots are the UV data at 300 K of vitreous germania of Fioretto *et al.* and P. Benassi *et al.* (Private Communication)

The comparison to the silica values of Benassi *et al.* (Benassi *et al.* 1996) shows an interesting difference. In silica, the condition $\Gamma = v\boldsymbol{Q}$ (full width at half maximum equal to nominal phonon frequency, the point where the phonons start to be overdamped) is reached at an energy of 12 meV, corresponding to a $\boldsymbol{Q}$-value of 0.32 Å^{-1}. According to our measurements, this point is reached for vitreous germania at 19.3 meV, corresponding to a $\boldsymbol{Q}$-value of 0.84 Å^{-1}. Since one probably should scale the energy transfer with the sound velocity, this implies that the Brillouin damping is a factor 2.6 weaker in vitreous germania than in vitreous silica. We will return to this point in the discussion of the vibrational density of states.

5.5.3 The investigation of the high-*Q* region by TOF spectrometer

At higher ***Q***, the mode merges in a broad feature, almost ***Q*** independent, as pointed out by Figure 5.9. Here we present the TOF data at three selected ***Q*** values. The semi-log plot enhances the high frequency inelastic broad contribution, which at high ***Q*** flattens at energy of 30 meV. The DOS, associated to this branch, as well as the quantity $g(\omega)/\omega^2$, show a definite bump at this energy. Thanks to the adequate energy resolution, a second inelastic feature can be revealed at low frequencies. The excitation, corresponding to a peak above the Debye level in the $g(\omega)/\omega^2$, is centred around 3.5 meV, and is ***Q*** independent. We identify this low frequency band as the high ***Q*** counterpart of the low-frequency excitation observed on IN3. The question is whether this excess of states, identified at high ***Q*** as the Boson Peak, is associated with the flattening of the acoustic transverse dynamics at high ***Q*** (Pilla *et al.* 2000) or whether it is some contribution from other excitations.

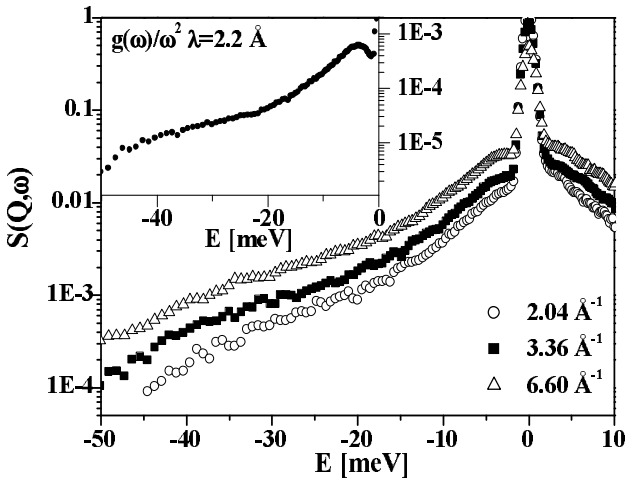

Figure 5.9: TOF neutron scattering spectra of v-GeO_2 at 300K, obtained for an incident wavelength of λ=1.53 Å, reported for three different ***Q***-values. Two modes are present, respectively, in the low and high frequency region. In the insert, the ratio between the DOS and the frequency square, obtained from the TOF data at λ =2.2 Å, is reported.

5.5.4 Molecular Dynamics Simulations (MD)

The experimental data were compared with Molecular Dynamics Simulations (MD) on v-GeO_2. In a cubic box of length 32 Å, 680 molecules were simulated interacting through a van Best type potential proposed by Taraskin and Elliott (1997, 1999, 2002). Full details on the simulations will be published elsewhere (Pilla *et al.* 2004). The density of the system was ρ=3.6 g/cm^3 like in the experimental sample.

As shown in Figure 5.10, both the simulated longitudinal and transverse current spectra show the existence of two excitations.

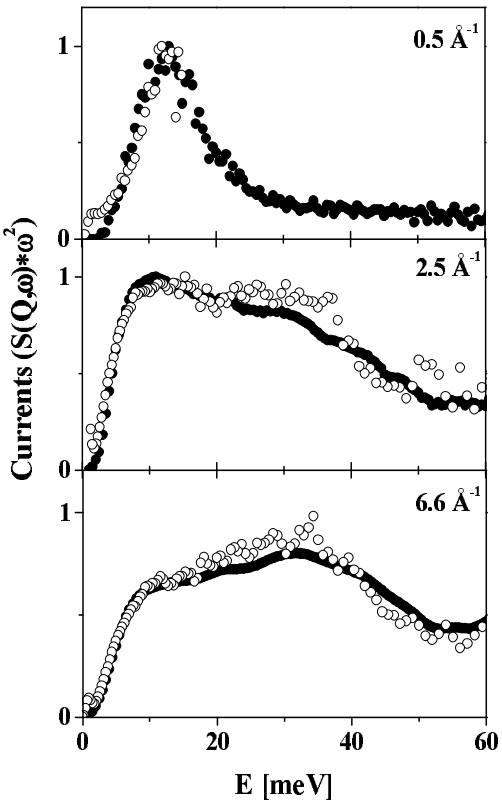

Figure 5.10: The longitudinal current spectra obtained by INS measurements (open dots) are reported together with the simulated ones (full dots), for three selected ***Q***-values. The spectrum at Q=0.5 Å^{-1} refer to IN1 data while the high ***Q*** spectra to the IN4 data.

The high frequency excitation disperses with $\boldsymbol{Q}$, and its propagation velocity is in excellent agreement with the hydrodynamic value (3600 m/s). This excitation appears at each $\boldsymbol{Q}$ value in the longitudinal current spectra down to the minimum simulated $\boldsymbol{Q}$ (0.2 $Å^{-1}$) where it merges in the sound branch, thus confirming the longitudinal character of the excitation. On the other side, the low frequency excitation is always present in the transverse current spectra, while it appears in the longitudinal current spectra only at Q>0.6 $Å^{-1}$. This low frequency feature disperses at low $\boldsymbol{Q}$ with a sound velocity of ~13 meV Å and becomes almost dispersionless at Q=1 $Å^{-1}$.

The MD results show that, as a consequence of lack of translational invariance, the pure symmetry character of the two modes is rapidly lost, and at large Q both modes contribute in similar amounts to longitudinal and transverse current spectra.

The good agreement between simulated and experimental correlation functions is shown in Figure 5.10. Here we report the comparison between simulated and measured current spectra, where the character of the two inelastic features is clearly enhanced.

The high-energy mode originates from the LA branch and its position for Q-values higher than ~1$Å^{-1}$ oscillates around ~30 meV. In the low energy range another feature peaked at about 10 meV in the longitudinal current spectra and at about 5 meV in the scattering spectra is present both in experiment and in simulation (though slightly weaker in the simulation).

The dynamic maps can give another qualitative example of the agreement between simulated and experimental data, as reported in Figure 5.11, 5.12a and 5.12b.

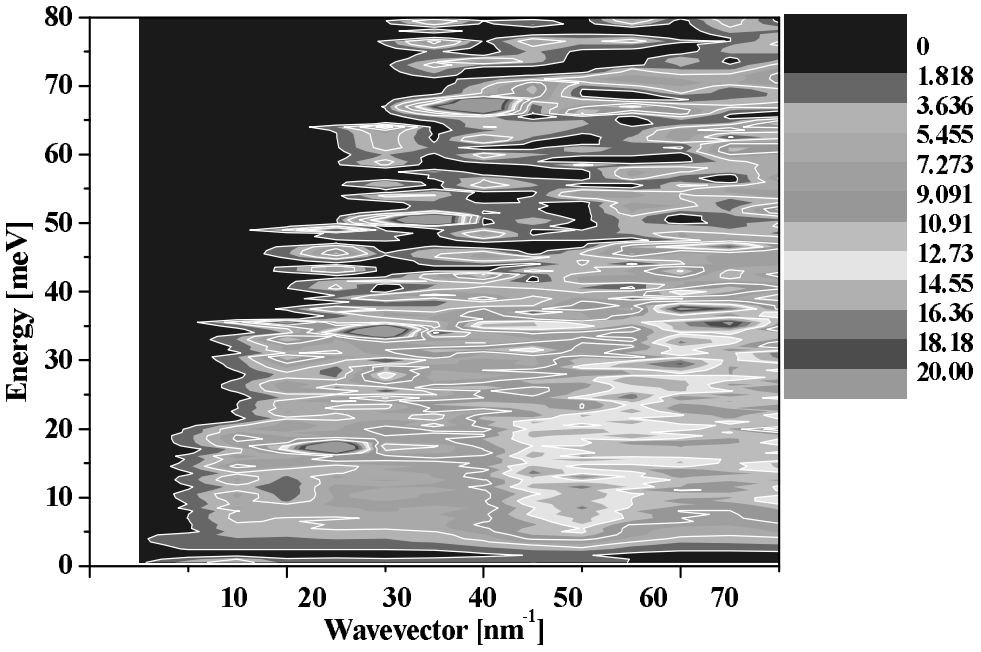

Figure 5.11: Experimental current maps for vitreous germania

In the comparison, the qualitative agreement between the experimental and simulated current maps is evident at low frequency where around 10 meV. In this frequency region the presence of a mode which disperses up to 1 Å^{-1} and then which assumes a constant trend around 10 meV, can be noticed in the simulated transverse current map (Figure 5.12) as well as the experimental map (Figure 5.11).

At high frequency values other modes are present and disperse as well up to 1 Å^{-1}. At higher Q-values in the simulated longitudinal current map it oscillates around 30-40 meV while it does not disperse in the experimental current map.

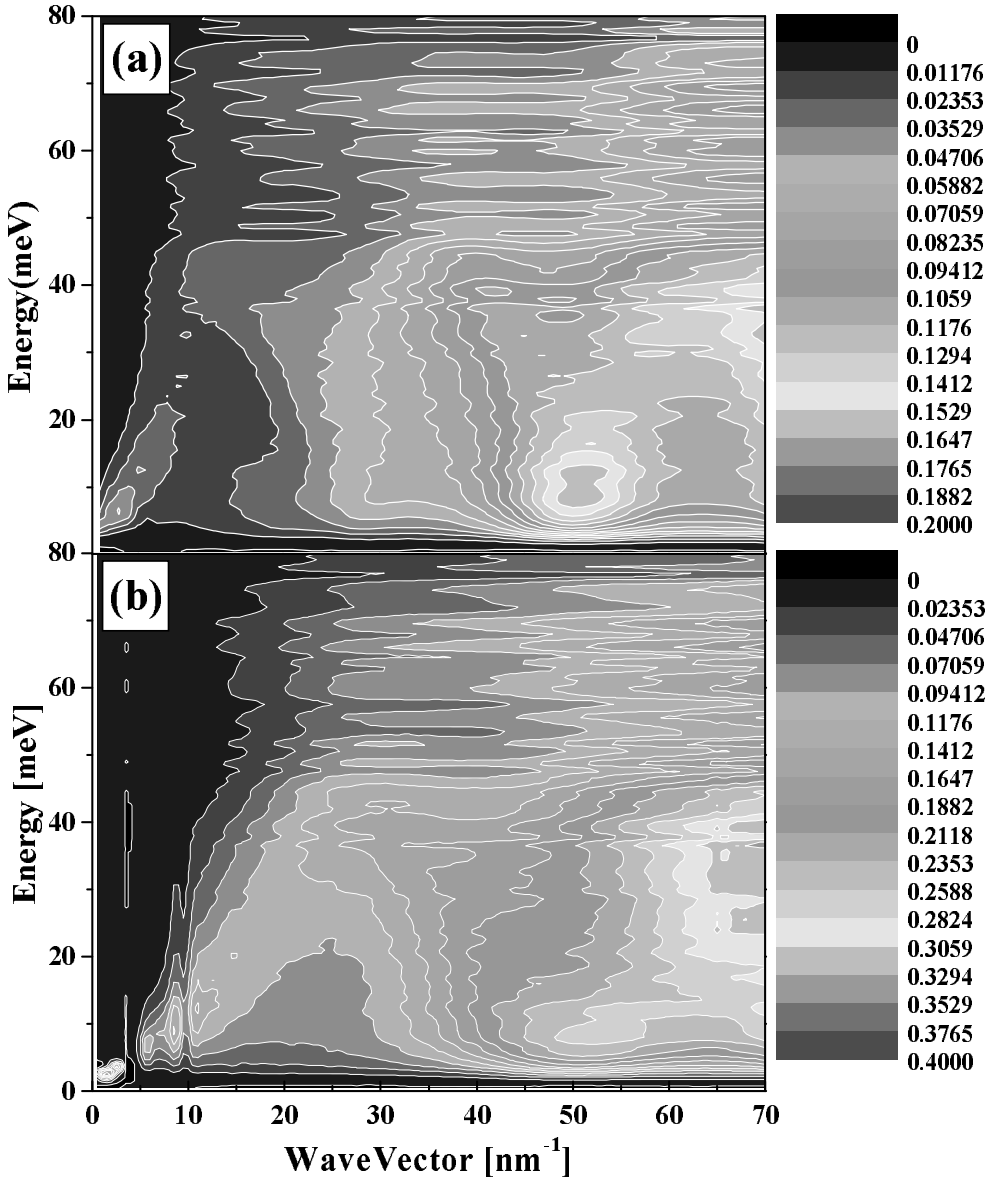

Figure 5.12: Simulated Longitudinal (a) and Transverse (b) current maps for vitreous germania

5.5.5 The dispersion branches

To get quantitative information on the excitations energy and on its Q-dependence, the overall measured scattering spectra have been fitted convoluting the proper instrumental resolution with a delta function and a Damped Harmonic Oscillator (DHO) function, modelling the elastic and inelastic structure respectively.

The DHO frequencies, obtained from the fitting procedure by using the formula 5.2, are reported in Figure 5.13 (open and full dots). The corresponding dispersion curves obtained from MD simulations are plotted in the same figure (straight line). The overall behaviour of the dispersion curves is consistent with the interpretation here proposed. In particular, the dispersion curves observed by INS measurements are well reproduced by the simulated LA and TA branches. A velocity of about 3650±100 m/s is associated with the LA mode, in good agreement with the ultrasonic value (3600 m/s) (Soga 1969) and with the results of Brillouin light scattering measurement carried out on the same sample, i.e. 3640±100 m/s.

Exploiting the results of the simulation at the lowest Q value, we could estimate a propagation velocity of the TA mode, equal to 2000±100 m/s, which matches the velocity of transverse phonon measured by Brillouin light scattering of 2150±100 m/s. In the high Q region, the measured excitations shows an almost flat trend as a function of Q, while the simulated ones oscillates around a mean value at about 5 (TA) and 30 meV (LA). This behaviour shows that the long-range component of the potential has to be improved to properly simulate the real system.

Though the dispersion picture derived from the simulation and from the neutron data is reasonably consistent, it is rather unsatisfactory as a general explanation of the vibrations in glasses. According to this picture, all vibrations at the boson peak and above are heavily damped. There is general agreement that such a high damping cannot be a true anharmonic damping. It is rather thought to be a consequence of squeezing the vibrational excitations into the crystal picture of a well-defined wave vector for each vibrational excitation.

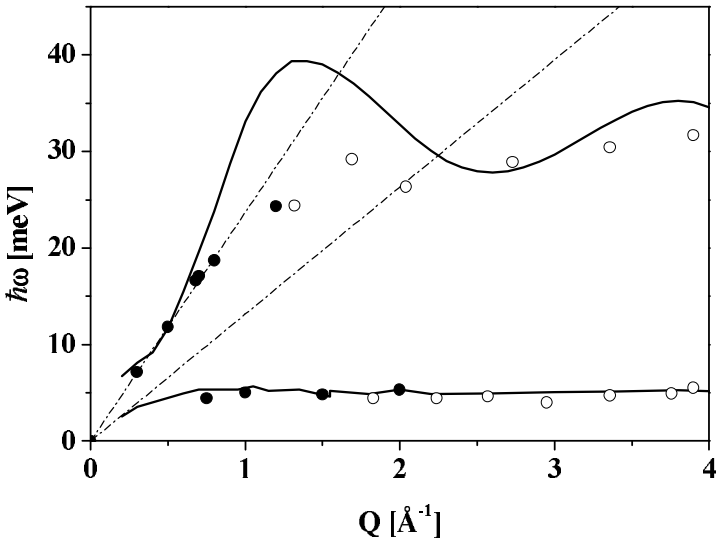

Figure 5.13: Dispersion relations of v-GeO_2 as resulted from the fitting procedure described in the text. The TAS (full dots) and TOF (open dots) fit results are compared with the main maxima of the simulated L (higher branch) and T (lower branch) scattering spectra (straight lines). The dashed and dot-dashed lines are the L and T sound velocity as measured by Brillouin Light Scattering.

One would therefore prefer to describe the vibrations in terms of long-lived excitations, which do not have a well-defined wavevector, only obeying the momentum transfer selection rule at very low wave vectors and properly described by a vibrational density of states. The evaluation of the neutron time-of-flight data in terms of such a picture will be the topic of the next chapter.

REFERENCES

AHMAD N., *Phys. Rev.* **B 48**, 13512 (1993)

ANDERSON O.L. and BÖMMEL H.E., *J. Am. Ceram. Soc.* **38**, 125 (1955)

BENASSI P., PILLA O., MAZZACURATI V., MONTAGNA M., RUOCCO G. and SIGNORELLI G., *Phys. Rev.* **B 44**, 11734 (1991).

BENASSI P., KRISCH M., MASCIOVECCHIO C., MAZZACURATI V., MONACO G., RUOCCO G., SETTE F., and VERBENI R., *Phys. Rev. Lett.* 77, 3835 (1996)

CAPONI S., FONTANA A., MONTAGNA M., PILLA O., ROSSI F., TERKI F., and WOIGNIER T., *J. Non-Cryst. Solids* **322**, 29 (2003)

CARINI G., D'ANGELO G., TRIPODO G., FONTANA A., LEONARDI A., SAUNDERS G. A., and BRODIN A., *Phys. Rev.* **B 52**, 9342 (1995)

FLUBACHER P., LEADBETTER A. J., MORRISON J. A. and STOICHEFF B. P., *J. Phys. Chem. Solids* **12**, 53 (1959);

FONTANA A., DELL'ANNA R., MONTAGNA M., ROSSI F., VILIANI G., RUOCCO G., SAMPOLI M., BUCHENAU U. and WISCHNEWSKI A., *Europhys. Lett.* **47**, 56 (1999).

HASS M., *J. Phys. Chem. Solids* **31**, 415 (1970).

HEHLEN B., COURTENS E., VACHER R., YAMANAKA A., KATAOKA M. AND NOUEK. I, *Phys. Rev. Lett.* **84,** 5355 (2000)

HORBACH J., KOB W. and BINDER K., *Chem. Geol.* **174**, 87 (2001)

HUNKLINGER S. and ARNOLD W.: *"Physical Acoustics"*, Ed. W.P. Mason and R.N. Thurston, **Vol. XII**, 155-215 (Academic, New York 1976).

JÄCKLE J. in *Amorphous Solids*, Edited by W.A. Phillips (Springer-Verlag, New York, 1981).

PILLA O., CUNSOLO A., FONTANA A., MASCIOVECCHIO C., MONACO G., MONTAGNA M., RUOCCO G., SCOPIGNO T. and SETTE F., *Phys. Rev. Lett.* **85**, 2136 (2000)

PILLA O., CAPONI S., FONTANA A., GONCALVES JR, MONTAGNA M., ROSSI F., VILIANI G., ANGELANI L., RUOCCO G., MONACO G. and SETTE F., *J. Phys.: Condens. Matter* **16** (2004)

RAT E., FORET M., COURTENS E., VACHER R. and ARAI M., *Phys. Rev. Lett.* **83**, 1355 (1999)

RUOCCO G., SETTE F, DI LEONARDO R., FIORETTO D., KRISCH M., LORENZEN M., MASCIOVECCHIO C., MONACO G., PIGNON F. and SCOPIGNO T., *Phys. Rev. Lett.* **83**, 5583 (1999)

RUZICKA B., SCOPIGNO T., CAPONI S., FONTANA A., PILLA O., GIURA P., MONACO G., PONTECORVO E., RUOCCO G. and SETTE F., *Phys. Rev.* **B 69**, 100201(R) (2004)

SOGA N. *Journal of Applied Physics* **40**, 3382 (1969)

TARASKIN S.N. and ELLIOTT S.R., *Phys. Rev.* **B 56**, 8605 (1997)

TARASKIN S.N. and ELLIOTT S.R., *Phys. Rev.* **B 59**, 8572 (1999)

TARASKIN S.N. and ELLIOTT S.R., *Phys. Rev.* **B 65**, 052201 (2002)

TERKI F., PILLIEZ J.N., WOIGNIER T., PELOUS J., FONTANA A., ROSSI F., MONTAGNA M., FERRARI M., CICOGNANI G., DIANOUX A.J., *Phil. Mag.* **B 79**, 2081-2089, (1999).

VACHER R. AND PELOUS J., *Phys. Rev.* **B 14**, 823 (1976).

VACHER R., PELOUS J., and COURTENS E. *Phys. Rev.* **B 56**, R481 (1997).

WINTERLING G., *Phys. Rev.* **B 12**, 2432 (1975).

6. Beyond the incoherent approximation

The aim of this part of the thesis is to evaluate the neutron time-of-flight spectra in terms of the extension of the incoherent approximation "extended approximation" described in chapter 4. As we will see, this approach yields much more information on the vibrations in vitreous silica and vitreous germania than the dispersion scheme described in chapter 5.

Le but de cette partie de la thèse est d'évaluer les spectres de temps-de-vol de neutrons en termes de l'extension de l'approximation incohérente ("extended approximation"(décrite dans le chapitre 4. Cette approche va nous donner beaucoup plus d'informations sur les vibrations des oxydes de silice et de germanium vitreux que la procédure standard de dispersion que nous avons décrite dans le chapitre 5.

6.1 The dynamical structure factor of vitreous silica

All information about the structure and the dynamics of the material are contained in the scattering law $S(\boldsymbol{Q},\omega)$, which can be divided into coherent and incoherent parts (as seen in Chapter 4). The coherent scattering law contains information about the correlation in time and space between different atoms while the incoherent part treats the self-correlation, i.e. the moving of a particular atom around its equilibrium position.

All the structural information can be obtained performing diffraction experiments

where we can measure directly the static structure factor $S(\boldsymbol{Q})$.

By performing TOF experiments, the same information can be extracted from the scattering law $S(\boldsymbol{Q},\omega)$, by integrating over the whole frequency range (Formula 3.15, Chapter 3). The $S(\boldsymbol{Q})$ obtained is equal to 1 for incoherent scattering and oscillates around 1 for the coherent one.

The TOF experimental data described in the previous chapter, were corrected for multiple scattering and normalised to the diffraction data. To determine $S(\boldsymbol{Q})$ from a our data set, one integrates the scattering over a single detector or a detector group, *correcting for the change in momentum transfer* $\boldsymbol{Q}$ *as the frequency changes*. This has the advantage that a bad detector does not corrupt its neighbours. The procedure is justified in silica, where most of the inelastic scattering stems from the boson peak region, close to the elastic line.

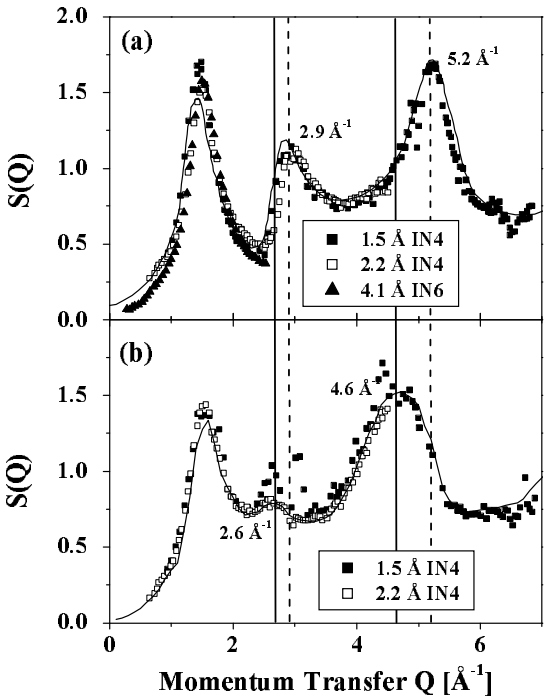

Figure 6.1: Comparison of $S(\boldsymbol{Q})$ calculated from time-of-flight data collected using a wavelength of 1.5 Å (full squares), 2.2 Å (open squares) and 4.1 Å (full trangles) to the $S(\boldsymbol{Q})$ from the diffraction experiments in literature (Johnson *et al.* 1983, Kohara and Suzuya 2002, Suzuya *et al.* 1997) (continuous line) for vitreous silica (a) and vitreous germania (b).

In Figure 6.1, TOF data for vitreous silica and vitreous germania, obtained at room temperature with different spectrometers and different incident wavelengths (resolutions), are represented in comparison with the diffraction data taken from literature (Johnson *et al.* 1983, Kohara and Suzuya, 2002).

The comparison with vitreous germania shows that the second and the third peak in $S(\boldsymbol{Q})$ shift to lower momentum transfer with respect to the vitreous silica case. This is caused by the increased Ge-O distance (1.73 Å) in germania (Suzuya *et al.* 1997) as compared to the Si-O distance of 1.6 Å in silica (Johnson *et al.* 1983). The corner connected GeO_4-tetrahedra in germania are 8% larger than the corner connected SiO_4-tetrahedra in silica. Nevertheless, the first sharp diffraction peak is more or less at the same place in both substances, which shows that the larger tetrahedra in germania are more densely packed.

By looking at only the $S(\boldsymbol{Q})$ calculated in this way, all information about the frequency dependence of the vibrations of atoms are lost.

A way out of this difficulty is to introduce the dynamic structure factor $S_\omega(\boldsymbol{Q})$ which depends on the frequency window and, like $S(\boldsymbol{Q})$, oscillates around 1 for coherent scattering and is equal to 1 for the incoherent scattering. It is close to $S(\boldsymbol{Q})$ for zero energy transfer. The experimental determination of the dynamical structure factor is taking the integral over a small frequency window of the scattering law $S(\boldsymbol{Q},\omega)$ as shown in Chapter 4.

Another important characteristic of the $S_\omega(\boldsymbol{Q})$ is that it can be divided into elastic and inelastic part. The elastic part takes into account the position of atoms and it is very similar for its shape to the static structure factor $S(\boldsymbol{Q})$ (even if it is not integrated over the full energy range). On the other hand, the inelastic part takes into account both the positions and the displacement $\boldsymbol{u}_j$ of atoms. This means that it can give information about the origin of the vibrations in glasses. It is also characterised by several oscillations, which die out at high $\boldsymbol{Q}$.

Figure 6.2a shows the boson peak frequency window from 2 to 6 meV in vitreous silica for all three sets of data.

The pronounced oscillations around the dashed line (calculated from the incoherent approximation as explained in the following) are clearly observed. Germania (Figure 6.2b) shows rather similar oscillations in the same window in but the second peak is less pronounced. In the interpretation of the early IN6 experiment on silica (Buchenau *et al.* 1986, Wischnewski *et al.* 1998), this means that the librational motion of the corner-connected tetrahedra is less important than in silica.

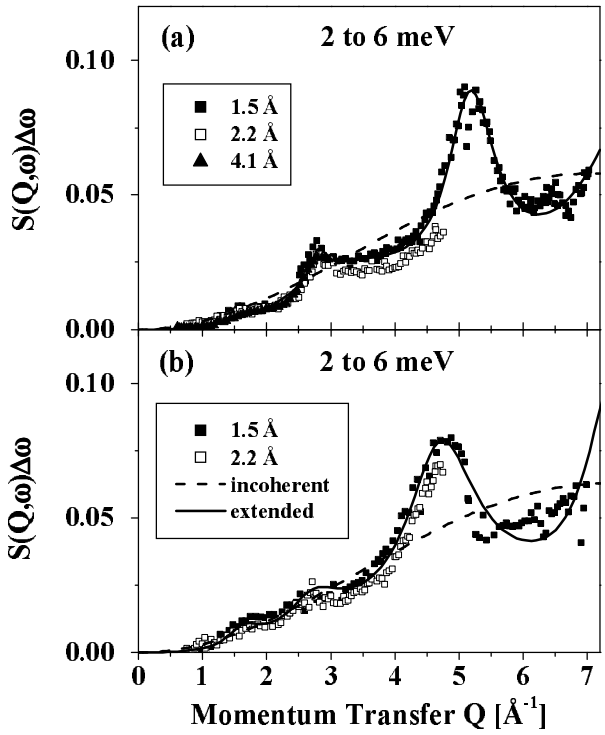

Figure 6.2: Inelastic dynamic structure factor $S_\omega(Q)$ for vitreous silica (a) and vitreous germania (b) calculated from TOF data collected at IN4 and IN6 for three different wavelengths (full squares λ=1.53 Å, open squares λ= 2.2 Å, full triangles λ= 4.12 Å) integrating over the frequency region of the Boson Peak. The dashed line is the incoherent approximation and the continuous line is the extension of the incoherent approximation described in the following sections.

As one goes up in energy transfer, the amplitude of the oscillations decreases

gradually and the deviations of the coherent from the incoherent approximation get smaller and smaller, and the last one seems to be appropriate within experimental error. This development is shown for vitreous silica in Figure 6.3 (a-c).

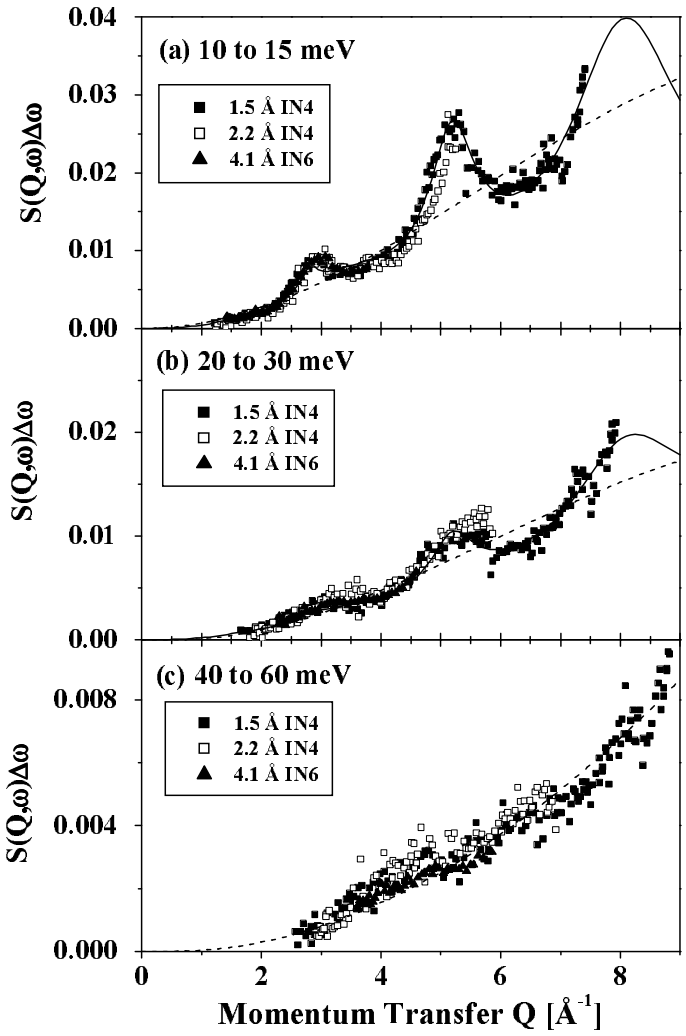

Figure 6.3: The development of the inelastic dynamic structure factor of vitreous silica above the boson peak frequency regions: (a) from 10 to 15 meV, (b) from 20 to 30 meV, (c) from 40 to 60 meV. The dashed line is the incoherent approximation and the continuous line is the extended of the incoherent approximation discussed in the following sections.

6.2 The vibrational density of states

6.2.1 The incoherent approximation

The next step is to calculate the vibrational density of states from these data sets, applying the incoherent approximation described in Chapter 4. The usual way to determine the so-called *generalised vibrational density of states* from neutron data is to calculate first of all the multiphonon scattering self-consistently, using the gaussian approximation. The result is a first estimate of the vibrational density of states, from which it is possible to calculate the $\gamma(t)$ of the intermediate scattering function of the average atom in the gaussian approximation

$$S(Q,t) = e^{-Q^2\gamma(t)} \qquad 6.1$$

where t is the time. $S(\boldsymbol{Q},\omega)$ is then obtained by Fourier transform from $S(\boldsymbol{Q},t)$ (formula 4.15, Chapter 4). The vibrational density of states at a given energy frequency is corrected by comparing calculated and measured scattering. This provides an improved density of states, taking the multiphonon effects into account. The procedure is iterated until the density of states does no longer change.

For vitreous silica, the dashed lines in Figure 6.2 and Figure 6.3 are the fit with $S_\omega(\boldsymbol{Q})=1$, the traditional way of evaluation in the incoherent approximation. Obviously, they are not in good agreement with the experimental data in such a case as coherent glasses, because they do not reproduce the oscillations of the measured scattering law. The simplest way of improving the scheme is to determine an appropriate empirical dynamical structure factor $S_\omega(\boldsymbol{Q})$, oscillating around 1 to keep consistency. One then can compare the measurement to the product $S_\omega(\boldsymbol{Q})\cdot S_{inc}(\boldsymbol{Q},\omega)$ instead of the incoherent approximation $S_{inc}(\boldsymbol{Q},\omega)$ alone, still having a consistent treatment of the multiphonon effects. This will be done in the next section.

The results for the three measurements are compared in Figure 6.4. They agree reasonably well with each other, even though the incoherent approximation is not

good at the boson peak.

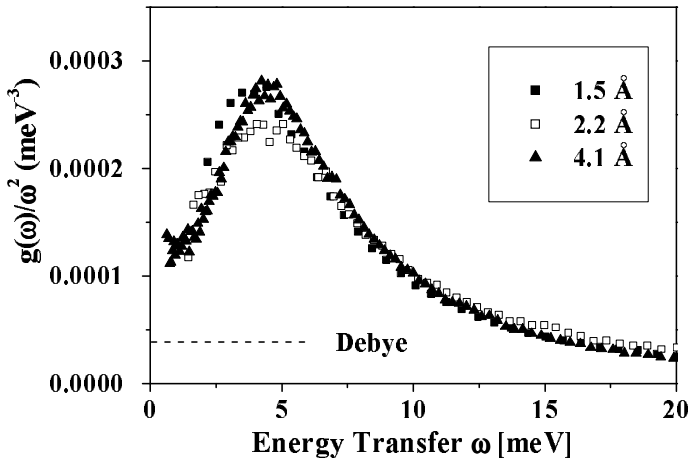

Figure 6.4: Vibrational density of states $g(\omega)$ of silica calculated on the basis of the incoherent approximation, plotted as $g(\omega)/\omega^2$ between 0 and 20 meV.

6.2.2 Beyond the incoherent approximation

To go beyond the incoherent approximation, we start by calculating the dynamic structure factor $S_{\text{boson}}(\boldsymbol{Q})$ ($S_{\omega}(\boldsymbol{Q})$ at the boson peak) via the formula

$$S_{\text{boson}}(\boldsymbol{Q}) = \frac{S_{\text{boson}}(\boldsymbol{Q},\omega)}{\frac{1}{\pi}\int_0^{\infty} \mathrm{e}^{-\gamma(t)Q^2} \cos\omega t \, \mathrm{d}t} \qquad 6.2$$

taking $\gamma(t)$ from the evaluation in terms of the incoherent approximation described in the precious subsection. $S_{\text{boson}}(\boldsymbol{Q},\omega)$ is determined from the measured $S(\boldsymbol{Q},\omega)$ via:

$$S_{\text{boson}}(\boldsymbol{Q},\omega) = \frac{\int_{\omega_{\min}}^{\omega_{\max}} S(\boldsymbol{Q},\omega)\,\mathrm{d}\omega}{\omega_{\max} - \omega_{\min}} \qquad 6.3$$

where $\omega_{\min}$ and $\omega_{\max}$ denote the lower and upper limit of the boson peak frequency regio, respectively. In vitreous silica and germania with their boson peak at an energy

transfer of about 4 meV, ω_{min} and ω_{max} were chosen corresponding to energy transfers of 2 and 6 meV, respectively. Figure 6.5a shows the result for the three sets of data of silica and Figure 6.5b those for the two IN4 measurements of germania.

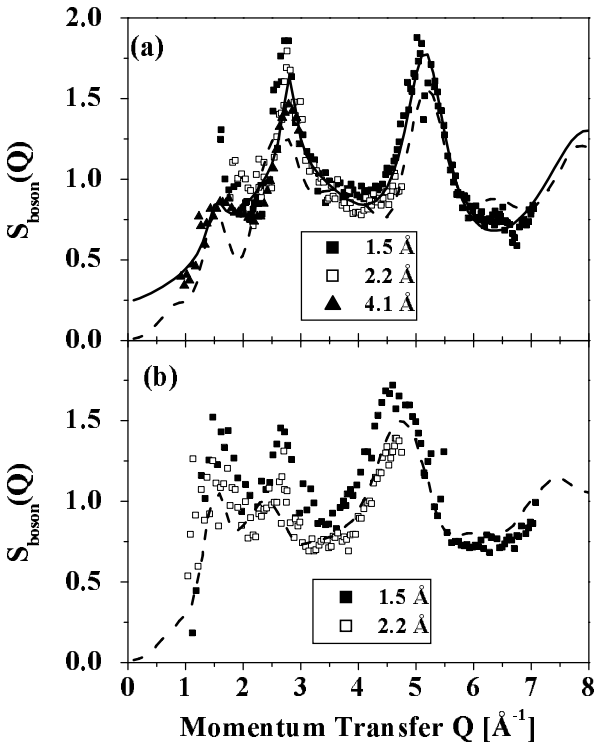

Figure 6.5: Inelastic dynamic structure factor $S_{boson}(Q)$ in the boson peak region for (a) silica and (b) germania. The continuous line is the fit with five lorentzians, the dashed line is the sum of 0.45 $S(Q)$ and 0.55 tetrahedra libration in the case of silica and 0.75 and 0.25 for germania.

The next step is to quantify the fading-away of the oscillations with increasing frequency. For this, we fit the data point of Figure 6.5a in term of a sum of five lorentzians (the continuous line in Figure 6.5a). This purely empirical dynamic structure factor oscillates around 1 in the momentum transfer region of the three measurements. One can use it to replace the incoherent approximation $S_\omega(Q) = 1$, to get a description of the scattering in terms of an effective density of states. Figure 6.2 shows that it gives a much better agreement with the experiment than the incoherent

approximation, at least in the frequency region of the boson peak.

As one goes up in frequency, the oscillations of the dynamic structure factor begin to get weaker. On can follow this behaviour quantitatively by fitting the inelastic intensities in subsequent frequency windows in terms of the expression:

$$S_{\omega}(\boldsymbol{Q}) = r_{\text{incoh}}(E) + [1 - r_{\text{incoh}}(E)] S_{\text{boson}}(\boldsymbol{Q}) \qquad 6.4$$

where $r_{\text{incoh}}(E)$ is the energy-dependent fraction of incoherent scattering, going from 0 to 1 as one goes from the boson peak up to higher frequencies (Figure 6.6).

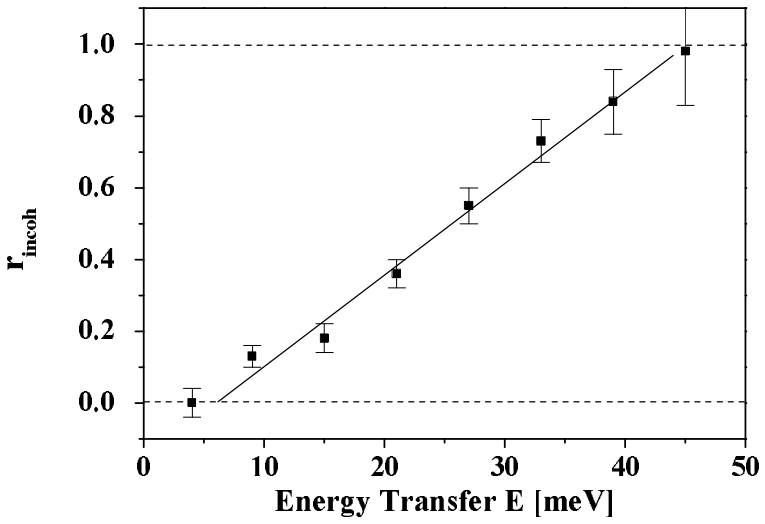

Figure 6.6: Gradual increase of the fraction r_{incoh} of the incoherent scattering in vitreous silica with increasing energy transfer (from a simultaneous fit to all three sets of data).

Knowing the change of r_{incoh} with frequency, one now has a well-defined coherent inelastic dynamic structure factor $S_{\text{dyn}}(\boldsymbol{Q},\omega)=S_{\omega}(\boldsymbol{Q})\cdot S_{\text{inc}}(\boldsymbol{Q},\omega)$ where $S_{\omega}(\boldsymbol{Q})$ oscillates around 1 (the value for incoherent scattering) with changing momentum transfer $\boldsymbol{Q}$. In this way, it is possible to obtain the good fit reported in Figure 6.3.

So within experimental accuracy the peaks in the coherent inelastic dynamic structure factor of silica do not shift; they merely fade away to make room for a full validity of the incoherent approximation above 40 meV. The same is true for germania, where the oscillations fade even more quickly.

We will see in the following that one needs a correction of that effective density of states, to account for mass and scattering cross section effects. But to be able to do that, one needs first to analyse the observed $S_\omega(Q)$ in terms of specific atomic motions. This will be done in the following section.

6.2.3 Analysis of the coherent inelastic dynamic structure factor $S_\omega(Q)$

The next question is: what does the dynamic structure factor $S_\omega(Q)$ at the boson peak tell us about the eigenvector of the vibrational modes?

The first investigation of that question in vitreous silica was done on the IN6 spectrometer (Buchenau *et al.* 1986). Therefore the momentum transfer range was limited to values lower than 3 $Å^{-1}$, a factor of two lower than the range covered here.

Let us recall what one knows about the frequency region of the boson peak, both from the quartz crystal (Schober *et al.* 1993) and from the silica glass (Buchenau *et al.* 1986, Wischnewski *et al.* 1998) studies.

In the literature, the boson peak is explained in terms of long-wavelength sound waves (translational motion) and librations of the SiO_4 tetrahedra (Figure 6.7). The first contribution links the dynamic structure factor to the static structure factor, $S_\omega(Q)=S(Q)$ (Carpenter and Pelizzari 1975), while the tetrahedra librations can be described by $S_\omega(Q)= S_{rot}(Q)$, where $S_{rot}(Q)$ is calculated from the motional model of Figure 6.7. One expects a mixture of long-wavelength sound waves and SiO_4-tetrahedra librations.

The large momentum transfer range of the present investigation allows extending the earlier work (Buchenau *et al.* 1986) to a determination of the ratio between sound waves and coupled librations (a libration is a rotational vibration) at the boson peak.

Figure 6.8 compares the two structure factors $S(Q)$ and $S_{rot}(Q)$. They differ mainly at the first and second peak. Thus a strong first peak in $S_{boson}(Q)$ means a large sound

wave fraction in the boson peak modes, a strong second peak a large tetrahedra libration fraction.

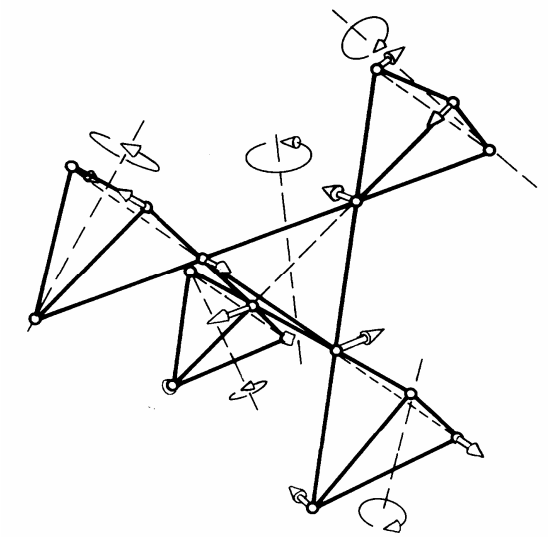

Figure 6.7: Coupled rotation of five corner-connected SiO_4- or tetrahedra GeO_4- (Buchenau *et al.* 1986)

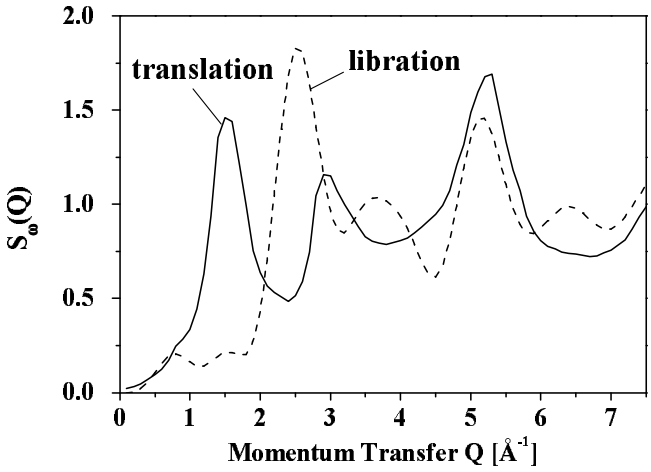

Figure 6.8 Comparison of the translation structure factor $S(Q)$ (continuous line) with the structure factor $S_{rot}(Q)$ (dashed line) of the coupled libration of five corner-connected SiO_4- tetrahedra.

The tetrahedra rotation was calculated for the motional model of Figure 6.7 and is shown as the dashed line in Figure 6.8. The $S(\boldsymbol{Q})$, the continuous line in Figure 6.8, is

expected for any in-phase motion of neighbouring atoms, for instance for long-wavelength sound waves.

The position of the peaks in Figure 6.5a demonstrates a sum of both structure factors is needed to explain the measurement; one can neither explain it in terms of only coupled tetrahedra libration nor in terms of a pure in-phase motion of neighbouring atoms. The experiment requires a mixture of about equal parts of both for its explanation. The best fit supplies a fraction of 0.55 of tetrahedra libration signal and 0.45 of translation.

This information goes beyond the one of the old experiment (Buchenau *et al.* 1986), which only showed that one needs tetrahedra libration to explain the inelastic dynamic structure factor. Here we show that one needs a sizeable part of long-wavelength translational motion as well. As we will see, this part is markedly larger than the expectation of the sound wave Debye model.

6.2.4 Density of states in the coherent approximation and specific heat

Now that we know what kind of vibrational modes we deal with, we can extend the incoherent approximation to take the coherent oscillations of the dynamic structure into account. For vitreous silica we take the signal at the boson peak to consist of 55 % tetrahedra libration signal and 45 % in-phase motion of neighbouring atoms. Since the tetrahedra libration is essentially oxygen motion, the neutron signal from a tetrahedra libration mode is enhanced by the mass factor $\overline{m}/m_O = 20/16$, where $\overline{m}$ is the average mass and m_O is the oxygen mass. The neutron signal of the mode is further enhanced by the scattering cross-section ratio $3\sigma_O/(2\sigma_O + \sigma_{Si})$, where $\sigma_O = 4.24$ barn is the oxygen atom scattering cross section, and $\sigma_{Si} = 2.18$ barn is the one of the silicon atom. Both factors together supply a signal factor of 1.49 for tetrahedra libration in vitreous silica. This has to be taken into account when a

density of states is calculated from the neutron data (Figure 6.9).

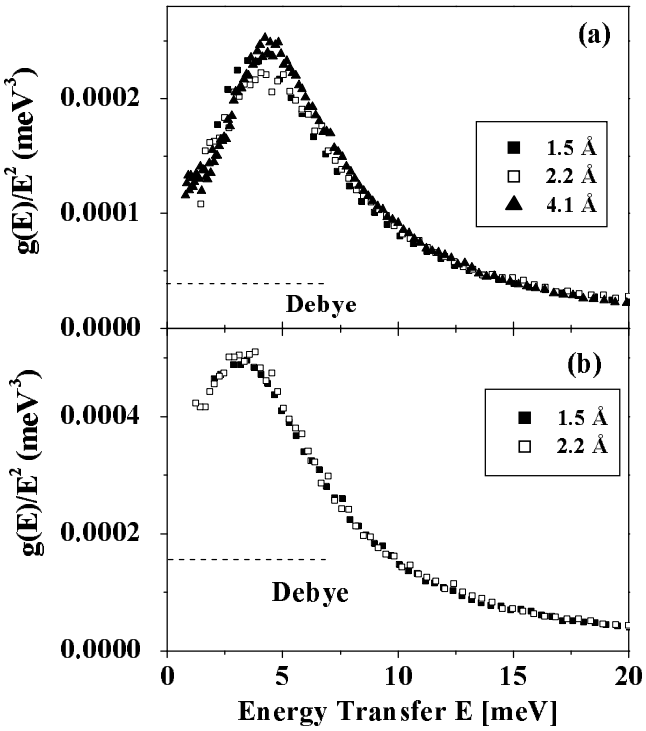

Figure 6.9 Vibrational density of states obtained using the extended approximation for the different TOF data sets of vitreous silica (a) and for vitreous germania (b)

To check the vibrational density of states obtained in the previous section from the extended approximation against earlier results in literature, the heat capacity was calculated from the 4.1Å data (Figure 6.10a) and compared with the data measured on the same sample (Buchenau *et al.* 1986).

Figure 6.10 shows the comparison between the measured heat capacity data (Buchenau *et al.* 1986) of vitreous silica to the result of the evaluation of the neutron data. As it turns out, the correction of the enhancement factor is essential to get a good agreement. Without the correction, the heat capacity calculated from the neutron data is clearly too high (Figure 6.10a).

So the comparison corroborates the assignment of 55 % pure oxygen signal and 45 % average motion at the boson peak in vitreous silica. Similarly, Figure 10b shows

good agreement between measured and calculated heat capacity data in vitreous germania where the correction is smaller (we have only 25 % tetrahedra libration at the boson peak).

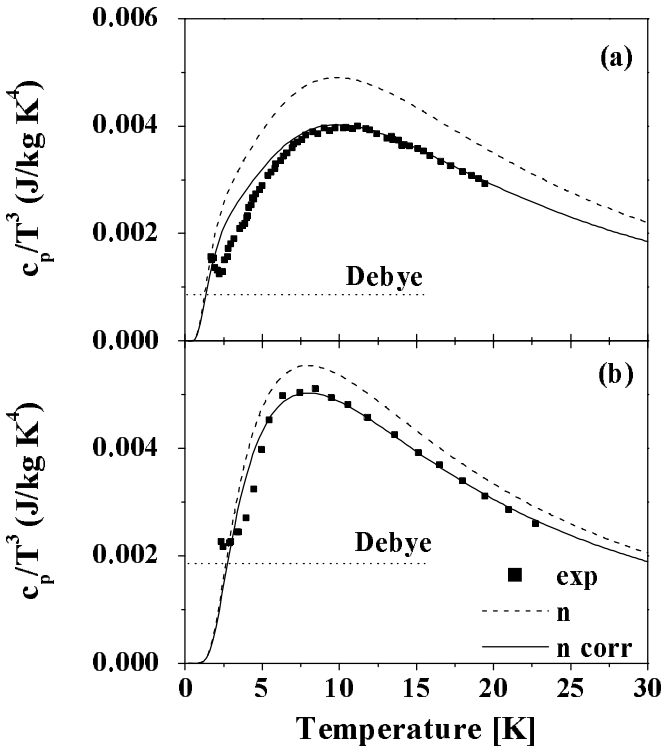

Figure 6.10: (a) Comparison of measured heat capacity data of vitreous silica (solid squares, Buchenau *et al.* 1986) with the ones calculated from the 4.1 Å neutron data with (full line) and without (dashed line) correction for the tetrahedra libration signal. (b) Comparison of measured heat capacity data of vitreous germania (solid squares, Antoniou and Morrison 1965) with the ones calculated from the 2.5 Å neutron data with and without correction for the tetrahedra libration signal.

6.2.5 The influence of the phonon damping

The analysis of the dynamic structure factor at the boson peak in subsection 6.2.3 suggested a signal ratio of 55:45 for librations to sound waves in vitreous silica. In vitreous germania, this ratio was even lower, 25:75. In both cases, the simple Debye expectation would predict a lower number of sound waves between 2 and 6 meV that is directly observed in Figure 6.9a and 6.9b.

However, we know that the simple Debye expectation is not correct. We do not have a simple sound wave picture. From the x-ray Brillouin data of vitreous silica (Benassi *et al.* 1996) and from the neutron Brillouin data in Chapter 5, we already know that at least the longitudinal phonons are strongly damped in both glasses. From the plateau in the thermal conductivity at low temperatures (Zeller and Pohl 1971), one infers that the transverse phonons experience a similar damping (one can also see that from the simulation results for the transverse currents in Chapter 5).

With this knowledge, we can go one step beyond the simple Debye expectation, calculating the scattering response for Debye phonons with the damping observed in the x-ray or neutron Brillouin experiments, replacing the δ-function of each Debye phonon by a DHO function with the appropriate damping. For simplicity, we assume the damping of a transverse wave to be equal to the one of the longitudinal wave at the same frequency, taking the observed Q^2-law for the longitudinal waves. This procedure does not change the overall scattered sound wave intensity, but shifts a part of it into the low-frequency range, as shown in Figure 6.11. The comparison in Figure 6.11 provides at least a qualitative explanation of the high amount of sound waves observed in the boson peak region, a higher amount than the one expected on the basis of the simple Debye picture.

Finally, a ratio of 55:45 in vitreous silica and 25:75 in vitreous germania means that the sound waves in silica coexist with three times more librational excitations than in germania. This is a clear hint that the reason for the 2.6 times stronger damping of the sound waves in silica is due to a coupling between sound waves and additional

modes, rather than a scattering by structural inhomogenieties.

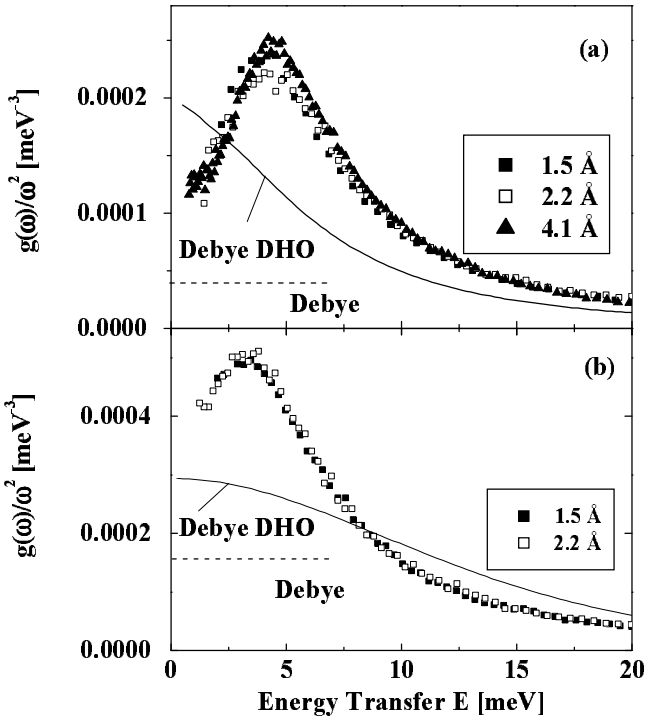

Figure 6.11 Comparison of the measured vibrational density of states with the DHO-damped Debye expectation (continuous lines) for (a) vitreous silica (b) vitreous germania .

REFERENCES

BENASSI P., KRISCH M., MASCIOVECCHIO C., MAZZACURATI V., MONACO G., RUOCCO G., SETTE F., and VERBENI R., *Phys. Rev. Lett.* **77**, 3835 (1996).

BUCHENAU U., PRAGER M., NÜCKER N., DIANOUX A. J., AHMAD N. and PHILLIPS W. A., *Phys. Rev.* **B 34**, 5665 (1986).

CARPENTER J. M. and PELIZZARI C. A., *Phys. Rev.* **B 12**, 2391 (1975).

JOHNSON P.A.V., WRIGHT A.C. and SINCLAIR R.N., *Journal of Non-Cryst. Solids* **58**, 109 (1983)

KOHARA S. and SUZUYA K., *Phys. Chem. Glasses* **43C**, 51 (2002).

SHOBER H., STRUCH D., NÜTZEL K. and DORNER B., *J. Phys.: Condens. Matter* **5**, 6155 (1993).

SUZUYA K., PRICE D.L., SABOUNGI M.L. and OHNO H., *Nucl. Instr. and Meth.* **B 133**, 57 (1997)

WISCHNEWSKI A., BUCHENAU U., DIANOUX A.J., KAMITAKAHARA W.A., and ZARESTKY J. L., *Phys. Rev.* **B 57**, 2663 (1998).

ZELLER R.C.and POHL R.O. *Phys. Rev.* **B 4**, 2029 (1971).

7. The Raman coupling function $C(\omega)$ for strong glasses

In this Chapter, inelastic Raman and neutron scattering spectra are reported for the network glass formers SiO_2 and GeO_2 measured at temperature from 10 and 300K. The scattering data are compared to obtain the Raman coupling function $C(\omega)$ and in particular, its low frequency limit.

Dans ce chapitre, nous présentons les spectres de diffusion inélastique Raman et de neutrons pour les verres de SiO_2 et GeO_2 que nous avons mesurés, pour des températures allant de 10 K jusqu'à 300K. Les données obtenues seront ensuite comparées entre eles pour obtenir le coefficient de couplage $C(\omega)$ et, en particulier, sa limite à basse fréquences.

7.1 Introduction

The results obtained until now are useful for the study of the Raman Coupling Function $C(\omega)$ for vitreous germania and for the comparison with the $C(\omega)$ previous calculated for vitreous silica (Fontana *et al.* 1999).

Different theoretical models have been so far proposed for the frequency dependence of $C(\omega)$ under different approximations. In particular, in the case of slightly distorted plane wave vibrations, $C(\omega)$ has been proposed to follow a ω^2 low frequency

dependence (Nemanich and Solin 1977, Winterling 1975, Martin and Galeener 1981), while in the fracton-like model (Alexander and Orbach 1982, Duval *et al.* 1987, Fontana *et al.* 1987, Fontana *et al.* 1997) the coupling function follows a power law, $C(\omega) \propto \omega^{\alpha}$, even if is not yet clear if this exponent depends on the fractal and/or spectral dimension, or not (Dell'Anna *et al.* 1998). The soft-potential model predicts a constant $C(\omega)$ (Karpov *et al.* 1983, Karpov and Parshin 1985). It should be noted however, that even if all these models predict a power - law frequency behavior for $C(\omega)$, a complete understanding on the value of the exponents is still lacking.

On the experimental side, the direct comparison between Raman scattering and inelastic neutron scattering measurements is the most faithful procedure to evaluate $C(\omega)$ to appraise the validity of the proposed models (Fontana *et al.* 1990). Though some efforts in this direction have been made on SiO_2 (Fontana *et al.* 1999), a definite conclusion on the spectral shape of $C(\omega)$ has not yet been acquired (Sokolov *et al.* 1993, 1995), because of the presence in the light scattering experiments of both a weak luminescence background and, in the lowest energy region, the quasi-elastic scattering (QES) contribution treated in Chapter 5 (Phillips 1981, Carini *et al.* 1995). The luminescence background induce a great uncertainty in the determination of the density of states from the experimental data (Sokolov *et al.* 1993, 1995), and it is necessary to minimize this influence as explained in Chapter 4. The data for silica (presented by Fontana *et al.* 1999) were re-analysed in order to take into account the luminescence contribution and compare with the new data collected for germania. The results obtained confirm the universal behaviour of $C(\omega)$ for strong glasses.

7.2 The general shape of $C(\omega)$

Figure 7.1 shows VV and HV Raman spectra measured at room temperature for both polarisations, for vitreous silica (a) and vitreous germania (b).

These data show typical features of the Raman scattering in glasses:

1. the presence of Boson peak in 20-100 cm^{-1} frequency range;
2. the presence in vv spectra of a intense and broad band in the intermediates frequency range;

Over 40 meV in Raman spectra of v-GeO_2 two bands, connected to the optical modes are present. The spectral shape of HV Raman data are clearly similar to the $g(\omega)/\omega^2$ obtained by neutron data, for v-SiO_2 (Figure 7.2a) and v-GeO_2 (Figure 7.2b).

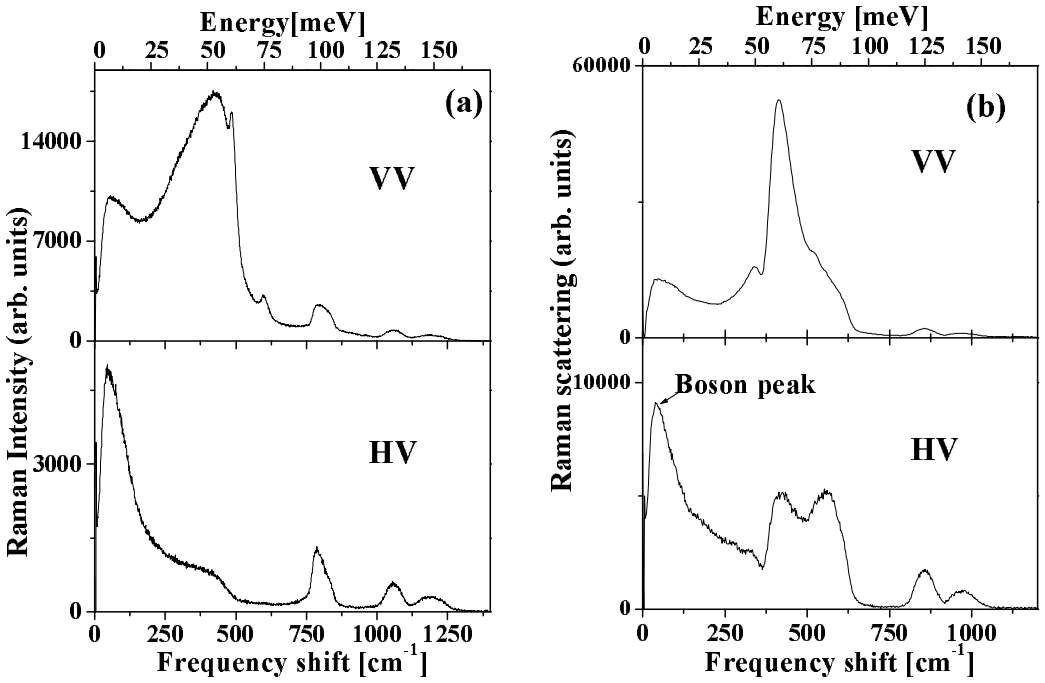

Figure 7.1: VV and HV Raman spectra measured at room temperature on v-SiO_2 and v-GeO_2

The comparison can be cast in a quantitative way if one considers the ratio $C(\omega)$ between the Raman intensity ($I_R(\omega)$) and neutron VDOS ($g_N(\omega)$) data expressed by the formula (7.1):

$$C(\omega) = \frac{I_R(\omega) \cdot \omega}{[n(\omega, T) + 1] \cdot g_N(\omega)} \tag{7.1}$$

The ratio are shown in Figure 7.3, for both polarisations, in the frequency range between 0 and 700 cm^{-1} for vitreous silica (Figure 7.3a-c) and between 0 and 400 cm^{-1} (Figure 7.3b-d) for vitreous germania.

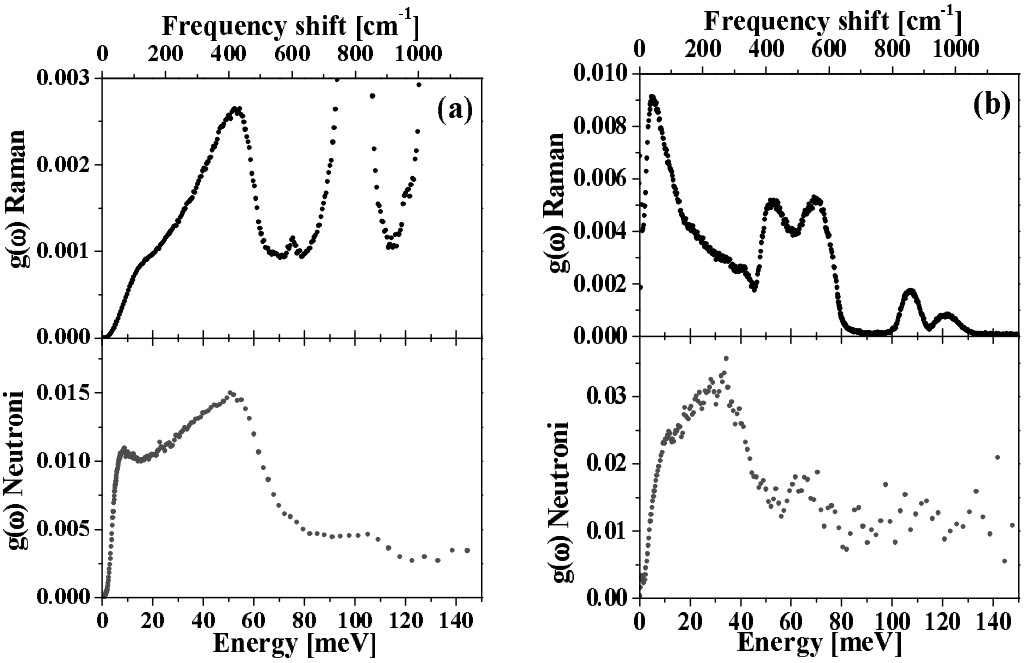

Figure 7.2: Comparison between HV Raman spectra and neutron VDOS for vitreous silica (a) and vitreous germania (b) in the range between 0 cm^{-1} and 1200 cm^{-1}

In particular for HV polarization we observe a linear behaviour (Figures 7.3c and 7.3d or better in the particular range shown in Figure 7.4) of $C(\omega)$ in the boson peak frequency range (around 60 cm^{-1} in Raman spectra as show in Figure 7.3c and 7.3d) followed by a nearly constant plateau up to high frequency where the molecular modes begin to appear (Mariotto *et al.* 1981, Masciovecchio *et al.* 1999, Fontana *et al.* 1999).

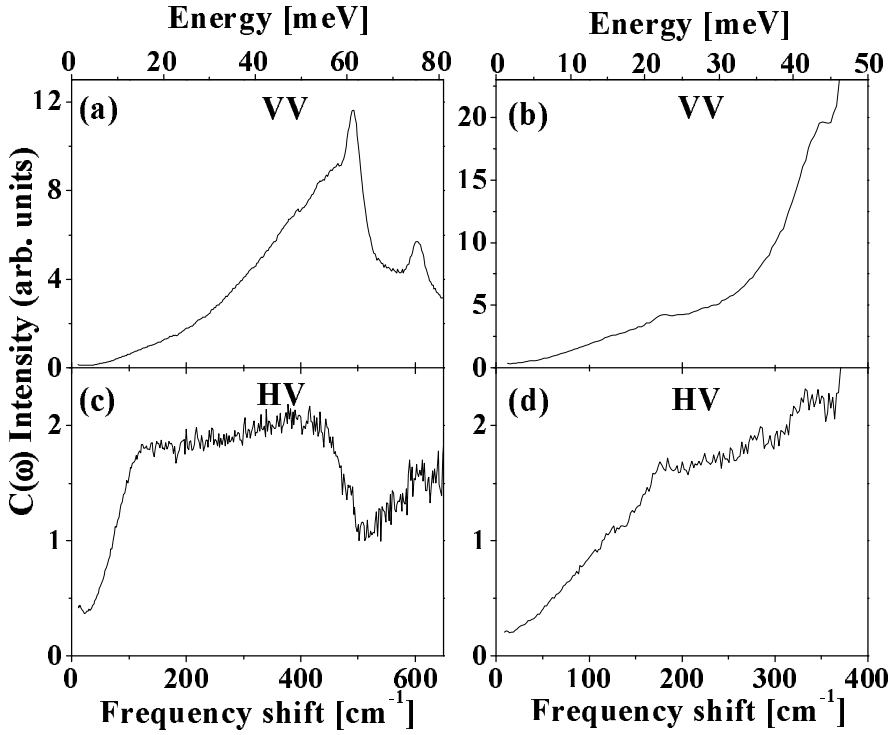

Figure 7.3: $C(\omega)$ for v-SiO_2 and v-GeO_2 calculated by the ratio of both polarizations of Raman with neutron scattering data.

This last frequency is near to the maximum value of acoustic phonons in the corresponding crystalline counterparts at the Brillouin zone edge (Leadbetter 1973). $C_{VV}(\omega)$ behaves in a completely different way showing an almost ω^2-behaviour up to 400 cm^{-1}. Over 400 cm^{-1} several peaks are present indicating a different sensibility to optical modes of the Raman scattering respect to that of neutron scattering.

For the v-GeO_2 glass the situation is slightly different. The resemblance of C_{VV} and C_{HV} could be due to a partial depolarization of light caused by microscopic bubbles inside the sample. So the evaluation of $C(\omega)$ in this system is approximate and can do only an indication. This last experimental result demonstrates that on the experimental side the shape of $C(\omega)$ can be strongly modified by spurious effects.

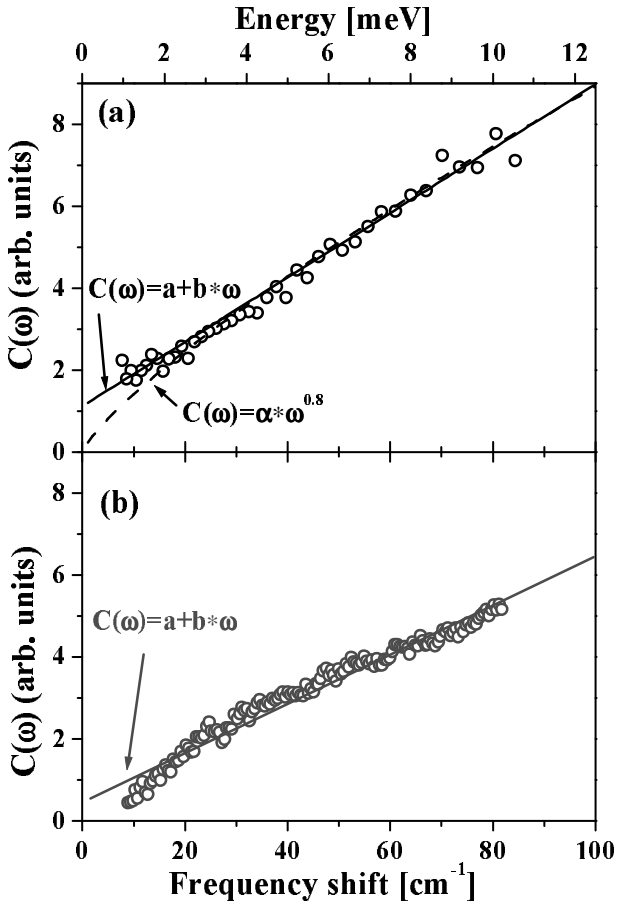

Figure 7.4: The $C(\omega)$ for vitreous silica (a) and vitreous germania (b) obtained by Raman and neutron scattering data collected at 50K

In Figure 7.4 we show the ratio between the Raman and neutron scattering (at 50K for both the samples). The $C(\omega)$ results to be a linear function of the frequency in the BP region, thus explaining the shift towards high frequencies observed in the BP maximum, in Raman scattering respect to neutron one. It is worth to note that $C(\omega)$ does not tend to zero decreasing the frequency but saturate at constant value (Fontana *et al.* 1999).

7.3 Discussion of the results of the $C(\omega)$

The key to understand of the experimental Raman spectra is the breakdown of the wave-vector selection rule of Raman scattering from crystals. This brings to a continuous first order vibrational spectrum in glasses instead of the discrete Raman spectrum observed in crystals. Two properties of glasses are responsible for this fundamental difference. Firstly, in glasses the coupling between the atomic displacement and the fluctuation of dielectric susceptibility is itself a random quantity because of the irregular atomic bonding: this aspect of disorder is referred to as *electrical disorder*. Secondly the vibrational modes of the glasses are not plane waves, except for the very low frequencies. The disorder that causes the distortion of the vibrational modes is named *mechanical disorder*.

From experimental results it is evident that the Raman coupling function in the optic mode region (over 400 cm^{-1}) is clearly band dependent, but still $C(\omega)$ is expected to vary weakly with frequency over any particular band.

In the intermediate frequency range (80-400 cm^{-1}) we assist to two different evidences:

i) $C_{HV}(\omega)$ has a constant value up to high frequencies where the molecular modes begin to appear. This demonstrates that the Raman and the neutron scattering measurements yield the same quantity, i.e. the density of states.

ii) $C_{VV}(\omega)$shows a nearly ω^2-behaviour up to 400 cm^{-1}.

In the low frequency region (ω<80 cm^{-1}), the two types of disorder cited above are characterised by correlation function of elastic-optics and vibrational properties of the sample: theoretical models predict a quadratic dependence of the Raman coupling function $C_{HV}(\omega)$ and $C_{VV}(\omega)$, at low frequency (corresponding to the acoustic region).

On the contrary the experiment data show that in the range 10-80 cm^{-1}, $C(\omega)$ does not follow a simple power law as shown in Figure 7.4.

7.4 The comparison with the specific heat

A check of the validity of the spectral shape of the $C(\omega)$ can be obtained by calculating from the Raman depolarised spectrum the specific heat and comparing the results with the specific heat calculated by the fit of the experimental $C(\omega)$.

The specific heat in the range 2K-30K is reported in Figure 7.5 for vitreous silica and vitreous germania.

The excess of the density of states with respect to the Debye in the spectra is evident by the presence of the bump centred at about 8 K.

The excess specific heat around the maximum of C_p/T^3 *versus* T is comparable with the Debye contribution for the systems under investigation. The Debye level was calculated from the experimental sound velocities (see table 1, Chapter 2) by:

$$C_{Debye} = \frac{2\pi^2 k_B^4 T^3}{5\hbar^3 \rho \bar{v}^3} \tag{7.2}$$

in J g^{-1} K^{-1}, where $\bar{v}$ is the *mean sound velocity* (in cm/s) expressed by:

$$\bar{v}^3 = 3\frac{1}{\frac{1}{v_L^3} + \frac{1}{v_T^3}} \tag{7.3}$$

and ρ is the mass density measured in g/ cm^3.

The specific heat can be calculated by the formula:

$$C_p \approx C_v = 3Nk_B \int_0^{\omega_0} g(\omega)\left(\frac{\hbar\omega}{k_B T}\right)^2 \times \frac{e^{\hbar\omega/k_B T}}{\left[e^{\hbar\omega/k_B T} - 1\right]^2} d\omega \tag{7.4}$$

where N is the number density, ω_0 the highest vibrational frequency and $g(\omega)$ is the density of states obtained by low temperature Raman spectra:

$$g(\omega) = \frac{\omega}{n(\omega, T)+1}\frac{I_R(\omega, T)}{C(\omega)} \tag{7.5}$$

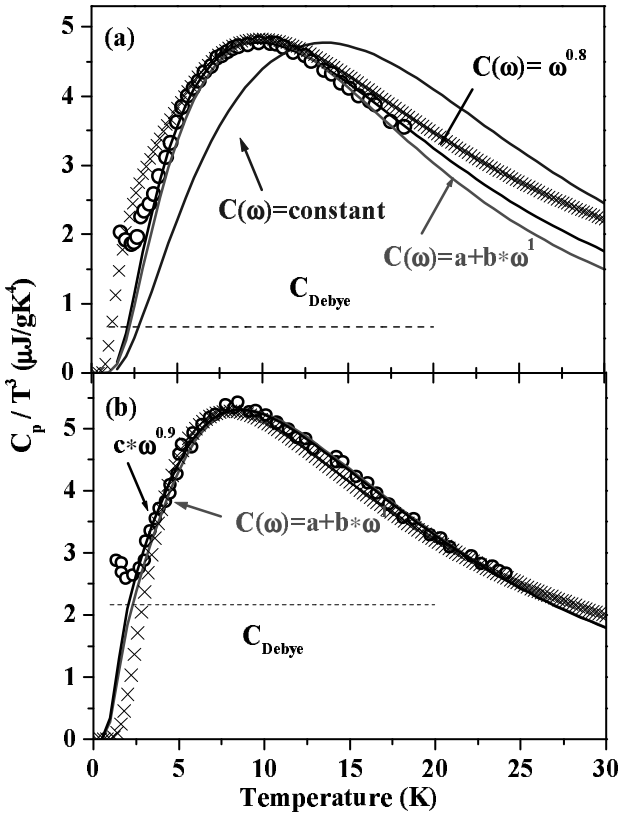

Figure 7.5: Comparison between the specific heat calculated by Raman data (open dots) and by neutron data (crosses) with respect to the Debye value (dashed line), for vitreous silica (a) and vitreous germania (b). The continuous lines represent the specific heat calculated assuming different trends of the C(ω).

In Figure 7.5 the fits of the specific heat taking the magnitude of $g(\omega)$ as a fitting parameter are also reported.

The behaviour of $C(\omega)$ can be assumed to have two different functional shapes :

$$C(\omega) \propto \omega^{\alpha} \tag{7.6}$$

or

$$C(\omega) = a + b\omega \tag{7.7}$$

The two fits can be considered satisfactory for both studied glasses, using the equation the fits can be considered as satisfactory for $0.7 < \alpha < 0.9$.

At T=0 the fitted curves fall to zero because we are not doing any assumption on the spectral behaviour below the instrumental limit of a few cm^{-1}, just truncating the integration range. This approximation does not affect the validity of the fit since we are not interested in the very low temperature/frequencies region which is rather connected to other modes, two level systems for example.

The functions for $C(\omega)$ expressed by the equations fit in an equally good way the experimental data, in the BP frequency range. This is not surprising because this method has a limited precision, which is due to the fact that the specific heat depends on the integral of density of states.

Nevertheless this method give a qualitative insight of the general shape of the $C(\omega)$. In fact if a constant $C(\omega)$ was used, as predicted by the soft potential model, we obtain the fit reported in Figure 7.5a for vitreous silica, which is clearly unsatisfactory.

The linear behaviour found by Raman to neutron ratio is in agreement with that obtained fitting the specific heat excess, even if the two fitting functions for $C(\omega)$ expressed by the equations are appreciably different only in the low frequency limit.

The Raman coupling function, analysed in strong glasses determined either by fitting the specific heat data and measured directly by the Raman to neutron ratio, has an universal linear frequency dependence in the BP frequency range.

In Figure 7.5 the two fitting functions are superimposed to the results for the $C(\omega)$ obtained from neutron and depolarised Raman scattering spectra. The experimental data below 20 cm^{-1}-30 cm^{-1} show that $C_{HV}(\omega)$ extrapolate to a non-vanishing value for $\omega \rightarrow 0$, confirming the previous conclusions reported for vitreous silica (Fontana *et al.* 1999). Thus, even if both equations 7.6 and 7.7 fit equally well the specific heat data, only equation 7.7 is adequate in describing the experimental $C(\omega)$.

This non-vanishing value of $C(\omega \rightarrow 0)$ gives interesting suggestions about the characteristics of vibrations in a topologically disordered systems (Fontana *et al.* 1999).

To defined the general behaviour of $C(\omega)$, different glasses, characterised by different structure and fragility, have been studied by Raman and neutron scattering techniques. The treatment of data is in progress

REFERENCE:

ALEXANDER S. and ORBACH R., *J. Phys. (Paris) Lett.* **43**, L625 (1982)

CARINI G., D'ANGELO G., TRIPODO G., FONTANA A., LEONARDI A., SAUNDERS G. A., and BRODIN A., Phys. Rev. **B 52**, 9342 (1995)

DELL'ANNA R., RUOCCO G., SAMPOLI M. and G. VILLANI, *Phys. Rev. Lett.* **80**, 1236 (1998)

DUVAL E., MARIOTTO G., MONTAGNA M., PILLA O., VILIANI G. and BARLAND M., *Europhys. Lett.* **3**, 333 (1987)

FONTANA A., ROCCA F., and FONTANA M. P., *Phys. Rev. Lett.* **58**, 503 (1987)

FONTANA A., ROCCA F., FONTANA M. P., ROSI B. and DIANOUX A. J., *Phys. Rev.* **B 41**, 3778 (1990)

FONTANA A., ROSSI F., CARINI G., D'ANGELO G., TRIPODO G. and BARTOLOTTA A., *Phys. Rev. Lett.* 78, 1078 (1997)

FONTANA A., DELL'ANNA R., MONTAGNA M., ROSSI F., VILIANI G., RUOCCO G., SAMPOLI M., BUCHENAU U. and WISCHNEWSKI A., *Europhys. Lett.* **47**, 56 (1999).

KARPOV V. G., KLINGER M. I., and IGNAT'EV F. N., Zh. Eksp. Teor. Fiz. 84,760 (1983)

KARPOV V. G. and PARSHIN D. A., *Zh. Eksp. Teor. Fiz.* 88, 2212 (1985)

LEADBETTER A. J., "*Chemical Applications of Thermal Neutron Scattering*", Willis B.T.M., editor (OUP), p. 146 (1973)

MARIOTTO G., FONTANA A., CAZZANELLI E., ROCCA F., FONTANA M.P., MAZZACURATI V., and SIGNORELLI G., *Phys. Rev.* **B 23**, 4782 (1981)

MARTIN R.M. and GALEENER F.L., *Phys. Rev.* **B 23**, 3071 (1981)

MASCIOVECCHIO C., MAZZACURATI V., MONACO G., RUOCCO G., SCOPIGNO T., SETTE F., BENASSI P, CUNSOLO A., FONTANA A., KRISCH M., MERMET A., MONTAGNA M., ROSSI F., SAMPOLI M., SIGNORELLI G., and VERBENI R., *Phil. Magazine* **B 79**, 2013 (1999), and references therein

NEMANICH R.J. and SOLIN S.A., *Solid State Commun.* **23**, 417 (1977)

PHILLIPS W.A., "*Amorphous Solids: Low-Temperature properties*", (Springer, Berlin, 1981)

SOKOLOVA.P., KISLIUK A., QUITMANN D., and DUVAL E., *Phys. Rev* **B 48**, 7692 (1993).

SOKOLOV A. P., BUCHENAU U., STEFFEN W., FRICK B., and WISCHNEWSKI A., *Phys. Rev.* **B 52**, R9815 (1995- II).

WINTERLING G., *Phys. Rev.* **B 12**, 2432 (1975).

8. Conclusions

A new procedure to extract the density of states extending the usual incoherent approximation, an important result for coherent systems, has been developed. The introduction of the *dynamical structure factor* $S_\omega(\boldsymbol{Q})$ provides a better agreement between theory and experiment data and allows the analysis of the vibrational eigenvectors. In this way the *true* vibrational density of states can be calculated and used for the following studies about:

1. the origin of the Quasi-Elastic Scattering in strong glasses
2. the low frequency limit of the Raman coupling function $C(\omega)$, comparing neutron with Raman scattering data.

8. Conclusions

Nous avons développé une nouvelle procédure pour extraire la densité d'états, basée sur l'extension de l'approximation incohérente standard. Il s'agit là d'un résultat très important dans le cas de systèmes cohérents. L'introduction du facteur dynamique $S(Q,\omega)$ a fourni un meilleur accord entre la théorie et les données experiementales et a permi l'analyse des vecteurs propres vibrationnels.

Dans cette façon, il devient possible d'accéder à la 'vraie' densité d'états qui peut employée pour les études de:

1. *l'analyse de l'origine du quasi-élastique dans les verres forts*
2. *la limite à basse fréquence de la fonction de couplage en diffusion Raman $C(\omega)$, en comparant les données de diffusion neutronique et Raman.*

The second important result obtained is the existence of longitudinal and transverse branches in the strong glass former v-GeO_2 as well as the corresponding crystals.

Each subject has been developed by using different techniques such as Raman and neutron scattering, in order to obtain complementary information about the behaviour of our samples. In particular, the neutron scattering experiments have been carried out on Time-of-Flight and Three Axis spectrometers in order to investigate the dynamics of vitreous systems over a wide range of energies and wave vectors exchanged.

The systems under study were two typical strong glasses (v-SiO_2 and v-GeO_2) which have been widely studied experimentally and numerically in the last twenty years (in particular vitreous silica). The choice of vitreous germania was decided because of its lower sound velocity which allows the direct observation by INS, of the dispersion relation over the ($\boldsymbol{Q}$,ω)

Le deuxième résultat important qui a été obtenu est la mise en évidence de l'existence des branches longitudinales et transverses dans le verre fort v-GeO_2 tout comme dans le cristal correspondant.

Chaque sujet a été développé en employant différentes techniques telles que la diffusion Raman de la lumière et la diffusion des neutrons, dans le but d'obtenir des informations complémentaires sur le comportement de nos échantillons. En particulier, les expériences de diffusion de neutrons ont été effectuées sur des spectromètres Temps-de-Vol et Trois-Axes afin d'étudier la dynamique des systèmes vitreux sur une grande gamme d'échange d'énergie et de vecteur d'onde.

Les systèmes étudiés étaient deux verres forts typiques (v-SiO_2 et v-GeO_2) qui ont été largement étudiés tant du coté expérimental que numérique durant les dernières vingt années (et tout particulièrement la silice). Le choix de l'oxyde de germanium vitreux a été décidé en raison de sa vitesse du son inférieure à celle de la silice, ce qui permet l'observation directe par

region intermediate between hydrodynamic and single particle dynamics. We found clear presence of two well-defined peaks with an associated dispersion, which were assigned to LA and TA modes. The experimental results are compared with the corresponding dispersion curves calculated from the Molecular Dynamics simulations showing that they can be well reproduced by the simulated LA and TA branches, confirming our interpretation. To our knowledge, this is the first time that in a strong glass, like v-GeO_2, the presence of well-defined Brillouin peaks with an associated dispersion was observed directly from INS data. The comparison between experimental and simulated dispersion curves supported the hypothesis that in v-GeO_2 the Boson Peak (BP) can be ascribed to the quasi-transverse acoustic modes, whose dispersion relation becomes $\boldsymbol{Q}$-independent at large $\boldsymbol{Q}$ giving rise to the mode excess found at the BP energy. But the analysis of the coherent dynamic

diffusion inélastique des neutrons de la relation de dispersion dans le plan dynamique (Q, ω), intermédiaire entre l'hydrodynamique et la dynamique de la simple particule. Nous avons mis clairement en évidence la présence de deux pics bien définis dont les dispersions associées, qui ont été assignés aux modes LA et TA. La comparaison des résultats expérimentaux aux courbes de dispersion calculées à partir des simulations de dynamique moléculaire prouve qu'ils peuvent être bien reproduits par les branches simulées de LA et de TA, confirmant ainsi notre interprétation. A notre connaissance, c'est la première fois que dans un verre fort, comme v-GeO_2, la présence de pics Brillouin bien définis et avec une dispersion associée a été observée directement par des expériences de diffusion de neutrons. La comparaison entre les courbes de dispersion expérimentales et simulées conforte l'hypothèse que dans v-GeO_2 le pic de Bose (BP) peut être attribué aux modes acoustiques quasi-transverses, dont la relation de dispersion devient indépendante de Q à grand Q, en

structure factor at the boson peak shows that one has not only sound waves, but some coupled tetrahedra libration as well.

As far as Raman spectroscopy is concerned, the experimental results obtained by using this technique, have been compared with neutron data to extract information about the particular features of glassy systems at very low frequencies.

For the QES, our work proposes the interpretation to explain the origin of this particular characteristic in glasses. In fact, the common behaviour of Raman and neutron data with another scattering technique like Brillouin scattering suggests that the temperature-dependent extra-scattering is due to the same mechanisms.

The understanding of the origin of the QES allows a better calculation of the low frequency limit of the Raman coupling function $C(\omega)$. Performing low temperature measurements for our samples by Raman and neutron scattering measurement, a linear behaviour non-vanishing, for $\omega \rightarrow 0$, of the

provoquant l'excès de mode trouvé à l'énergie du BP. Mais l'analyse du facteur dynamique de structure cohérent au pic de Bose prouve qu'on n'a pas seulement des ondes du son, mais aussi bien des librations de tétrahèdres couplés.

Pour ce qui concerne la spectroscopie Raman, les résultats expérimentaux obtenus par cette technique ont été comparés aux données de diffusion neutronique pour obtenir des informations sur les propriétés particulières des systèmes vitreux à très basses fréquences. Pour le QES, notre travail propose une interprétation pour expliquer l'origine de cette caractéristique particulière dans les verres. En fait, le comportement commun de données Raman et de neutron avec une autre technique de diffusion comme la diffusion Brillouin suggère que la diffusion supplémentaire qui est dépendante de la température, soit due aux mêmes mécanismes.

La compréhension de l'origine du QES permet un meilleur calcul de la limite à basse fréquence de la fonction de couplage $C(\omega)$. Les mesures à basse température pour nos échantillons par

$C(\omega)$ has been obtained. We believe that this is a general trend of $C(\omega)$ at low frequency because the same results have been found in many others glasses, characterised by different structure and fragility from the strong glasses studied here.

diffusion Raman et de neutrons montrent un comportement linéaire de $C(\omega)$ qui n'est pas dispersif lorsque $\omega \to 0$. Nous croyons que la fonction de couplage $C(\omega)$ présente un comportement universel parce que les mêmes résultats ont été trouvés dans beaucoup d'autres systèmes vitreux à basse fréquence, caractérisés par des structures et une fragilité différentes comparativement aux verres forts étudiés ici.

9. List of Related Papers

- E.Fabiani, M.A.Gonzalez, S.Caponi, A.Fontana, M.Montagna, O.Pilla, F.Rossi and C.P.E.Varsamis, ***"Neutron scattering studies of vitreous germania"***, *Journal of Non-Crystalline Solids* **322** (2003) 7–10

- O. Pilla, A. Fontana, M. Montagna, F. Rossi, G.Viliani, M.A.Gonzalez, E.Fabiani and C.P.E.Varsamis, ***"Vibrational Dynamic of 'strong' glasses : the case of v-SiO_2 and v-GeO_2 "***, *Journal of Non-Crystalline Solids* **322** (2003) 53–57

- E. Fabiani, L. E. Bove, A. Fontana, O. Pilla and C. Petrillo, ***"Dynamic Structure Factor of Vitreous Germania"***, *Physica* **B 350**, (2004) e1099-e1102

- A. Fontana, F. Rossi, S. Caponi, E. Fabiani, U. Buchenau and A. Wischnewski, ***"Evidences of Quasi-elastic Scattering in Vitreous Silica: a Raman and Neutron scattering study"***, *Journal of Non-Crystalline Solids* (submitted, July 2004)

- L. E. Bove, E. Fabiani, A. Fontana, O. Pilla, F. Paoletti and C. Petrillo, ***"Vibrational dynamics of vitreous GeO_2 at THz frequency"***, *Europhysics Letters* vol.**71** N° **4,** (2005) 563-569

- E. Fabiani, A. Fontana, U. Buchenau, ***"Neutron scattering study of the vibrations in vitreous silica and vitreous germania"***, *Phys. Rev.* **B** (submitted)

- A. Fontana, O. Pilla, F. Rossi, E. Fabiani, ***"The Raman coupling function in v-GeO_2 and v-SiO_2: a light and neutron scattering study"***, (submitted)

- A. Fontana, F. Rossi, E. Fabiani, ***"The study of Raman Coupling Function from fragile to strong glasses"***, (to be submitted)

ABSTRACT

The main task of this thesis is to perform a systematic investigation of the dynamics of glassy materials at temperatures T much smaller than Tg, the glass transition temperature. Both theoretical and experimental studies performed over the last two decades on different aspects of the glassy state, have established a number of peculiar properties that concern low energy dynamics and manifest themselves in low temperature specific heat, thermal conductivity, and inelastic scattering experiments. Some of the fundamental questions in this field, in particular about the microscopic nature of the dynamics and the origin of the "universal" features concerning the density of vibrational states in glasses, have not found a generally accepted answer. In order to explain some features of strong glasses, different systems have been investigated. Here we present new results on two strong glasses, vitreous silica (v-SiO_2) and vitreous germania (v-GeO_2). The technique employed was Inelastic Neutron Scattering (INS). The studies of these samples have been done in order to:
(i) develop a new procedure to extract the density of states from coherent systems extending the usual incoherent approximation;
(ii) study the QES of our samples at very low frequency range (in order to compare with Brillouin data and to asses a correlation with the mechanism causing the sound attenuation);
(iii) compare of the previous scattering data above-mentioned, in order to calculate the Raman coupling function $C(\omega)$ and its low frequency limit;
(iv) finally, investigate v-GeO_2 to asses that both longitudinal and transverse acoustic branches are still somewhat defined also in glassy system.

ABSTRACT

Le but principal de cette thèse est d'effectuer une recherche systématique sur la dynamique des matériaux vitreux à des températures T beaucoup plus petites que la température de transition vitreuse Tg. Des études théoriques et expérimentales, exécutées pendant les deux dernières décennies sur différents aspects de l'état vitreux, ont établi un certain nombre de propriétés particulières qui concernent la dynamique à basse énergie et qui se manifestent dans la chaleur spécifique à basse température, dans la conductivité thermique, et dans la diffusion inélastique expérimentale. Certaines questions fondamentales dans ce domaine, relatives à la nature microscopique de la dynamique et à l'origine des caractéristiques "universelles" de la densité des états vibrationnels (VDOS) dans les verres, n'ont pas trouvé actuellement une réponse généralement admise. Afin de expliquer certaines caractéristiques des verres, nous avons étudié deux verres forts, le quartz fondu (v-SiO_2) et l'oxyde de germanium vitreux (v-GeO_2). La technique utilisée est la dispersion inélastique des neutrons. Les études de ces échantillons avaient pour objectifs:
(i) le développement d'une nouvelle procédure pour extraire la VDOS à partir des systèmes cohérents en étendant l'approximation incohérente habituelle;
(ii) l'étude de la diffusion quasiélastique de nos échantillons dans la région de très de basse fréquence;
(iii) la comparaison des données de dispersion précédemment mentionnées, afin de calculer la fonction de couplage Raman $C(\omega)$ et sa limite à basse fréquence;
(iv) l'étude du v-GeO_2 afin de prouver que les branches acoustiques longitudinales et transversales sont aussi définies dans le système vitreux.